

Technical University of Denmark



Wake models developed during the Wind Shadow Project

Larsen, Søren Ejling; Ott, Søren; Pena Diaz, Alfredo; Berg, Jacob; Nielsen, Morten; Rathmann, Ole Steen; Ejsing Jørgensen, Hans

Publication date:
2011

Document Version
Publisher's PDF, also known as Version of record

[Link back to DTU Orbit](#)

Citation (APA):
Larsen, S. E., Ott, S., Pena Diaz, A., Berg, J., Nielsen, M., Rathmann, O., & Ejsing Jørgensen, H. (2011). Wake models developed during the Wind Shadow Project. Roskilde: Danmarks Tekniske Universitet, Risø Nationallaboratoriet for Bæredygtig Energi. (Denmark. Forskningscenter Risoe. Risoe-R; No. 1793(EN)).

DTU Library
Technical Information Center of Denmark

General rights

Copyright and moral rights for the publications made accessible in the public portal are retained by the authors and/or other copyright owners and it is a condition of accessing publications that users recognise and abide by the legal requirements associated with these rights.

- Users may download and print one copy of any publication from the public portal for the purpose of private study or research.
- You may not further distribute the material or use it for any profit-making activity or commercial gain
- You may freely distribute the URL identifying the publication in the public portal

If you believe that this document breaches copyright please contact us providing details, and we will remove access to the work immediately and investigate your claim.

Wake models developed during the Wind Shadow Project

Risø-R-Report

S. Larsen, S. Ott, A. Peña, J. Berg,
M. Nielsen, O. Rathmann, H. Jørgensen
Risø-R-1793(EN)
November 2011



Author: S. Larsen, S. Ott, A. Peña, J. Berg,
M. Nielsen, O. Rathmann, H. Jørgensen
Title: Wake models developed during the Wind Shadow Project
Division: Wind Energy

Abstract

The Wind Shadow project has developed and validated improved models for determining the wakes losses, and thereby the array efficiency of very large, closely packed wind farms. The rationale behind the project has been that the existing software has been covering these types of wind farms poorly, both with respect to the densely packed turbines and the large fetches needed to describe the collective shadow effects of one farm to the next.

Further the project has developed the necessary software for the use of the models.

Guidelines with recommendations for the use of the models are included in the model deliverables.

The project has been carried out as a collaborative project between Risø DTU, DONG, Vattenfall, DNV and VESTAS, and it has been financed by energinet.dk grant no. 10086.

Risø-R-1793(EN)
November 2011

ISSN 0106-2840
ISBN 978-87-550-3936-0

Contract no.:

Group's own reg. no.:
(Føniks PSP-element)

Sponsorship:

Cover :

Pages:
Tables:
References:

Information Service Department
Risø National Laboratory for
Sustainable Energy
Technical University of Denmark
P.O.Box 49
DK-4000 Roskilde
Denmark
Telephone +45 46774005
bibl@risoe.dtu.dk
Fax +45 46774013
www.risoe.dtu.dk

Contents

Preface 5

Overview of the Modeling effort 7

Conclusions 11.

References 12.

Attachments

Peña, A. And O. Rathmann; The atmospheric stability dependent infinite wind farm and wake decay constant.

Ott, S. , J. Berg and M. Nielsen: Linearised CFD Models for Wakes. Risø-R-1772

Preface

The aim of the Wind Shadow project has been to develop and validate an improved model for determining the wakes losses, and thereby the array efficiency of very large, closely packed windfarms. The rationale behind the project has been that the existing software has been covering these types of wind farms poorly, both with respect to the densely packed turbines and the large fetches needed to describe the collective shadow effects of one farm to the next.

Further the project has aimed to develop the necessary software for the use of the model.

The final results of the project are two models, FUGA and the Wake Park Boundary Layer Model, allowing the user to estimate the effects of wakes behind wind individual turbines as well as behind whole wind farms while the original WASP Park model (Mortensen et al.2007), remains a possibility for smaller wind farms.

These results are summarized in the two reports 1) by Ott et al. (2011) giving the detailed description of the FUGA model and description of validation studies of within farm and between farm wakes, 2) by Peña et al (2011) describing the Wake-Park Boundary Layer model; these two publications are attached to this report. Finally the present report provides short overview and inter-comparison of the two models, as well as recommendations and guidelines for when and how to use them. Further references are found in the two reports

The Fuga model will in the future undergo further development, both with respect to terrain and stability, and ability to handle multiple types of wind turbines (like the WASP wind farm model); It is presently best suited for studies of offshore wind energy, neutral atmospheric conditions and farms with one type wind turbine only. On the other hand, here the validation of the model both for within farm and between farms against data is well documented.

The Wake Park Boundary Layer Model combines two well known wind farm models; the WASP Park model (Mortensen et al, 2007) and the infinite wind farm model by Frandsen (1992). It is well adapted to use with the WASP Park model. It uses an iterative technique to gradually modify the wake expansion coefficients used in the WASP Park model to the values of consistent with those of the Infinite Farm, as the fetches within the farm grow larger (Rathmann et al, 2010). Also the Wake Park Boundary Layer Model is under further development, and is now able to predict the wake wind deficit for a range of atmospheric stability conditions.

The modeling efforts described in this reporting has been a key activity within the present PSO Wind Shadow project, Energinet. dk 10086. Additionally it has been supported by the Carbon Trust as part of the Offshore Wind Accelerator Project, and by the EU TOPFARM project.

The following organizations have participated in the Wind Shadow project:

Wind Energy Division, Risø DTU, Det Norske Veritas (DNV), DONG, Vattenfall, VESTAS. Here Risø DTU has been the main model developer, while the industrial participants are all main-users of the farm efficient models.

The developed models are distributed to the participants in the Wind Shadow project for testing and validation. Similarly participants in the Carbon Trust and the EU TOPFARM project, will all get access to the developed models as stand-alone models.

Overview of the developed models.

A. Peña, S. Ott, O. Rathmann, M. Nielsen, S. Larsen (Risø DTU)

During the Wind Shadow project, two models were developed/improved: **Fuga** and the **Wake-Park BL-adjusted**. Although they can estimate similar wake-related parameters, they are based on two completely different approaches. Fuga is based on CFD, whereas the Wake-Park BL adjusted model is based on an engineering approach to model the wake and the interaction of a wind farm with the atmospheric boundary layer. Both models are in their current versions documented to be able to handle neutral atmospheric conditions only (although stability dependent versions has been developed, but not yet validated against data), and 'single-type-wind-turbine' wind farms. However, the Park wake model, used in WASP and basis of the Wake-Park BL adjusted model, can perform wake estimates for wind farms with different turbines' types. So one can use the results for the wake decay coefficient of the Wake-Park BL adjusted model directly in WASP and model 'multiple type' wind farms. However, less agreement with data is expected when using the WASP Park model for large compared to small-medium size wind farms. The characteristics of the two models are described below in parallel, while the relevant key publications are attached in the end of the report.

Models	
Fuga	Wake-Park Boundary-Layer (BL) model
Background	
<p>A new wake model called Fuga has been made in the course of three projects. Refinement of numerical methods and adaptation to multiple wind turbine types—of the first drafts of the model developed under the TOPFARM project—were made in the WindShadow project and the Carbon Trust Offshore Wind Accelerator project sponsored the development of a graphical user interface and model validations. The model explicitly represents the wakes from individual turbines. Thus it is possible to study turbine-to-turbine interactions and estimate annual energy productions from individual turbines in a wind farm or even a cluster of wind farms. Below we briefly describe version 1.5 of the model. The plan is to include wake meandering in the future by combining the model with the dynamic wake model developed in the TOPFARM project. At the moment (June 2011) Fuga cannot deal with more than one turbine type in one calculation, but this will also be changed in the near future (a mathematica version can deal with more than one type).</p>	<p>The Wake-Park Boundary-Layer (BL) adjusted model combines the results of two models: the infinite wind farm boundary layer (IWFBL) model of Frandsen (1992), later extended and corrected by Frandsen et al. (2006), and the WASP Park wake model (Mortensen et al., 2007). The IWFBL model computes the wind speed reduction of an infinite wind farm array. The WASP Park model can be also evaluated for an infinite wind farm, but the wake decay coefficient, which is a 'free', but constant parameter of the Park model, can be "adjusted" so that the infinite Park model matches the wind speed reduction of the IWFBL model. Since wind farms are not infinite, the WASP Park model is modified, allowing it to run for a real 'definite' wind farm with a wake decay coefficient that will be asymptotically reduced from a recommended value to that "adjusted" in the previous step.</p>

Fuga	Wake-Park Boundary-Layer (BL) model
The model	
<p>A technical comprehensive description of the model can be found in Ott (2011), where the model equations and solution methods are explained.</p> <p>The model starts from a specific set of non-linear computational fluid dynamics (CFD) equations. Models based on the Reynolds average Navier-Stokes (RANS) equations with a closure based on an eddy viscosity have been considered. The $E - \epsilon$ closure and the mixing length closure are examples of such models. Perturbation theory is then applied to the equations with the drag force from the turbines acting as a 'small' perturbation, and only first order perturbations are considered. The first order perturbation is governed by linear equations and we have developed very fast solution methods for them. The gain in speed of around 10^5 is the main advantage of the linearization. The price to pay for this is that the solutions to the linearized equations are only approximate solutions to the original equations. It is also clear that a linearized model can never be better than the non-linear model it was made from. There are many different CFD models around and it is difficult to point out one as the best and obvious choice for linearization. There have in fact been many problems with CFD models applied to wakes. Ott (2011) compared linearized versions of three different CFD models with data and found one model to be distinctly better than the two others. This model is the simplest possible closure, where the eddy viscosity is assumed to have the same value ($\kappa u_* z$) as over a flat (sea) surface without any turbines. In other words, the simple closure completely ignores any influence a wake may have on the turbulent mixing that governs wake decay. All other models have a feed back mechanism that modifies the eddy viscosity in wakes and which is based on turbulence theory. It can therefore be argued that the success of the simple model actually demonstrates a lack of basic understanding of how turbulent mixing works in wakes.</p>	<p>The WAsP Park model is a momentum-based model that estimates the wind speed deficit behind a wind turbine in a similar fashion as the model of Jensen (1983), i.e. the wake is modeled to increase in width with distance from a turbine at a linear rate or decay (therefore the concept of wake decay coefficient), but it also accounts for the interaction of neighboring wakes to estimate a combined wind speed reduction (Katic et al., 1986). Rathmann et al. (2010) solved analytically the WAsP Park model for an infinite wind farm, so that it can be compared to an IWFBL model.</p> <p>An IWFBL model, on the other hand, inherently assumes an infinite wind farm and computes the wind speed deficit of the whole infinite array by estimating the asymptotic overall mean wind speed at hub height within the wind farm. This can be performed by different means and Frandsen (1992) did it by dividing the atmospheric boundary layer in two layers: one above hub height, affected by the roughness of the wind farm, and another below hub height affected by the roughness of the surface. The above-hub and below-hub wind profiles are required to match at hub height and the difference in shears between the two layers is equal to the effect of the turbines and the array layout.</p> <p>As stated in the background, once the IWFBL model estimates the wind speed deficit for a given wind farm layout with a certain turbine type, the modified (infinite) Park wake model iteratively tries to match that wind speed deficit by adjusting the wake decay coefficient. This "infinite adjusted wake decay coefficient" is kept as a minimum asymptotic value. Then the standard WAsP Park procedure is internally applied using a 'high' wake decay value, e.g the WAsP recommended wake decay coefficients (0.05 for offshore and 0.075 for onshore sites), for the first row of turbines and for the following (already wake affected) the value will be reduced via a relaxation constant towards the "infinite wake decay coefficient" every time a new row is encountered. The Wake-Park BL adjusted model is described in the paper by Rathmann et al. (2010).</p> <p>One of the main advantages of the model is that it is fast, very fast (for Horns Rev 1 calculations, it takes less than 1 s).</p>

Fuga	Wake-Park Boundary-Layer (BL) model
Assumptions and interpretations (1)	
<ul style="list-style-type: none"> • Neutral stratification. For offshore locations the atmospheric stability is determined mainly by the difference of temperature between air and water. These two temperatures are in turn determined by the different histories of the air and the water. Most often air and water are brought in from different places so it is quite unlikely that they end up being the same. Neutral stability is therefore quite rare offshore. Nonetheless, the assumption seems to work because stable and unstable conditions have opposite effects on energy production which somehow compensate in the long run. • Statistical stationarity Statistical properties of the flow are assumed to be constant in time. This is the basis for the Reynolds decomposition of the flow into a mean flow and a fluctuating, turbulent part. • Boussinesque approximations. The term is actually used for three different approximations. Here we make use of two of them. The first consists in neglecting compressibility and only letting density differences play a role in the buoyancy term. Thus the effect on the inertia is neglected. This assumption is believed to be fully justified for atmospheric flow. The second is the representation of Reynolds stresses by means of an eddy viscosity. This means that the mean flow is calculated as if the fluid was sticky like sirup with a large viscosity ('stickiness') caused by turbulent mixing of momentum between neighboring fluid elements. This assumption is more controversial. • The rotor is represented by an actuator disk. This means that rotor drag forces are distributed evenly over the rotor plane, which is assumed to be vertical and perpendicular to the local free wind at the hub position. The local free wind for a given turbine is the wind speed at the hub when the turbine drag is neglected (while the drag from all other turbines is not neglected). The drag is calculated as $\frac{1}{2}\rho C_T \pi R^2 U_f^2$, where U_f is the local free wind and it is assumed to point opposite to the global free wind. • A simple closure is used based on eddy viscosity which is set equal to the value ku_*z of the free stream. • Air density is assumed to be constant. 	<ul style="list-style-type: none"> • Neutral stratification. The final graphic interface of the model is presently able to handle neutral atmospheric conditions, although the model itself has already been extended for unstable and stable static atmospheric conditions and a paper with the model extension is in preparation (A. Peña, personal communication). A user-friendly interface of the stability dependent model is planned to be developed within few months. • Turbine type The model requires all turbines of the wind farm to be of the same type and hub height, a restriction due to the IWFB model by Frandsen (1992). • Boundary Layer The IWFB model by Frandsen (1992) assumes that there are two boundary layers in the wind farm (above and below hub height). The momentum fluxes are assumed to be constant through the layers (not the same for the two though). • Thrust coefficient It is assumed to be homogeneously distributed in the rotor disk. • Wind profiles and geostrophic wind The wind profile above hub height approaches the geostrophic wind value. The hub height wind speed within the wind farm however is estimated from a simplified geostrophic drag law, which uses resistant law constants close to those normally assumed for neutral conditions and middle latitudes (Troen and Petersen, 1989). • Wake expansion This is linear and the rate of expansion is given by the wake decay coefficient in the same way as the model by Jensen (1983). • Wake deficit It is based on the model by Jensen (1983), so the wind speed deficit is a function of the induction factor (estimated from the thrust turbine characteristics), the wake decay coefficient, and the ratio between the downwind distance and the rotor diameter. • Wake interference The total wake deficit is a combination of four types of wakes: directly upwind, adjacently upwind, ground-reflected directly upwind and ground-reflected adjacently upwind. The resulting speed deficit is calculated following a quadratic summation rule as described by Katic et al. (1986).

Fuga	Wake-Park Boundary-Layer (BL) model
<p>CFD lives in an idealized model world. The global free flow (flow over open water with no turbines) is usually assumed to be horizontally homogeneous with respect to speed and direction, and a turbine wake becomes straight. The real world is more complicated. First the flow is not stationary, and the wind speed and direction can vary substantially in time and in space. We need such assumption to define a Reynolds decomposition. For practicality we may regard a 10-min time series as a piece of an infinite, stationary time series, but care must be taken when dealing with wakes. The important thing is that the small scales of the flow (small eddies with life times much shorter than 10 min) are not greatly influenced by the non-stationarity of the flow. Small eddies easily adapt to conditions changing over 10 min and contribute only to the fluctuating part of the model flow and their effects can be described by an eddy viscosity. Very big eddies that live much longer than 10 min are also easy because they only contribute to the assumed mean flow. Then there are the eddies with sizes in between. Eddies larger than the typical wake width move big parts of the wake more-or-less as an entity without causing much mixing with the surrounding air. The result is the meandering that makes the wake axis twist, turn and flap. The effect of these large eddies is not well described by an eddy viscosity, but the question is whether CFD does that. To some extent medium size eddies are caused by factors that are not built into the model. These factors could be gravity waves, differential heating due to passing clouds etc. Compared to the real world, the model world should contain fewer medium size eddies. It should be noted that in the 'simple' closure we use, the eddy viscosity is the same as in the free flow. Thus the eddy viscosity K is determined from the logarithmic wind profile of the free flow through $KdU/dz = u_*^2$, describing the vertical turbulent transport of momentum. But vertical transport is not much affected by meandering because meandering mainly involves horizontal motion. With this closure it seems plausible to interpret model results as if meandering was absent, so model results should be taken with a grain of salt since we should imagine the straight model wakes be replaced by real, meandering wakes. Thus the model predicts multiple wakes in the special situations where the wind blows right down the turbine rows. In reality we never see many wakes inside each another as the model predicts. The wake from the first turbine may hit the next one so that a combined wake is formed, but the chances that the combined wake hits the third turbine are not large. Visualizations of LES simulations made by Calaf et al. (2010) seem to support this. Real wakes are therefore considerably more messy than the model predicts. When the model predicts that the wake from a turbine hits another turbine for a particular direction, it may not happen in the real world. Conversely, wakes may hit turbines even when the model predicts otherwise. The total number of hits is the same, so averaged quantities such the annual energy production is only marginally affected by meandering.</p>	

Fuga	Wake-Park Boundary-Layer (BL) model
Recommendations	
<p>In its present form Fuga predicts the mean flow. It does not predict turbulence or fluctuations caused by turbulence. This makes the model well suited for annual production estimates. It is about one million times faster to run than a conventional RANS model which makes it possible to compute a very large number of flow cases involving a large number of turbines in a relatively short time. The model could therefore be used to optimize the positioning of turbines in wind farms or the positioning of wind farms within clusters of windfarms.</p> <p>The model has been validated mainly against data from offshore wind farms, and this should be its primary use. It would work even for an onshore wind farm, but only in flat terrain. It is not recommended for use in non-uniform or very rough terrain.</p> <p>The model is limited to neutral stability. It probably under-predicts production in unstable conditions and over-predicts in stable conditions, so there will be a tendency that these errors even out on average. The validation was made against all available data, not just neutral. We therefore recommend using it for all stabilities for farms with climatology similar to Horns Rev and Nysted.</p> <p>The model shows good agreement with data for long range shadow effects when results are compared with wind speeds measured at the two met mast east of Horns Rev 1. It is possible that long range shadow effects are affected by stability, but it has not been investigated in much detail.</p>	<ul style="list-style-type: none"> • Although the traditional WAsP Park model is recommended for small wind farms with extensions up to 3 km, the Wake-Park BL model can be used for very large wind farms with many rows, so that the wake decay approaches its infinite value. • The model can be used and is recommended to use over flat and homogenous terrain only. It has been tested at offshore sites only. • Wind farms with regular arrays/layouts are recommended, although not mandatory. • For model evaluation, neutral stability wind farm data should be used. It over-predicts production under stable conditions and under-predicts under unstable conditions, so it is ideal for annual wake losses studies where the stability is close to neutral.
Work flow	
<p>You receive Fuga as a zip file. Just unzip it and run the graphical user interface (GUI) called fuga.exe. The first time it runs it will generate generic look-up tables which will be used to speed up all later calculations.</p> <p>Fuga is used together with WAsP and use is made of WAsP files containing wind farm layout, wind turbine data and wind climatology. The basic work flow is described in the help system of the GUI.</p>	<p>You receive the Wake-Park Boundary-Layer (BL) model as a zip file. Unzip it and run the graphical user interface (GUI) called WakeParkBLAdjustedPr.exe. A manual for the use of GUI is also given in the zip file (WakeParkBL-Adjusted-Manual.pdf). In addition to the normal input data that the standard WAsP Park-model needs, i.e. a wind turbine generator type (WTG) (in the zip file an example 'HornsRevTurb.wtg' is given), the program requires a .dat file with the coordinates of the turbines in the wind farm (the example HorsnRevAIllyout.dat is also given). The user should also input parameters such as latitude (approximate), surface roughness length and the dimensionless inter-turbine distances along and across the wind direction S_r and S_f (scaled by rotor diameter). The ratio between S_f and S_r is only required approximately, but the product should represent the average horizontal area per turbine.</p>

Fuga	Wake-Park Boundary-Layer (BL) model
Validation	
<p>Ott (2011) also shows validations against production data from Horns Rev 1 and Nysted as well as a comparison with directly measured wind data from an onshore turbine (data from the Nibe experiment). The comparisons with data show substantial agreement. It should be noted that the model does not have any adjustable parameters and it is therefore not possible to tune it to data.</p> <p>Independent, and equally successful, validations of Fuga have been presented by Gribben (2011) on behalf of Carbon Trust. These validations include additional data from the North Hoyle wind farm and comparisons with wind data from met masts at Horns Rev 1.</p>	<p>The model has been validated against production and wind speed data from Horns Rev 1 and Nysted and some of the validation is shown by Rathmann et al. (2010). The comparisons show good agreement and substantial improvement compared to the traditional WASP Park model. It should be noted that the only adjustable parameters are the initial wake decay coefficient, where the WASP recommended values can be certainly used, and the relaxation constant which only gives the percentage of reduction of the wake decay towards its infinite value.</p>

Conclusions

The developed models will undergo further development, in relation to terrain, and stability, and more diverse wind turbine features, and it is finally planned that the models are integrated into the WASP program packet, and hence will be available for the users of the WASP program (Mortensen et al. 2007). Hereby also all the facilities in the WASP program will be available for the users of the new wake models as well.

The detailed developments for the two models described in this report, are published and for completeness, the publications are here presented in the two attachments

References

- Calaf, M., C. Meneveau, and J. Meyers, 2010: Large eddy simulations study of fully developed wind-turbine array boundary layers. *Physics of Fluids*, **22**, 015110.
- Frandsen, S., 1992: On the wind speed reduction in the center of large clusters of wind turbines. *J. Wind Eng. Ind. Aerodyn.*, **39**, 251–265.
- Frandsen, S., R. Barthelmie, S. Pryor, O. Rathmann, S. Larsen, J. Højstrup, and M. Thøgersen, 2006: Analytical modelling of wind speed deficit in large offshore wind farms. *Wind Energy*, **9**, 39–53.
- Gribben, B., 2011: Wake effects developments in the offshore wind accelerator. *AWEA Wind Resource Assessment Technology Workshop. Brussels, May 10–11*, URL <http://www.ewea.org/index.php?id=2102>.
- Jensen, N. O., 1983: A note on wind generator interaction. Tech. Rep. Risø-M-2411(EN), Risø National Laboratory, Roskilde, 16 pp.
- Katic, I., J. Højstrup, and N. O. Jensen, 1986: A simple model for cluster efficiency. *Proceedings of the European Wind Energy Association Conference & Exhibition, Rome*.
- Mortensen, N. G., D. N. Heathfield, L. Myllerup, L. Landberg, and O. Rathmann, 2007: Getting started with WAsP 9. Tech. Rep. Risø-I-2571(EN), Risø National Laboratory, Roskilde, Denmark, http://www.wasp.dk/Download/DownloadFiles/General/Getting_Started_with_WAsP_9.pdf.
- Ott, S. J. Bergh, and M. Nielsen ,2011:Linearised CFD models for wakes.Tech. Rep.Risø–R–1772(EN), <http://www.risoe.dk/rispubl/VEA/ris-R-1772.htm>.
- Peña, A, S. Ott, O.Rathmann, M. Nielsen, and S. Larsen (2011). Guidelines for the use of the wake models developed under the WindShadow project.
- Peña, A. and O. Rathmann (2011) The atmospheric stability dependent infinite wind farm and the wake decay constant. Submitted to Wind Energy, and attached as appendix to this report.
- Rathmann, O. S., S. Frandsen, and M. Nielsen, 2010: Wake decay constant for the infinite wind turbine array. *Proceedings of the European Wind Energy Association Conference & Exhibition, Warsaw*.
- Troen, I. and E. L. Petersen, 1989: European wind atlas. Tech. rep., Risø National Laboratory.

Risø DTU is the National Laboratory for Sustainable Energy. Our research focuses on development of energy technologies and systems with minimal effect on climate, and contributes to innovation, education and policy. Risø has large experimental facilities and interdisciplinary research environments, and includes the national centre for nuclear technologies.

Risø DTU
National Laboratory for Sustainable Energy
Technical University of Denmark

Frederiksborgvej 399
PO Box 49
DK-4000 Roskilde
Denmark
Phone +45 4677 4677
Fax +45 4677 5688

www.risoe.dtu.dk

The atmospheric stability dependent infinite wind farm and wake decay coefficient

Alfredo Peña* and Ole Rathmann

*aldi@risoe.dtu.dk

*Wind Energy Division,
Risø National Laboratory for Sustainable Energy,
Technical University of Denmark, Roskilde, DK*

October 5, 2011

Abstract

The infinite wind farm boundary-layer (IWFBL) model of Frandsen (Frandsen, 1992) is extended to take into account the atmospheric stability effect on the wind speed reduction using two approaches. These extended models are compared to the IWFBL model of Emeis (Emeis, 2010) and to two momentum-based wake models, the Park wake model used in WAsP and that of Jensen (Jensen, 1983), which are evaluated for an infinite wind farm and an infinite row of turbines, respectively. The models show similar behavior for the wind speed reduction when accounting for a number of surface roughness lengths, turbine to turbine separations and wind speeds under neutral conditions. For a wide range of atmospheric stability and surface roughness conditions, the two approaches of the extended IWFBL model of Frandsen show a much higher wind speed reduction dependency on the state of the atmosphere than on roughness length. We further adjust the wake decay coefficient of the Park wake model for an infinite wind farm to match the wind speed reduction estimated by both approaches of the extended IWFBL model of Frandsen for different roughness lengths, turbine to turbine distances and atmospheric stability conditions. For an infinite wind farm, it is found that the WAsP-recommended values for the wake decay coefficient of the Park wake model are too large compared to the adjusted values for a wide atmospheric stability range, a number of roughness lengths and turbine to turbine distances, except for smooth roughnesses both in combination with very unstable conditions and very short turbine separations.

Keywords: atmospheric stability, boundary-layer model, infinite wind farm, Park wake model, wake decay coefficient, wind speed reduction

1 Introduction

Most wind park wake (WPW) models are able to estimate wind speed reductions within the wind farm for a wide range of wind speeds, assuming neutral atmospheric conditions in most cases. These models, such as the Park wake model (Katic et al., 1986) implemented in the Wind Atlas Analysis and Application Program (WAsP) (Mortensen et al., 2007), predict well the energy yield losses due to wakes when analyzing long terms of meteorological (met) and wind farm data. This is partly because in a long term, the atmospheric stability conditions are close to neutral. According to Troen and Petersen (1989), the long-term atmospheric stability is just little biased to the stable side over land and to the unstable side over water from the analysis of met stations over Northern Europe.

When analyzing wind farm and met data from the Horns Rev I wind farm in the Danish North Sea, Jensen (2007) estimated that the annual mean array efficiency reduces from 91.5%

under unstable to 85.3% under stable atmospheric conditions. For the Nysted wind farm in the Danish Baltic Sea, Barthelmie and Jensen (2010) also estimated wind farm efficiency reductions from unstable to stable atmospheric conditions, but up to $\sim 9\%$ for the wind speed range 9–10 m s^{-1} . Since wind farm operators do not want to know the annual energy production of the wind farm only, but would also like to forecast the wind farm energy output for a given set of meteorological conditions, which can rapidly change as shown in Vincent et al. (2010), we need to be able to run the WPW models for different meteorological conditions, which include the state of the atmosphere.

Inclusion of the atmospheric stability dependency in the WPW models is not straightforward. Therefore, an alternative is to simply adjust the parameters in the models to match the observed/measured data. Barthelmie and Jensen (2010) found better agreement when comparing the Park wake model to the Nysted wind farm data using a lower wake decay coefficient (0.03) than that recommended in WAsP for offshore conditions (0.05). Interestingly, the amount of stable atmospheric conditions are relatively large at Nysted (Barthelmie and Jensen, 2010) compared to those in the North Sea (Sathe et al., 2011), implying that the more stable the atmosphere, the lower the wake decay coefficient for the Park wake model.

In this article, we adjust the wake decay coefficient of the Park wake model, evaluated for an infinite array of wind turbines, to match the wind speed reduction estimated by the infinite wind farm boundary-layer (IWFBL) model of Frandsen (Frandsen, 1992). The adjustment can be carried out for different wind speeds, turbine to turbine separations, surface roughness lengths and atmospheric stability conditions. Since Frandsen developed his model for neutral conditions only, we extend it for diabatic atmospheric conditions in a similar fashion as that applied by Emeis (Emeis, 2010), who extended the IWFBL model of Emeis and Frandsen (E&F) (Emeis and Frandsen, 1993), and in a somehow more consistent way that uses atmospheric stability corrections to the logarithmic wind profile and geostrophic wind. In the description of the model by Frandsen and its extension, we compare it to the results for the wind speed reduction of an infinite array of turbines of the IWFBL model of E&F, the momentum-based Park wake model and the simple wake model of Jensen (Jensen, 1983). We also show the differences between the recommended, the semi-empirical and the IWFBL-adjusted wake decay coefficients.

2 Momentum wake model for the infinite row of turbines

Jensen (Jensen, 1983) devised a momentum wake model, which estimates the wind speed reduction of an infinite row of turbines (hereafter IRT model). Assuming conservation of momentum in the wake and using the superposition principle on the wakes he found¹,

$$\frac{u_\infty}{u_{free}} = 1 - \left(\frac{a}{1-a} \right) \left(\frac{f}{1-f} \right); \quad f = (1-a) \left[\frac{1}{1+k_w(x/r_o)} \right]^2, \quad (1)$$

where u_{free} is the upstream undisturbed wind speed, u_∞ the wind speed at the last turbine in the infinite row, a the induction factor, k_w the momentum entrainment or wake decay coefficient, x the turbine to turbine distance along the row and r_o the initial wake radius behind a rotor.

Jensen (1983) did not explicitly state that r_o should be taken as the rotor radius r_r , but his paper contains indications of this. Also, when Jensen’s model was implemented in the Park model, $r_o = r_r$ was assumed. Here, we choose to follow the more realistic approach of Frandsen (1992), who used Jensen’s model with $r_o = r_1$, where r_1 is the radius of the Betz stream tube at a short distance downstream of the rotor, related to the rotor radius by $r_1 = r_r \sqrt{(1-a/2)/(1-a)}$ (Figure 1 shows the momentum wake model of Jensen for a single wake where the first wake-affected turbine faces u_1 ; in the infinite row the last turbine faces u_∞).

The ratio u_∞/u_{free} in Eq. (1) depends on wind speed, since $a = 1 - \sqrt{1-C_t}$, being C_t the turbine’s thrust coefficient, and on the surface roughness length z_o and turbine’s hub height h , since $k_w \approx 0.5/\ln(h/z_o)$. Although this approximation for k_w was given by Frandsen (1992) by semi-empirical means, it suggests that k_w is related to the flow characteristics because $0.5/\ln(h/z_o) \approx$

¹In the original derivation of Jensen (1983), he assumed $a = 2/3$, which corresponds to the value for maximum power extraction; here we show the general expression for u_∞/u_{free}

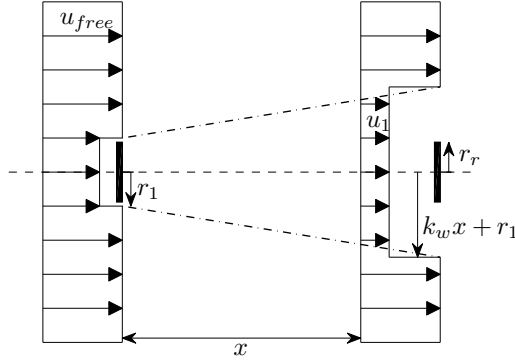


Figure 1: Momentum wake model concept by Jensen (Jensen, 1983)

u_{*free}/u_{hfree} , where u_{*free} is the undisturbed friction velocity and u_{hfree} —the undisturbed hub-height wind speed—is equal to $(u_{*free}/\kappa) \ln(h/z_o)$ under neutral stability conditions, with κ as the von Kármán constant (≈ 0.4).

3 Infinite wind farm boundary-layer (IWFBL) models

3.1 Review

The IWFBL model of Frandsen (Frandsen, 1992) assumes that within an infinite wind farm with the same turbine type and dimensions, two layers in the atmospheric boundary layer are distinguished, one above and one below h as shown in Figure 2. At h , the shear of both layers is linked as,

$$\rho u_{*2}^2 = \rho u_{*1}^2 + t, \quad (2)$$

where u_{*2} and u_{*1} are the friction velocities within the above and below layers, respectively, and t is the jump in shear due to the turbines. The latter is given as $t = \rho c_t u_h^2$, ρ being the air density, u_h the hub-height spatial average wind speed within the wind farm and c_t the areal homogeneously distributed thrust coefficient,

$$c_t = \frac{\pi}{8} \frac{C_t}{s_r s_f}, \quad (3)$$

where $s_r = x/D_r$ and $s_f = y/D_r$, y being the cross-wind turbine-turbine distance and D_r the rotor diameter.

Since the idea is to derive an expression for u_h using Eq. (2), Frandsen (1992) applied the logarithmic wind profile to estimate u_{*1} and u_{*2} at hub height from the true (z_o) and the effective (z_{oo}) wind farm roughness lengths, respectively

$$u_{*1} = \frac{u_h \kappa}{\ln(h/z_o)} \quad \text{and} \quad u_{*2} = \frac{u_h \kappa}{\ln(h/z_{oo})}. \quad (4)$$

Frandsen (1992) used a corrected version of the simplified geostrophic drag law of Jensen (1978),

$$u_* = \frac{\kappa G}{\ln\left(\frac{G}{f_p z_o}\right)}, \quad (5)$$

where G is the geostrophic wind speed and $f_p = f_c \exp(A_*)$, f_c being the Coriolis parameter and A_* a modified A -parameter from the resistant law constants, to estimate the effective roughness as a function of the velocity scales:

$$z_{oo} = \frac{G}{f_p} \exp\left(\frac{-\kappa G}{u_{*2}}\right). \quad (6)$$

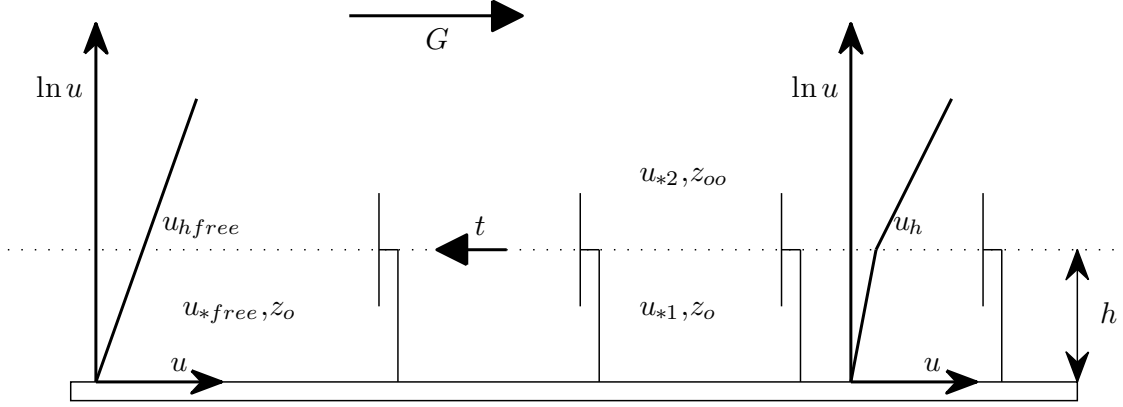


Figure 2: The infinite wind farm boundary-layer model concept of Frandsen (Frandsen, 1992)

Eq. (6) is then used to eliminate the z_{oo} dependency in u_{*2} in Eq. (4)-right, which results in

$$u_{*2} = \frac{\kappa (G - u_h)}{\ln\left(\frac{G}{hf_p}\right)}. \quad (7)$$

Defining $K_2 = (1/\kappa) \ln[G/(hf_p)]$ and $K_1 = (1/\kappa) \ln(h/z_o)$ and substituting u_{*1} and u_{*2} from Eqs. (4)-left and (7), respectively, into Eq. (2), the solution for u_h , i.e. the IWFBL model of Frandsen, is,

$$u_h = \frac{G}{1 + K_2 \sqrt{c_t + K_1^{-2}}}, \quad (8)$$

The wind speed reduction R_u for the IWFBL model of Frandsen is then given as,

$$R_u = \frac{1 + K_2 \sqrt{K_1^{-2}}}{1 + K_2 \sqrt{c_t + K_1^{-2}}}, \quad (9)$$

which is the ratio of u_h to the asymptotic overall mean wind speed at hub height, i.e. $u_h(c_t \neq 0)/u_h(c_t = 0)$.

E&F further developed another IWFBL model based on mixing-length theory and estimated R_u as,

$$R_u = \frac{1 + (\Delta z/l) \sqrt{c_s}}{1 + (\Delta z/l) \sqrt{c_{teff}}}, \quad (10)$$

where $c_s = K_1^{-2}$, $c_{teff} = c_t + c_s$, l is the mixing length and Δz the height interval between the turbines and the undisturbed flow. When comparing Eqs. (17) and (10), it can easily be demonstrated that they are identical if $\Delta z/l = K_2$. So, one of their main differences is that the IWFBL model of Frandsen depends on $u_{h,free}$ through both G (through K_2) and C_t (which for a wind turbine varies with wind speed), whereas the IWFBL model of E&F, Eq. (10), is only dependent on $u_{h,free}$ through C_t provided that l is wind speed independent.

For neutral atmospheric conditions, E&F suggested $\Delta z/l \approx 2/\kappa$, which in terms of the IWFBL model of Frandsen means $\ln[G/(hf_p)] \approx 2$. Such approximation for a place in rural Denmark ($z_o = 0.025$ m) or in the Danish North Sea ($z_o = 0.0002$ m), both assuming $h = 70$ m, $u_{h,free} = 10$ m s⁻¹ and $A_* = 4.53$, is rather low, since $\ln[G/(hf_p)] = 3.54$ and 2.73 , respectively². Therefore, R_u is generally lower for the IWFBL model of Frandsen than that for E&F. This, as shown later, is valid for a range of wind speeds and atmospheric stability conditions.

² G is estimated from the simplified geostrophic drag law, Eq. (5), and related to $u_{h,free}$ through the logarithmic wind profile similarly to Eq. (4)

The main “drawbacks” of the IWFBL model of E&F are that 1) Δz is rather difficult to estimate and 2) the mixing-length concept might be inappropriate when modeling wakes (Rethoré, 2009). The approach by Frandsen also has drawbacks related to 1) the assumption that at some level above the hub height the wind farm wind speed approaches the geostrophic wind speed value and 2) the value of A_* , since as a modified A -parameter of the geostrophic drag law, it depends on atmospheric stability among others (Zilitinkevich, 1975).

Figure 3 shows the wind speed reduction comparison between the IRT model and the IWFBL model of Frandsen for different turbine to turbine separations, s , and roughness lengths³. Unless otherwise stated, k_w is evaluated as $u_{*free}/u_{hfree} = \kappa/\ln(h/z_o)$.

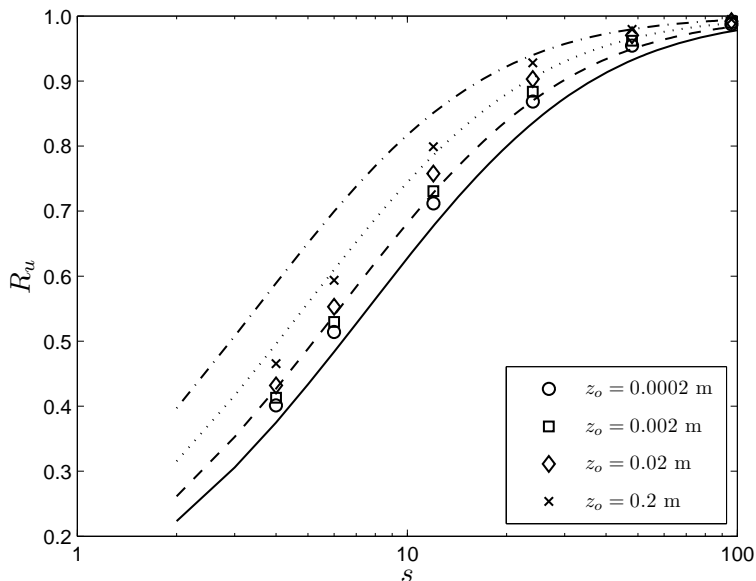


Figure 3: Wind speed reduction comparison between the IRT model of Jensen (Jensen, 1983) ($z_o = 0.0002$ m—solid, $z_o = 0.002$ m—dashed, $z_o = 0.02$ m—dotted and $z_o = 0.2$ m—dash-dotted lines) and the IWFBL model of Frandsen (Frandsen, 1992) (markers) for different dimensionless turbine-turbine separations and surface roughnesses. $C_t = 0.88$, $h = 70$ m, $u_{hfree} = 10$ m s⁻¹, $A_* = 4.53$ and latitude about Denmark

The two models show the same behavior and rather similar wind speed reductions for a wide range of z_o and s values; the larger the turbine to turbine distance and the larger the roughness, the lower the wind speed reduction. Figure 4 is similar to Figure 3, but for an offshore site only (where wind farms might become close to “infinite”) and includes the IWFBL model of E&F in the comparison. As mentioned, the values for R_u from the IWFBL model of E&F are larger than those from the approach by Frandsen, which shows similar results to the IRT model. Interestingly, the dependency on z_o of R_u is larger for the IRT model compared to the IWFBL models, although in the IRT model z_o is accounted for through the value of k_w only.

The previous comparisons are based on a fixed undisturbed hub-height wind speed and thus on a fixed C_t value. Figure 5 shows a similar comparison to that on Figure 4, but for a fixed turbine to turbine separation and different undisturbed hub-height wind speeds, which translate into a range of C_t values. For the analysis, we chose a C_t curve close to a MW wind turbine.

As illustrated, the IRT model results are close to those of the IWFBL model of Frandsen within the wind speed range 7–10 m s⁻¹ and to those of E&F within 11–14 m s⁻¹. Within the range 3–10 m s⁻¹, the IRT model and the IWFBL model of E&F do not largely vary because the C_t values are nearly constant. For all models and above ~ 10 m s⁻¹, R_u increases the higher the wind speed because of the reduction on C_t . R_u by Frandsen increases within the low wind speed range because of the relatively high weight of G in Eq. (17) (through K_2).

³for simplicity it is hereafter always assumed that $s_r = s_f = s$

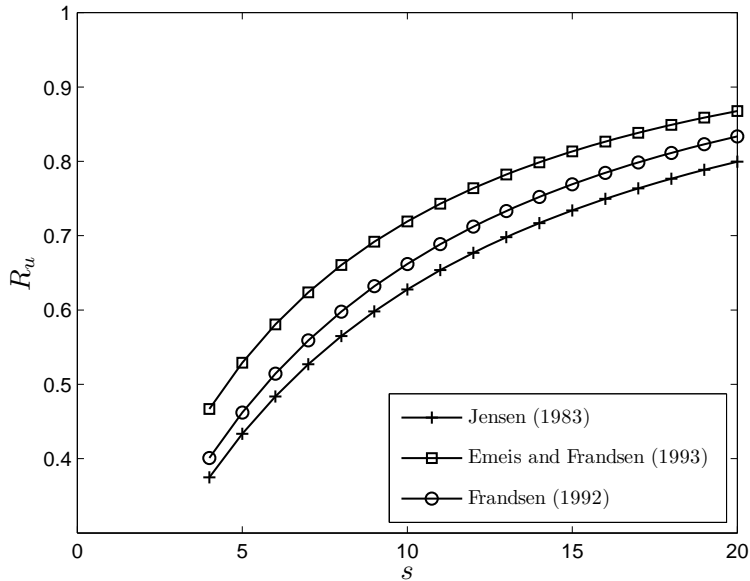


Figure 4: Wind speed reduction comparison between the IRT model of Jensen (Jensen, 1983) and the IWFBL models of Frandsen (Frandsen, 1992) and E&F (Emeis and Frandsen, 1993) for different dimensionless turbine-turbine separations. $C_t = 0.88$, $h = 70$ m, $u_{hfree} = 10$ m s⁻¹, $z_o = 0.0002$ m, $A_* = 4.53$ and latitude about Denmark

3.2 Stability dependency

We study two approaches to account for the effect of atmospheric stability in the IWFBL model of Frandsen; the first (hereafter known as version 1) is based on the approach developed by Emeis (2010) and the second (hereafter known as version 2) is based on the extension of the logarithmic wind profile and geostrophic wind to account for diabatic conditions.

3.2.1 Version 1

Emeis (Emeis, 2010) extended the IWFBL model of E&F to account for diabatic atmospheric stability conditions. Since R_u is a function of l in Eq. (10), it is rather simple to extend l for diabatic conditions using Monin-Obukhov similarity theory (MOST) (Monin and Obukhov, 1954), i.e. adding the dimensionless wind shear ϕ_m , which is a function of z/L , where z is the height above surface and L the Obukhov length.

This can be done in several ways and Emeis tried different forms including $l = \kappa z \phi_m^{-1}$, which was proven to be valid for the surface layer when compared to turbulence measurements and spectra (Peña et al., 2010b). Since $\Delta z/l$ and K_2 are equivalents, we can also extend Eqs. (8) and (17) using $\phi_m(h/L)$. Further, as Emeis did it for c_s , K_1 has to be extended for stability conditions by means of the stability correction of the logarithmic wind profile ψ_m , which comes from the integration of ϕ_m , so ψ_m is also a function of z/L . u_h and R_u for the extended IWFBL model (version 1) of Frandsen become, respectively,

$$u_h = \frac{G}{1 + \phi_m(h/L)K_2\sqrt{c_t + K_1^{-2}}} \quad (11)$$

and

$$R_u = \frac{1 + \phi_m(h/L)K_2\sqrt{K_1^{-2}}}{1 + \phi_m(h/L)K_2\sqrt{c_t + K_1^{-2}}}, \quad (12)$$

with $K_1 = (1/\kappa) [\ln(h/z_o) - \psi_m(h/L)]$.

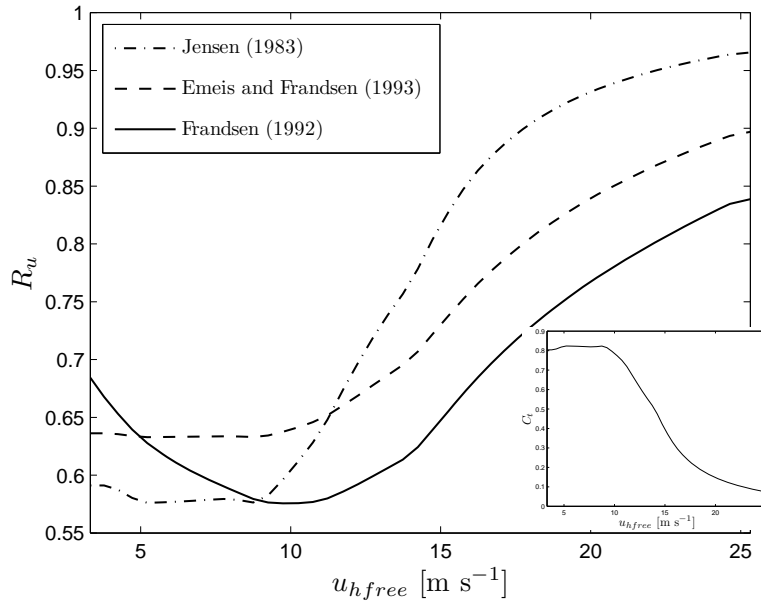


Figure 5: As Figure 4, but for a fixed dimensionless turbine-turbine separation $s = 7$ and a range of undisturbed hub-height wind speeds. The C_t curve is illustrated at the right bottom. $h = 70$ m, $A_* = 4.53$, $z_o = 0.0002$ m and latitude about Denmark

However, there is an inconsistency with this approach. u_h from Eq. (11) should equal $u_{h,free}$ when $c_t = 0$. They are indeed equal under neutral conditions because $\phi_m = 1$ and $\psi_m = 0$ for $h/L = 0$. When $h/L \neq 0$, on the other hand, $u_h(c_t = 0)$ from Eq. (11) becomes h -dependent and does not approach the $u_{h,free}$ value. Also, K_2 , which depends on the ratio G/f_p , should be stability dependent because both G and f_p in reality are. In this version of the extension, nevertheless, they are estimated using a constant A_* value (4.53).

3.2.2 Version 2

Another way to extend the IWFBL model of Frandsen is by including the stability correction function (ψ_m) to the logarithmic wind profiles within the two layers in Eq. (4), so that within the wind farm and at hub height,

$$u_{*1} = \frac{u_h \kappa}{\ln(h/z_o) - \psi_m(h/L)} \quad (13)$$

and

$$u_{*2} = \frac{u_h \kappa}{\ln(h/z_{oo}) - \psi_m(h/L)}. \quad (14)$$

One can work out the derivation of u_h , in a similar way as that explained in Section 3.1 (see steps between Eqs. (5)–(7)), and will find that K_1 needs to be extended as in “version 1”, i.e. $K_1 = (1/\kappa) [\ln(h/z_o) - \psi_m(h/L)]$ and that K_2 is also extended with ψ_m instead of ϕ_m , i.e. $K_2 = (1/\kappa) [\ln[G/(hf_p)] + \psi_m(h/L)]$. The expressions for u_h and R_u are then formally the same as those in Eqs. (8) and (17), also valid for neutral conditions.

However, G and f_p in the above expression for K_2 are also functions of atmospheric stability due to the stability dependency of the geostrophic drag law. This dependency is classically described by extending the resistance law parameters A and B to be functions of the dimensionless stability parameter $\mu_o = \kappa u_* / (f_c L)$. Despite disagreement among researchers on the forms of $A(\mu_o)$ and $B(\mu_o)$, due to the variety of data used in the different studies and their high uncertainty, it is possible to get empirical formulations for both (Jensen et al., 1984). On this basis, the dependency of A_* on atmospheric stability, $A_*(\mu_o)$ can be derived (see Appendix A for details).

For a given $u_{h,free}$ value and stability condition (a L -value at a given height), G can then iteratively be estimated using the simplified geostrophic drag law, Eq. (5) (now including the

above $A_*(\mu_o)$ stability dependence), and the upstream-undisturbed friction velocity u_{*free} derived from the diabatic wind profile,

$$u_{*free} = \frac{u_{hfree}\kappa}{\ln(h/z_o) - \psi_m(h/L)}. \quad (15)$$

Now, it is important to notice that in the non-neutral cases K_2 depends on u_* through A_* ,

$$K_2(u_*) = \frac{1}{\kappa} \left[\ln \left(\frac{G}{hf_c} \right) - A_*(\mu_o) + \psi_m(h/L) \right]. \quad (16)$$

Thus, R_u in Eq. (17) must be modified as,

$$R_u = \frac{1 + K_2(u_{*free})\sqrt{K_1^{-2}}}{1 + K_2(u_{*2})\sqrt{c_t + K_1^{-2}}}, \quad (17)$$

where u_{*2} is found iteratively from the stability-dependent simplified geostrophic drag law, but using the expression for z_{oo} for non-neutral conditions (see Appendix B for its derivation)

$$z_{oo} = h \exp \left[\frac{-\kappa}{\sqrt{c_t + K_1^{-2}}} - \psi_m(h/L) \right]. \quad (18)$$

This procedure ensures that Eq. (8) evaluated for $c_t = 0$ gives u_{hfree} .

3.2.3 Comparison

Figure 6 shows R_u given by both versions of the extended IWFBL model of Frandsen for a range of dimensionless atmospheric stabilities h/L , a number of roughness lengths and a fixed dimensionless turbine to turbine distance. For version 1 and for the range of atmospheric stabilities, R_u always increases with high roughness length values (similarly to Figure 3). The striking result is that the variation of R_u is much higher for this broad range of atmospheric stabilities than for the rather wide range of roughness lengths, with low and high wind speed reductions under unstable and stable atmospheric conditions, respectively.

The result for version 2 follows the behavior of that of version 1 for unstable conditions and near-stable conditions. However, at a given positive value of h/L (dependent on the given z_o value), R_u starts to increase with increasing stable conditions. This is because the reference height for wind speed u_{hfree} is simply too high ($h = 70$ m) compared to the boundary-layer height (BLH) that can indeed be below 50–70 m in stable and very stable conditions. MOST (strictly valid for $\sim 10\%$ of the BLH only) then predicts a too high stability correction when estimating u_{*free} , which is used for computing G in a range where the stability corrections to the geostrophic and simplified geostrophic drag laws are less applicable (ψ_m is more than four times higher for $h/L = 1.5$ than for $h/L = -1.5$). This can also be seen when comparing the behavior of the geostrophic wind speed with stability (Figure 7). There, G is normalized by a reference wind speed u_{ref} , which is taken equal to u_{hfree} and it is observed that assuming A_* to be constant, although u_{*free} is corrected for stability (as in version 1), G/u_{ref} decreases with increasing stable conditions. For version 2, G/u_{ref} increases up to a given positive μ_o value, where it starts to decrease. That μ_o value is related to the h/L range where R_u changes slope and later increases in Figure 6.

A way to avoid this is by using a reference wind speed, not at hub height but at a height well inside the surface boundary layer, where MOST is well applicable. Figure 8 shows the results for the wind speed reduction and normalized geostrophic wind using a reference wind speed at 10 m. In this case, both versions of the extension give the same wind speed reduction for neutral conditions and version 1 seems to be a “more conservative” approach, since the R_u variation from the neutral values is lower than that of version 2. However, we will continue using $h = 70$ m as the height for u_{ref} , because in most wind farms such reference wind speed is taken at hub height (the nacelle wind speed).

We can also compare the results for the model of Emeis, i.e. the atmospheric stability extended IWFBL model of E&F, and both versions of the extended IWFBL model of Frandsen for different

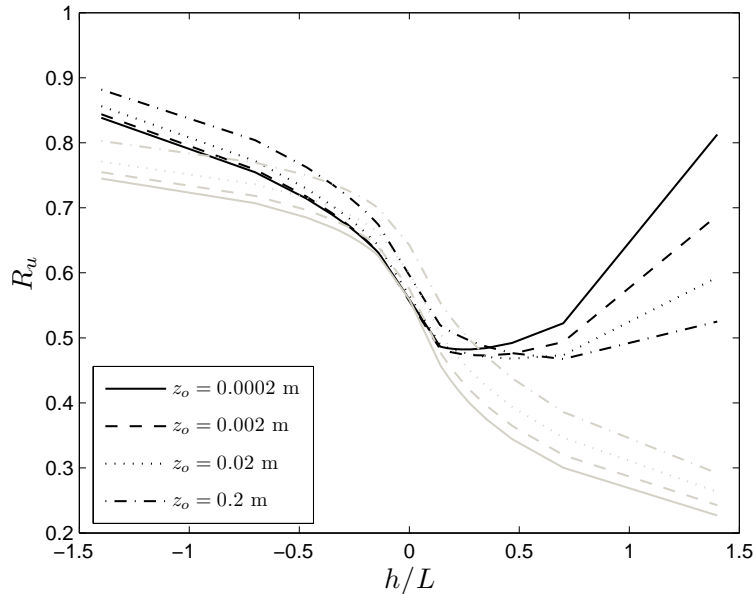


Figure 6: Wind speed reduction for both versions of the extended IWFB model of Frandsen for a range of dimensionless atmospheric stabilities, a number of surface roughnesses and a fixed dimensionless turbine-turbine distance $s = 7$ (versions 1 and 2 in light gray and black colors, respectively). $C_t = 0.88$, $h = 70$ m, $u_{hfree} = 10$ m s⁻¹, $A_* = 4.53$ (for version 1) and latitude about Denmark

atmospheric stability conditions and dimensionless turbine to turbine separations. This is illustrated in Figure 9 for an offshore site, where the models have the same behavior with separation distances and atmospheric stability. Versions 1 and 2 are identical for neutral conditions ($L = \infty$), whereas for version 2 R_u for stable conditions is close to that for neutral conditions and for version 1 R_u shows the lowest values. R_u for version 1 is systematically lower than that for the model of Emeis.

3.3 Wind profiles

For both versions of the extension of Frandsen’s IWFB model, u_{*free} is corrected for stability conditions as in Eq. (15) and required for the estimation of G (assuming a “neutral” constant A_* -value for version 1 and a stability corrected one for version 2), so that R_u and the spatial average wind profiles within the wind farm can be computed using Eqs. (13) and (14). Both versions of the extension can also use the expression for z_{oo} in Eq. (18), because this is neither dependent on G nor on K_2 .

The spatial average wind profiles within the wind farm then become,

$$u(z \leq h) = \frac{u_{*1}}{\kappa} \left[\ln \left(\frac{z}{z_o} \right) - \psi_m \left(\frac{z}{L} \right) \right] \quad (19)$$

and

$$u(z \geq h) = \frac{u_{*2}}{\kappa} \left[\ln \left(\frac{z}{z_{oo}} \right) - \psi_m \left(\frac{z}{L} \right) \right]. \quad (20)$$

Figure 10 illustrates wind profiles within an offshore wind farm for different dimensionless turbine to turbine separations, atmospheric stability conditions and for both versions of the extension. Except for $s = \infty$, a kink in the wind profile is distinguished at hub height ($h = 70$ m), as expected. It is interesting to note that all these wind profiles are computed using $u_{hfree} = 10$ m s⁻¹, which is equal to the estimation of u_h for both versions under neutral conditions and $s = \infty$ ($c_t = 0$), whereas for version 1 and $s = \infty$, $u_h < u_{hfree}$ for stable and unstable conditions, respectively.

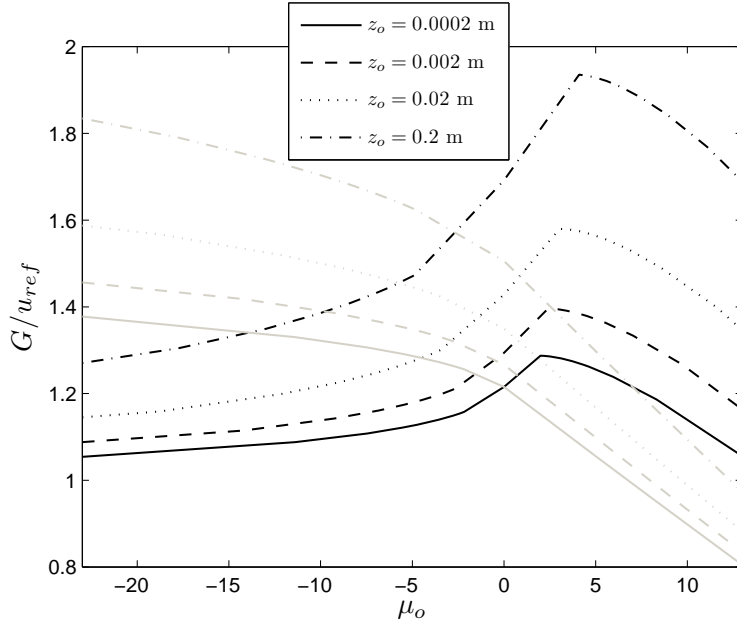


Figure 7: Normalized geostrophic wind speed for both versions of the extended IWFBL model of Frandsen for a range of dimensionless stabilities, a number of surface roughnesses and a fixed dimensionless turbine-turbine distance $s = 7$ (versions 1 and 2 in light gray and black colors, respectively). $C_t = 0.88$, $h = 70$ m, $u_{hfree} = u_{ref} = 10$ m s⁻¹, $A_* = 4.53$ (for version 1) and latitude about Denmark

This is due to the use of a constant “neutral” A_* value for the simplified geostrophic drag in version 1. For the value of R_u , this does not have a strong effect, since the wind speed reduction is computed based on $u_h(c_t = 0)$ not on u_{hfree} . For version 2, under all stability conditions and $s = \infty$, $u_h = u_{hfree}$. As illustrated, the two versions of the extension give the same wind profiles for neutral conditions. For the unstable and stable cases illustrated, the wind speeds of version 1 are lower than those of version 2, which is not always the case when using a reference wind speed at a height close to the surface.

It is important to notice that both layers (above and below h) are modeled using the approach of MOST. As h increases, e.g. with larger turbines, the above- h layer will be affected by the BLH and baroclinicity (among others) and the MOST approach is less valid. Also, the stable corrections from MOST predict very large wind shears for the above- h layer, which lead to wind speeds $u(s \neq 0)$ above the undisturbed ones $u(s = \infty)$ already at 200 m in Figure 10-bottom.

4 Infinite Park wake model

The Park wake model implemented in WAsP is based on the momentum wake model by Jensen (Figure 1), so the wind speed reduction is a function of k_w . The ground interaction of a wake is modeled by adding the wake reflected at the surface, i.e. a wake seemingly originating from a reflected “underground rotor”. The surface interaction is then modeled by considering the combined effect of the direct and the reflected wakes. Further, the efficiency of the wind turbine cluster is estimated by combining the effect of four types of overlapping wakes (Katic et al., 1986):

1. From directly upwind rotors.
2. Reflected “underground rotors” directly upwind.
3. Shading rotors upwind, but left or right to the wind direction.
4. Reflected shading “underground rotors” upwind but left or right to the wind direction.

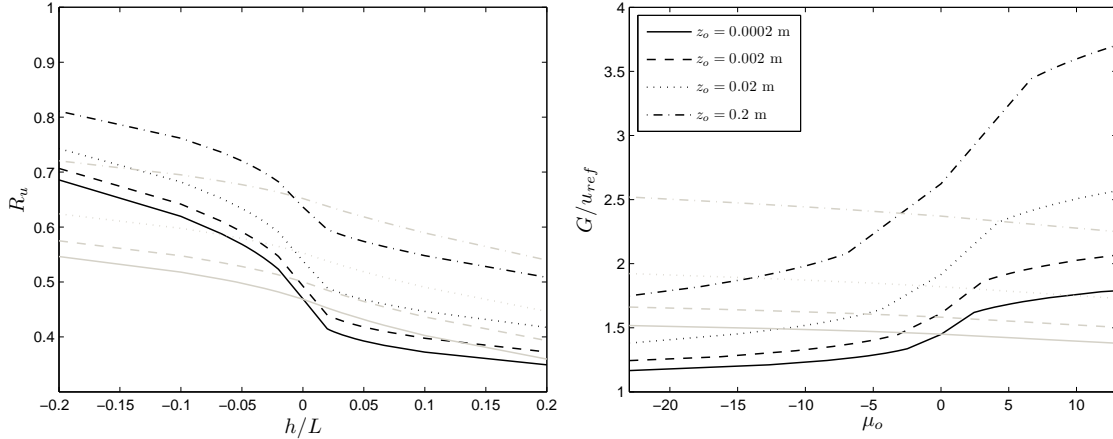


Figure 8: Left and right frames as in Figures 6 and 7, respectively, but for $h = 10$ m

The combined effect of two or more overlapping wakes on a downwind rotor was modeled through an empirical quadratic summation rule (Katic et al., 1986). Here, partial wake-overlap with a rotor is considered by applying the overlap fraction to the speed deficits of the individual wakes. Thus, the rotor diameter is required as an input to the model.

Rathmann et al. (2010) analytically solved the contribution of the four types of wakes (described above) for an asymptotically infinite number of wind turbines. This is described here as the “infinite Park wake model” (see Appendix C).

4.1 Adjusted wake decay coefficient for the infinite Park wake model

When using the Park wake model, the wake decay coefficient for the particular site is required. To a first approximation, it is common procedure to use $k_w = 0.050$ and $k_w = 0.075$ when performing wake analysis in WAsP over sea and land surfaces, respectively. However, k_w should be estimated for the particular z_o value and atmospheric stability condition of the site, since $k_w \approx u_{*free}/u_{hfree} = \kappa/[\ln(h/z_o) - \psi_m(h/L)]$, where the correction due to atmospheric stability is here already considered from that in Sections 2 and 3.

Figure 11 compares the wind speed reduction from the infinite Park wake (IPW) model when using $k_w = u_{*free}/u_{hfree}$, as above, to that from the IWFBM model by Frandsen for neutral conditions, different dimensionless turbine to turbine separations and a number of roughness lengths. The IPW model shows the same behavior as the IWFBM models, i.e. higher wind speed reductions the smoother the terrain and the shortest the turbine to turbine separations. Except for very short separations and low roughnesses, the IPW model shows lower wind speed reductions compared to the IWFBM model of Frandsen.

When the IPW model is matched to the IWFBM model of Frandsen to give the same wind speed reductions as those in Figure 11, k_w has to be adjusted, and thus, it becomes dependent not only on z_o , but on turbine separation as shown in Figure 12. The “adjusted” wake decay coefficients are generally much smaller than those normally used for wind energy calculations. In the range of turbine separations where most wind farms lie, i.e. s values between 5 – 9, k_w generally peaks the lowest, increasing for longer and shorter turbine separations and z_o values.

In a similar fashion, a constant turbine to turbine distance, e.g. $s = 7$, can be used to analyze the behavior of R_u for different atmospheric stability conditions and roughness lengths. This is illustrated in Figure 13. The wind speed reductions for the IPW model using $k_w = u_{*free}/u_{hfree}$ are generally lower than those for both versions of the extended IWFBM model by Frandsen, except for very unstable conditions and low roughness lengths. For version 2 it is observed an increase of R_u at a given positive h/L value because, as mentioned earlier, the reference wind speed is too high and MOST might be not longer valid. R_u does not vary with atmospheric stability in the IPW model as strongly (stability is accounted for through k_w only) as it does in both versions of the extended IWFBM model of Frandsen.

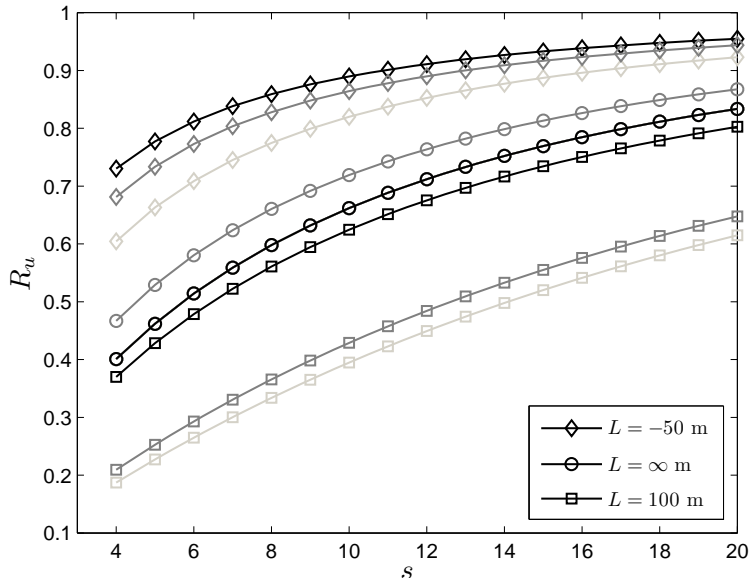


Figure 9: Comparison between the wind speed reduction from both versions of the extended IWFBL model by Frandsen (versions 1 and 2 in light gray and black colors, respectively) and the model by Emeis (Emeis, 2010) (dark grey) for different atmospheric stabilities and dimensionless turbine-turbine distances. $C_t = 0.88$, $h = 70$ m, $u_{hfree} = 10$ m s⁻¹, $A_* = 4.53$ (for version 1), $z_o = 0.0002$ m and latitude about Denmark

The correspondent adjusted wake decay coefficients, found when matching the wind speed reduction of the IPW model to that of both versions of the extended IWFBL model of Frandsen for the different atmospheric stability conditions in Figure 13, are illustrated in Figure 14. The behavior of k_w with stability when assuming $k_w = u_{*free}/u_{hfree}$ is similar to that found with the adjusted wake decay coefficients for all roughness lengths, i.e. a decrease of the wake decay coefficient the more stable the atmosphere, although the adjusted values (adjusted to both versions of the extended IWFBL model of Frandsen) tend to be much lower than the WASP-recommended ones, expect for very unstable conditions over smooth roughnesses. The increase of the adjusted k_w for version 2 is due to the increase in R_u at the same stable h/L range, which disappears when the reference undisturbed wind speed is taken at height within the surface boundary layer.

5 Discussion

In this paper, k_w in the Park wake model for the infinite wind farm is adjusted so that the model matches the value of the wind speed reduction of two versions of the extended IWFBL model of Frandsen. In a similar fashion, the adjustment can be performed using the IWFBL model of Emeis, which also shows that the WASP-recommended values for k_w are generally large except for a range of unstable conditions, with a more pronounced drop in k_w (compared to version 1) when the atmospheric conditions become stable as illustrated in Figure 14. Also the adjustment of k_w can be based on the IRT model by Jensen to match one of the IWFBL models. Here we choose the Park wake model because it considers (among others) the effect of adjacent turbines, is a commonly used model and the base of wind power calculations in WASP.

From our findings, we do not suggest to use the results for the wake decay coefficient when performing wind power calculations directly, since the analysis is performed based on the assumption of an infinite wind farm, and in reality only a couple of wind farms might be treated as such. An interesting approach was shown by Rathmann et al. (2010), in which after the k_w of the Park model is adjusted to the IWFBL model of Frandsen, the WASP-recommended k_w value is modified to approach the infinite k_w value for “deep” positions in the wind farm via a relaxation constant.

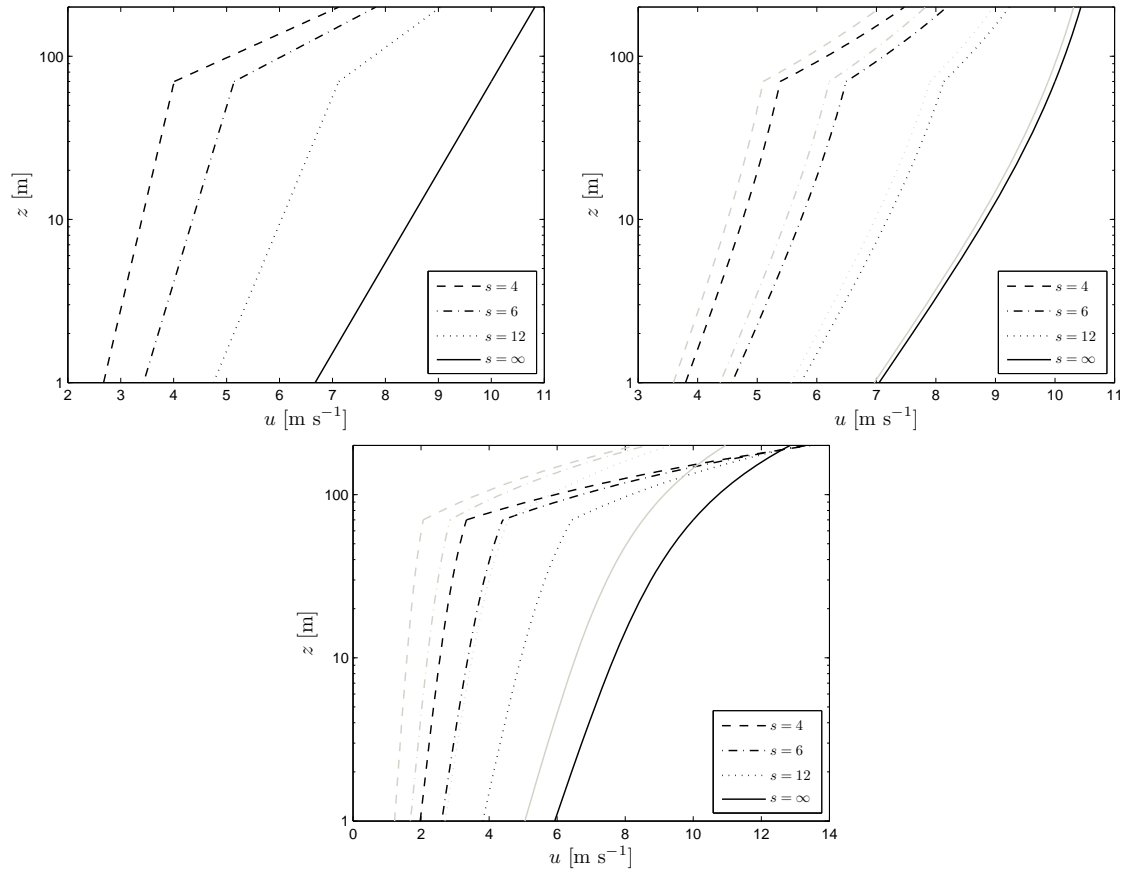


Figure 10: Spatial average wind profiles within an offshore wind farm ($z_o = 0.0002$ m) for a number of dimensionless turbine-turbine separations, atmospheric stabilities (top left: $L = \infty$ m–neutral, top right: $L = -200$ m–unstable, bottom: $L = 200$ m–stable) and for both versions of the extended IWFB model of Frandsen (versions 1 and 2 in light gray and black colors, respectively). $C_t = 0.88$, $h = 70$ m, $u_{h,free} = 10$ m s $^{-1}$, $A_* = 4.53$ (for version 1) and latitude about Denmark

Their approach agrees better than only assuming the WAsP-recommended values when compared to data from the Horns Rev and Nysted wind farms.

As wind turbines become larger, the IWFB models have to be extended to account for effects that are normally not considered for small-medium turbines, which are well inside the surface boundary layer, such as the BLH. As illustrated in Figure 10, particularly for stable conditions, the wind speed highly increases with height and the addition of the BLH as a wind profile parameter will damp such unrealistic growth, as shown in the wind profile models by Peña et al. (2008) over the sea, and Peña et al. (2010a) and Gryning et al. (2007) over land. Unfortunately, from our knowledge, there is still a lack of BLH data for wind energy purposes, which can be used for model comparison.

Frandsen (2007) attempted to compare theoretical wind farm efficiencies assuming that the change in roughness imposed by the infinite wind farm can be modeled as a smooth-to-rough generated internal boundary layer (IBL) to those derived from “traditional” IBL models such as that of Miyake (1965), also used in WAsP for natural roughness transitions, finding similar results for an infinite row of turbines. However, as shown in Floors et al. (2011), although the IBL models give good results for neutral atmospheric conditions, observations of the IBL height show a strong dependency on atmospheric stability, which is normally neglected in the IBL models because it is generally believed that the mechanical contribution dominates the IBL growth. Since from our results the efficiency of the wind farm strongly depends on atmospheric stability, the question arises on how the IBL models can be adjusted for wind farm efficiency analysis under different atmospheric conditions. Wind speeds within and downstream the wind farm are therefore needed

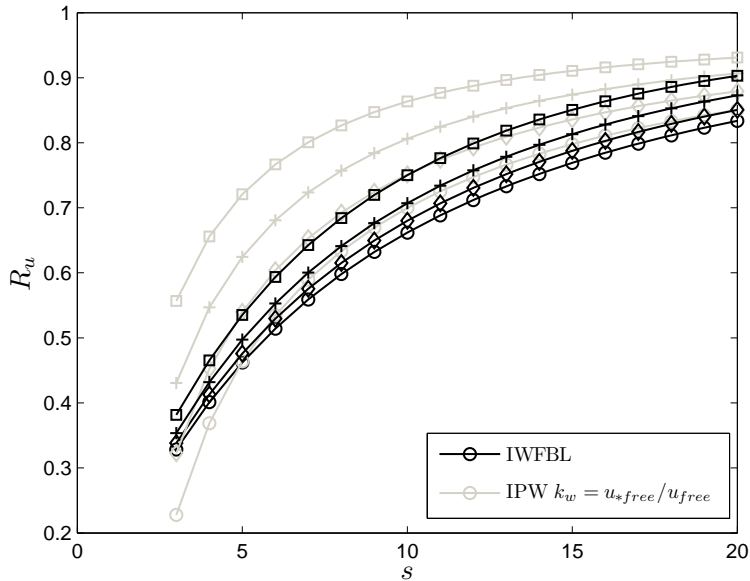


Figure 11: Comparison of the wind speed reduction between the IWFBL model of Frandsen (Frandsen, 1992) and the IPW model for neutral conditions, a number of z_o values ($\circ z_o = 0.0002$ m, $\diamond z_o = 0.002$ m, $+ z_o = 0.02$ m and $\square z_o = 0.2$ m) and dimensionless turbine-turbine separations. $h = 70$ m, $D_r = 80$ m, $A_* = 4.53$, $u_{hfree} = 10$ m s $^{-1}$ and latitude about Denmark

to validate, for example, how accurate Eq. (18) describes the wind farm characteristics by applying it to roughness models such as that in WAsP.

6 Conclusions

Two wake models based on conservation of momentum have been used to derive the wind speed reduction asymptotically reached by an infinite row of wind turbines, from the IRT model of Jensen, and by an infinite array of wind turbines, from the Park wake model, and compared to the wind speed reduction of two boundary-layer models for the infinite wind farm, those from Frandsen and E&F. All models show the same behavior for different dimensionless turbine to turbine separations and surface roughness lengths; the higher the roughness length and the longer the turbine separation, the lower the wind speed reduction. The IRT model shows very close wind speed reductions compared to those of the IWFBL model of Frandsen for neutral conditions, a range of roughness lengths and turbine separations assuming $k_w = u_{*free}/u_{hfree}$.

The IWFBL model of Frandsen has been extended to account for atmospheric stability conditions using two approaches and shows a similar behavior with stability when compared to the IWFBL model of Emeis (the stability extended model of E&F); the more stable the atmosphere, the higher the wind speed reduction, being the relative wind speed reduction due to stability much higher than that due to surface roughness lengths (a wide range of roughness lengths has been considered). For the range of stability conditions, the IWFBL model of Emeis estimates lower wind speed reductions than one of the versions for the extended model of Frandsen (version 1), i.e. u_h , the hub-height wind speed within the wind farm, is smaller for version 1 of the extended model of Frandsen. This is because the approach of Emeis implies $\Delta z/l = 2\phi_m/\kappa$, whereas from the geostrophic drag law approach by Frandsen $\Delta z/l > 2\phi_m/\kappa$. Compared to the other approach (version 2), the model by Emeis also estimates a lower wind speed reduction but for neutral conditions only.

The more consistent approach to the extension of the IWFBL model of Frandsen, version 2, shows that in order to get an increasing wind speed reduction when going from neutral to stable conditions, it is required that the inputs to the model (i.e. the reference wind speed and

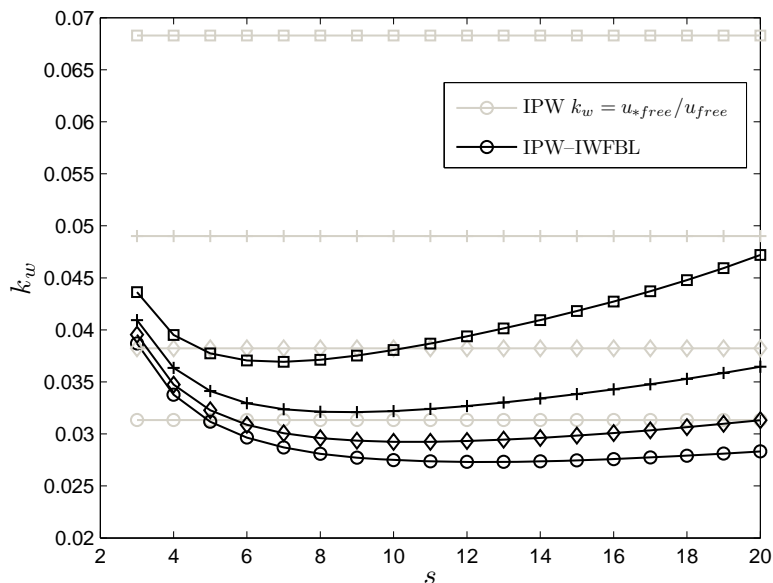


Figure 12: Variation of the wake decay coefficient assuming $k_w = u_{*free}/u_{free}$ and adjusted to match the IPW model to the IWFBL model by Frandsen (Frandsen, 1992) for neutral conditions, a number of z_o values (as in Figure 11) and dimensionless turbine-turbine separations. $h = 70$ m, $D_r = 80$ m, $A_* = 4.53$, $u_{hfree} = 10$ m s⁻¹ and latitude about Denmark

atmospheric stability) are given close to the surface where MOST is fully valid. This results in a good estimation of the stability-corrected undisturbed friction velocity, which in turn provides a well-behaved stability corrected geostrophic wind speed.

The IWFBL model by Frandsen is the only one of the four models that is dependent on wind speed not only through the C_t curve of the turbine, but because it is geostrophic wind speed dependent. Thus for a nearly constant C_t value, the wind speed reduction increases about 10% within the range 5–10 m s⁻¹. However, at this stage, it is difficult to judge the quality of the models, since the IWFBL models—for example—either assume, among others, a relation between the mixing length and the height where the wind is undisturbed or a relation between the geostrophic and the hub-height wind farm wind speed. Also, we do not validate the models against wind farm data, but we expect to do so in the near future.

Finally, and most importantly, we are able to calibrate the “more realistic” and more complex Park wake model to match the wind speed reduction of two versions of the extended IWFBL model of Frandsen for different wind speeds, roughnesses, turbine separations, turbine characteristics and atmospheric stability conditions by adjusting the value of the wake decay coefficient, considering an infinite array of wind turbines. Already for neutral conditions, the k_w values are generally much lower than those normally recommended by WAsP for wind power calculations for a number of surface roughness lengths. They are also strongly dependent on atmospheric stability, decreasing as the atmosphere becomes more stable, and lower than the WAsP-recommended values for a number of roughness lengths under unstable atmospheric conditions and much lower than those WAsP-recommended under stable atmospheric conditions.

Acknowledgements

This work could not be possible without the lifetime work efforts of the late Steen T. Frandsen. Funding from the Danish Public Service Obligation (PSO) to the “Windshadow” project, Energinet.dk 10086, is acknowledged. We would also like to thank Søren Ott from Risø DTU for the comments on the manuscript.

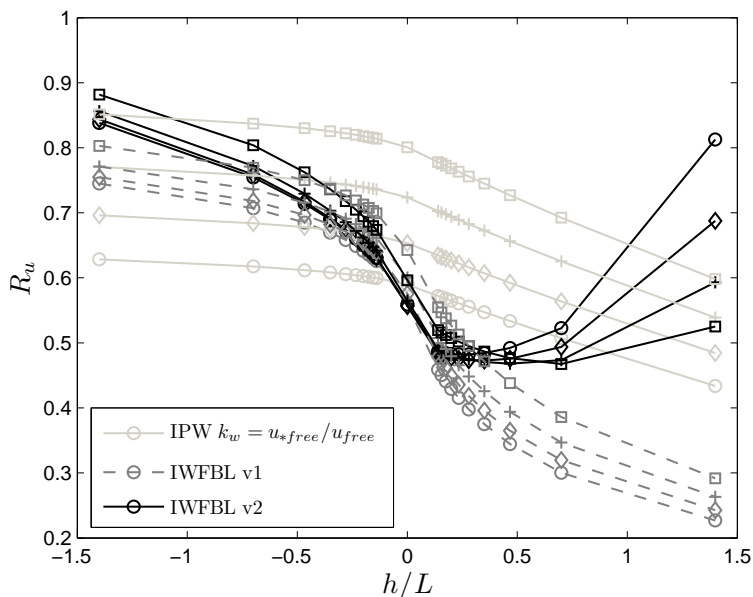


Figure 13: As in Figure 11 but for a range of dimensionless atmospheric stability conditions and a constant dimensionless turbine-turbine separation $s = 7$. $h = 70$ m, $D_r = 80$ m, $A_* = 4.53$ (for version 1), $u_{hfree} = 10$ m s⁻¹ and latitude about Denmark

Appendix A: Simplified geostrophic drag law dependency on atmospheric stability

The geostrophic drag law is given as

$$G = \frac{u_*}{\kappa} \left(\left[\ln \left(\frac{u_*}{f_c z_o} \right) - A(\mu_o) \right]^2 + B(\mu_o)^2 \right)^{1/2}, \quad (21)$$

where $A(\mu_o)$ and $B(\mu_o)$ depend on atmospheric stability since $\mu_o = \kappa u_*/(f_c L)$ (Zilitinkevich, 1975). Due to the scatter of the observations, there are numerous formulations for $A(\mu_o)$ and $B(\mu_o)$. We choose to use those of Jensen et al. (1984), but with the values for neutral conditions ($\mu_o = 0$) adjusted to match the recent results of Peña et al. (2010a) and in consistency with the values used for the European Wind Atlas (Troen and Petersen, 1989),

$$A(\mu_o \geq 0) = 1.7 - \mu_o^{1/2}, \quad (22)$$

$$A(\mu_o \leq 0) = 1.7 + \ln(1 - \mu_o), \quad (23)$$

$$B(\mu_o \geq 0) = 5 + \mu_o^{1/2}, \quad (24)$$

$$B(\mu_o \leq 0) = \frac{5 - \kappa}{1 - \mu_o/25} + \kappa. \quad (25)$$

In the original formulation of Jensen et al. (1984), $\mu_o = u_*/(f_c L)$. However, we choose to include κ in μ_o , as in Zilitinkevich (1975) and Long and Guffey (1977), because the points used by Jensen et al. (1984) to derive Eqs. (22)–(25) were taken from the study of the Wangara data by Clarke and Hess (1974), where $\mu_o = \kappa u_*/(f_c L)$.

For a range of dimensionless stabilities, G is computed from Eq. (21) using the forms in Eqs. (22)–(25). The result can then be used to estimate A_* from rearranging the simplified geostrophic drag law, Eq. (5),

$$A_* = \ln \left(\frac{G}{f_c z_o} \right) - \frac{\kappa G}{u_*}. \quad (26)$$

Figure 15 illustrates the results of such analysis, where an analytical form for $A_*(\mu_o)$ is also given.

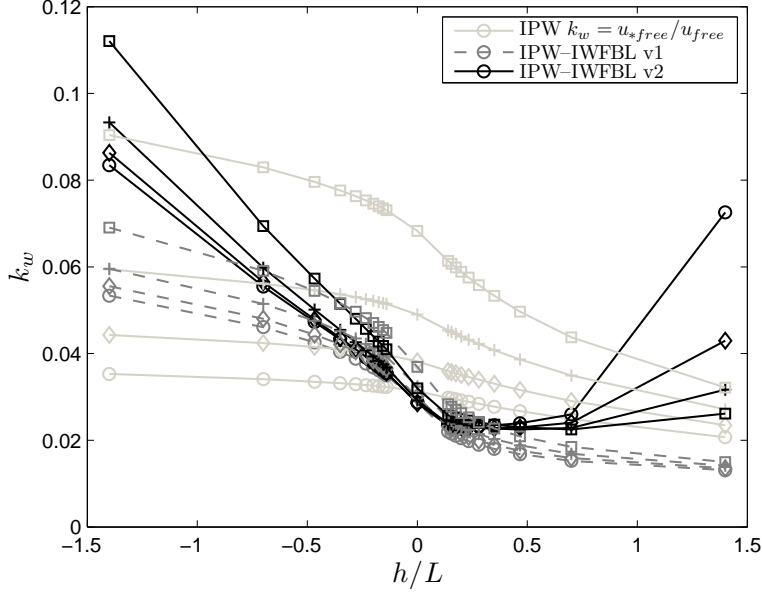


Figure 14: As in Figure 12 but for a range of dimensionless atmospheric stability conditions and a constant dimensionless turbine-turbine separation $s = 7$. $h = 70$ m, $D_r = 80$ m, $A_* = 4.53$ (for version 1), $u_{hfree} = 10$ m s⁻¹ and latitude about Denmark

Appendix B: Effective wind farm roughness length

From Eq. (14), one can easily derive

$$\ln\left(\frac{z_{oo}}{h}\right) = -\frac{\kappa u_h}{u_{*2}} - \psi_m(h/L), \quad (27)$$

where the ratio u_h/u_{*2} can be replaced by $1/\sqrt{(u_{*1}/u_h)^2 + c_t}$ from Eq. (2). Since $u_{*1}/u_h = K_1^{-1}$, Eq. (27) then reads as

$$\ln\left(\frac{z_{oo}}{h}\right) = -\frac{\kappa}{\sqrt{c_t + K_1^{-2}}} - \psi_m(h/L), \quad (28)$$

from which z_{oo} can be derived (Frandsen et al. (2006) deduced a similar form for neutral conditions only). It should be noted that the dependency on atmospheric stability of z_{oo} is only through $\psi_m(h/L)$ and K_1 which also depends on $\psi_m(h/L)$.

Appendix C: The infinite Park wake model

The total wake deficit $\delta_T = (1 - R_u)$ of the Park wake model implemented in WASP is estimated as the quadratic sum of four types of overlapping wakes,

$$\delta_T^2 = \delta_I^2 + \delta_{II}^2 + \delta_{III}^2 + \delta_{IV}^2. \quad (29)$$

The first term corresponds to the wakes directly upwind:

$$\delta_I^2 = \delta_o^2 \sum_{j=1}^{\infty} d_w(s_j)^{-4} = \delta_o^2 \sum_{j=1}^{\infty} (1 + 2k_w s_r j)^{-4}, \quad (30)$$

where δ_o is the initial wake deficit, $\delta_o = u_{hfree} (1 - \sqrt{1 - c_t})$, d_w is a dimensionless wake diameter, $d_w = D_w/D_r$, with D_w as the wake diameter, $D_w = D_r(1 + 2k_w s_r)$, and j is the number of rows upwind from the considered turbine.

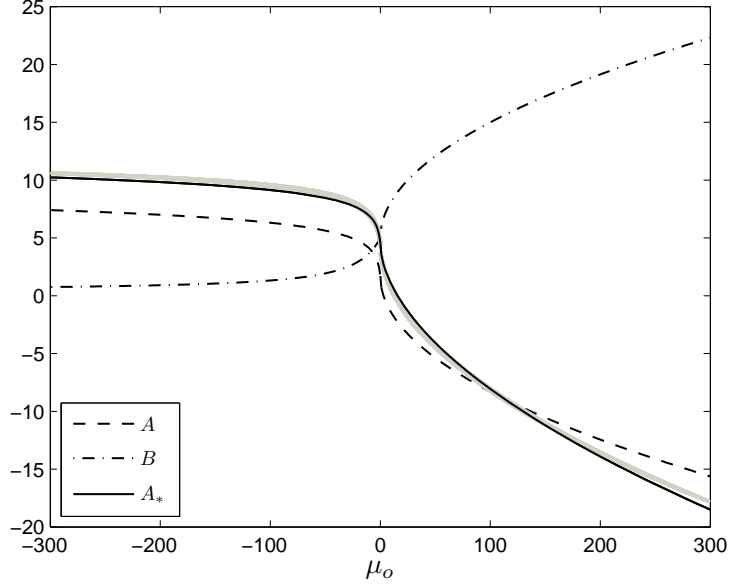


Figure 15: The dependency of the A , B and A_* parameters of the resistance laws on the dimensionless stability parameter μ_o . The gray points are the adjustment of A_* , Eq. (26), to match the geostrophic wind from Eq. (21). The solid line corresponds to the forms $A_*(\mu_o \geq 0) = 4.53 - \mu_o^{0.55}$ and $A_*(\mu_o \leq 0) = 4.53 + \ln(1 - \mu_o)$.

The second term corresponds to the reflected “underground rotors” directly upwind:

$$\delta_{II}^2 = \delta_o^2 \sum_{j=m_{II}}^{\infty} d_w(s_j)^{-4} = \delta_o^2 \sum_{j=m_{II}}^{\infty} (1 + 2k_w s_r j)^{-4}, \quad (31)$$

where m is the number of minimum rows to the first upwind row from where this type of wake has an effect on the considered turbine; in this case $m_{II} = (2h/D_r - 0.5)/(k_w s_r)$.

The third term corresponds to the shading rotors upwind, but left or right to the wind direction:

$$\delta_{III}^2 = \delta_o^2 \sum_{j=m_{III}}^{\infty} 2N_{III}(s_j) d_w(s_j)^{-4}, \quad (32)$$

where N_{III} is the number of turbines to the left and to the right of the wind direction that are able to throw their wake onto the considered turbine, $N_{III}(s_j) = d_w(s_j)/(2s_f)$, and $m_{III} = (s_f - 0.5)/(k_w s_r)$, so Eq. (32) becomes

$$\delta_{III}^2 = \delta_o^2 \sum_{j=m_{III}}^{\infty} \frac{d_w(s_j)}{s_f} d_w(s_j)^{-4} = \frac{\delta_o^2}{s_f} \sum_{j=m_{III}}^{\infty} (1 + 2k_w s_r j)^{-3}. \quad (33)$$

The four term corresponds to the reflected shading “underground rotors” upwind but left or right to the wind direction:

$$\delta_{IV}^2 = \delta_o^2 \sum_{j=m_{IV}}^{\infty} 2N_{IV}(s_j) d_w(s_j)^{-4}, \quad (34)$$

where $N_{IV}(s_j) = \sqrt{d_w(s_j)^2 - (4h/D_r)^2}/(2s_f)$ is the number of turbines to the left and to the right of the wind direction that are able to throw a reflected wake onto the considered turbine and $m_{IV} = (\sqrt{s_f^2 + (2h/D_r)^2} - 0.5)/(k_w s_r)$, so Eq. (34) becomes

$$\delta_{IV}^2 = \delta_o^2 \sum_{j=m_{IV}}^{\infty} \frac{\sqrt{d_w(s_j)^2 - (4h/D_r)^2}}{s_f} d_w(s_j)^{-4} = \frac{\delta_o^2}{s_f} \sum_{j=m_{IV}}^{\infty} \frac{\sqrt{(1 + 2k_w s_r j)^2 - (4h/D_r)^2}}{(1 + 2k_w s_r j)^4}. \quad (35)$$

The above infinite sums converge and can be approximated as

$$\delta_I^2 \approx \frac{\delta_o^2}{(1 + 2k_w s_r)^3} \left[\frac{1}{2(1 + 2k_w s_r)} + \frac{1}{6k_w s_r} \right], \quad (36)$$

$$\delta_{II}^2 \approx \frac{\delta_o^2}{128(h/D_r)^3} \left[\frac{1}{4(h/D_r)} + \frac{1}{3k_w s_r} \right], \quad (37)$$

$$\delta_{III}^2 \approx \frac{\delta_o^2}{16s_f^4} \left(1 + \frac{s_f/s_r}{k_w} \right), \quad \text{and} \quad (38)$$

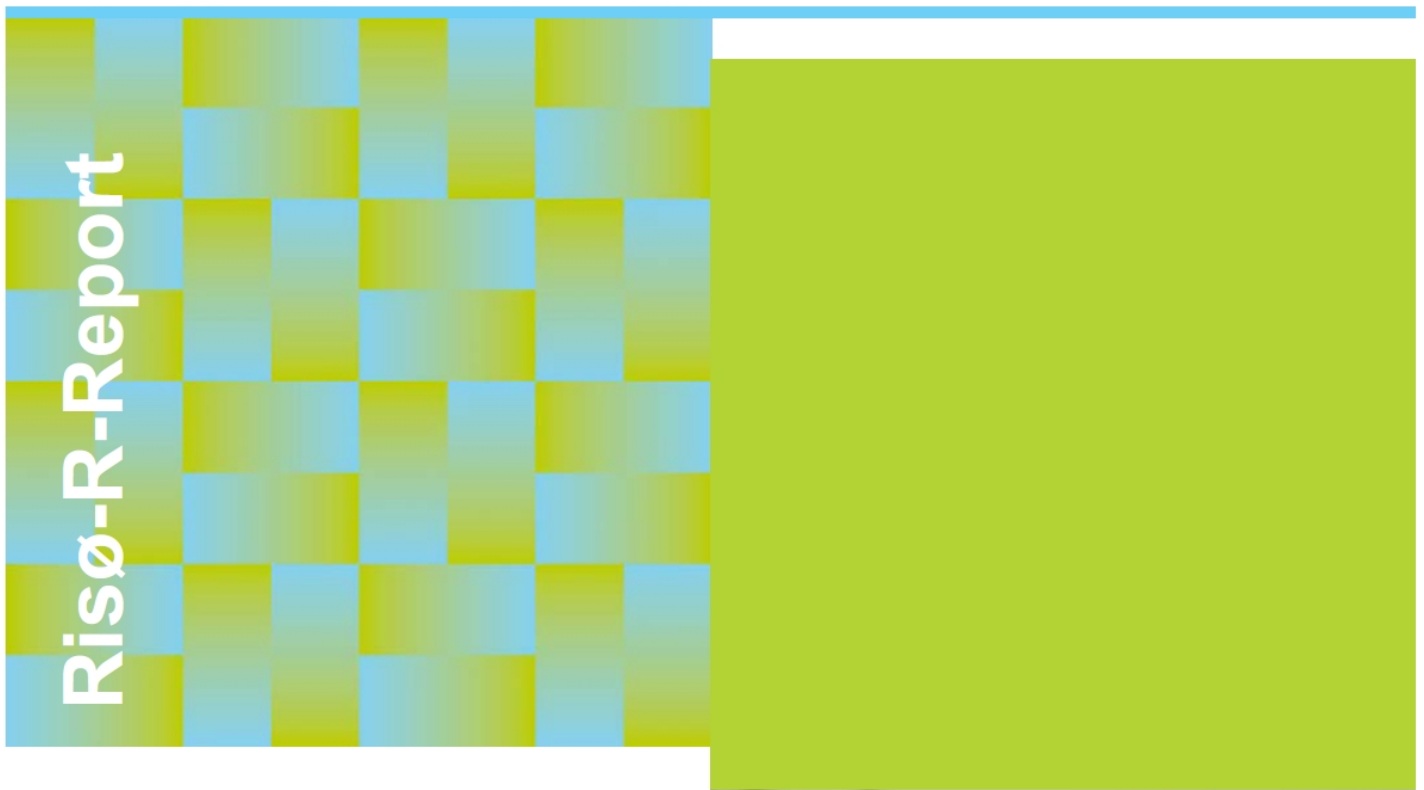
$$\delta_{IV}^2 \approx \frac{\delta_o^2}{16s_f^4} \left[(1 + 4[(h/D_r)/s_f]^2)^{-2} + \left(\frac{s_f/s_r}{k_w} \right) \left(\frac{1 - [1 + 4[(h/D_r)/s_f]^2]^{-3/2}}{6[(h/D_r)/s_f]^2} \right) \right]. \quad (39)$$

References

- Barthelmie, R. and L. E. Jensen, 2010: Evaluation of wind farm efficiency and wind turbine wakes at the Nysted offshore wind farm. *Wind Energy*, **13**, 573–586.
- Clarke, R. H. and G. D. Hess, 1974: Geostrophic departure and the functions a and b of rossby-number similarity theory. *Bound.-Layer Meteorol.*, **7**, 267–287.
- Emeis, S., 2010: A simple analytical wind park model considering atmospheric stability. *Wind Energy*, **13**, 459–469.
- Emeis, S. and S. Frandsen, 1993: Reduction of horizontal wind speed in a boundary layer with obstacles. *Bound.-Layer Meteorol.*, **64**, 297–305.
- Floors, R., S.-E. Gryning, A. Peña, and E. Batchvarova, 2011: Analysis of diabatic flow modification in the internal boundary layer. *Meteorol. Z.*, in review.
- Frandsen, S., 1992: On the wind speed reduction in the center of large clusters of wind turbines. *J. Wind Eng. Ind. Aero.*, **39**, 251–265.
- Frandsen, S., R. Barthelmie, S. Pryor, O. Rathmann, S. Larsen, J. Højstrup, and M. Thøgersen, 2006: Analytical modelling of wind speed deficit in large offshore wind farms. *Wind Energy*, **9**, 39–53.
- Frandsen, S. T., 2007: Turbulence and turbulence-generated structural loading in wind turbine clusters. Tech. Rep. Risoe-R-1188(EN), Risø DTU, Roskilde, 130 pp.
- Gryning, S.-E., E. Batchvarova, B. Brümmner, H. Jørgensen, and S. Larsen, 2007: On the extension of the wind profile over homogeneous terrain beyond the surface layer. *Bound.-Layer Meteorol.*, **124**, 251–268.
- Jensen, L. E., 2007: Array efficiency at Horns Rev and the effect of atmospheric stability. *Proceedings of the European Wind Energy Association Conference & Exhibition*, Milano.
- Jensen, N. O., 1978: Change of surface roughness and the planetary boundary layer. *Q. J. Royal Soc. Meteorol.*, **104**, 351–356.
- Jensen, N. O., 1983: A note on wind generator interaction. Tech. Rep. Risoe-M-2411(EN), Risø National Laboratory, Roskilde, 16 pp.
- Jensen, N. O., E. L. Petersen, and I. Troen, 1984: Extrapolation of mean wind statistics with special regard to wind energy applications. Tech. Rep. WCP-86, WMO/TF-No. 15, World Meteorological Organization, 85 pp.
- Katic, I., J. Højstrup, and N. O. Jensen, 1986: A simple model for cluster efficiency. *Proceedings of the European Wind Energy Association Conference & Exhibition*, Rome.
- Long, R. R. and L. J. Guffey, 1977: Drag and heat transfer relations for the planetary boundary layer. *Bound.-Layer Meteorol.*, **11**, 363–373.

- Miyake, M., 1965: Transformation of the atmospheric boundary layer over inhomogeneous surfaces. Tech. Rep. Unpublished MSc. Thesis, Sci. Rep. 5R-6, University of Washington, Seattle.
- Monin, A. S. and A. M. Obukhov, 1954: Osnovnye zakonomernosti turbulentnogo peremeshivaniya v prizemnom sloe atmosfery (Basic laws of turbulent mixing in the atmosphere near the ground). *Trudy Geofiz. Inst. AN SSSR*, **24** (151), 163–187.
- Mortensen, N. G., D. N. Heathfield, L. Myllerup, L. Landberg, and O. Rathmann, 2007: Getting started with WAsP 9. Tech. Rep. Risø-I-2571(EN), Risø National Laboratory, Roskilde, [http://www.wasp.dk/Download/DownloadFiles/General/Getting Started with WAsP 9.pdf](http://www.wasp.dk/Download/DownloadFiles/General/Getting%20Started%20with%20WAsP%209.pdf).
- Peña, A., S.-E. Gryning, and C. B. Hasager, 2008: Measurements and modelling of the wind speed profile in the marine atmospheric boundary layer. *Bound.-Layer Meteorol.*, **129**, 479–495.
- Peña, A., S.-E. Gryning, and C. B. Hasager, 2010a: Comparing mixing-length models of the diabatic wind profile over homogeneous terrain. *Theor. Appl. Climatol.*, **100**, 325–335.
- Peña, A., S.-E. Gryning, and J. Mann, 2010b: On the length-scale of the wind profile. *Q. J. Royal Meteorol. Soc.*, **136**, 2119–2131.
- Rathmann, O. S., S. Frandsen, and M. Nielsen, 2010: Wake decay constant for the infinite wind turbine array. *Proceedings of the European Wind Energy Association Conference & Exhibition*, Warsaw.
- Rethoré, P.-E., 2009: Wind turbine wake in atmospheric turbulence. Tech. Rep. Risoe-PhD-53(EN), Risø DTU, Roskilde, 170 pp.
- Sathe, A., S.-E. Gryning, and A. Peña, 2011: Comparison of the atmospheric stability and wind profiles at two wind farm sites over a long marine fetch in the North Sea. *Wind Energy*, in press.
- Troen, I. and E. L. Petersen, 1989: *European wind atlas*. Risø National Laboratory, Roskilde.
- Vincent, C. L., P. Pinson, and G. Giebel, 2010: Wind fluctuations over the North Sea. *Int. J. Climatol.*, in press.
- Zilitinkevich, S. S., 1975: Resistance laws and prediction equations for the depth of the planetary boundary layer. *J. Atmos. Sci.*, **32**, 741–752.

Linearised CFD Models for Wakes



Søren Ott, Jacob Berg and Morten Nielsen

Risø National Laboratory, Roskilde, Denmark
September 2011

Abstract

This report describes the development of a fast and reasonably accurate model for the prediction of energy production in offshore wind farms taking wake effects into account. The model has been implemented as a windows application called Fuga which can run in batch mode or as a graphical user interface. Fuga is briefly described. The model is based on a linearization technique which is described in some detail, and linearized, governing equations are derived and written in a standard form based on a mixed-spectral formulation. A new solution method is used to solve the equations which involves intensive use of look-up tables for storage of intermediate results. Due to the linearity of the model, multiple wakes from many turbines can be constructed from the wake of a single, solitary turbine. These are in turn constructed from Fourier components by a fast Fourier integral transform of results derived from generic look-up tables. Three different models, based on three different closures, are examined:

- the 'simple closure' using an unperturbed eddy viscosity $\kappa u_* z$
- the mixing length closure
- the $E-\varepsilon$ closure

Model results are evaluated against offshore wind farm production data from Horns Rev I and the Nysted wind farm, and a comparison with direct wake measurements in an onshore turbine (Nibe B) is also made. A very satisfactory agreement with data is found for the simple closure. The exception is the near wake, just behind the rotor, where all three linearized models fail. The mixing length closure underestimates wake effects in all cases. The $E-\varepsilon$ closure overestimates wake losses in the offshore farms while it predicts a too shallow and too wide the wake in the onshore case. The simple closure performs distinctly better than the other two. Wind speed data from the the Horns rev met masts are used to further validate Fuga results with the 'simple' closure.

Finally, Rødsand 1 and 2 are used as an example to illustrate the interaction between wind farms.

Approved by: Hans E. Jørgensen

Checked by: Søren E. Larsen

In no event will Risø National Laboratory or any person acting on behalf of Risø be liable for any damage, including any lost profits, lost savings, or other incidental or consequential damages arising out of the use or inability to use the results presented in this report, even if Risø has been advised of the possibility of such damage, or for any claim by any other party.

Contents

1	Introduction	<i>5</i>
2	Fuga	<i>6</i>
3	The governing equations	<i>10</i>
3.1	Closures	<i>10</i>
3.2	Actuator disk model	<i>13</i>
3.3	Boundary conditions	<i>13</i>
4	Linearization	<i>14</i>
4.1	The perturbation expansion	<i>14</i>
4.2	The mixed-spectral formulation	<i>15</i>
5	Numerical solution method	<i>17</i>
5.1	Standard form	<i>17</i>
5.2	Linear chasing	<i>18</i>
5.3	Orthogonal chasing	<i>19</i>
5.4	Numerical integration scheme	<i>21</i>
5.5	FFIT	<i>21</i>
5.6	Code verification and accuracy issues	<i>23</i>
6	Validation against data	<i>25</i>
7	Inter farm shadow effects	<i>30</i>
7.1	Farm wake validation	<i>30</i>
7.2	A case study: Rødsand 1 and 2	<i>32</i>
8	Conclusions	<i>35</i>
9	Acknowledgements	<i>36</i>
	Notation	<i>37</i>
	References	<i>38</i>

1 Introduction

Wake effects is an important issue in the planning of large offshore wind farms. Loss of energy production due to the wakes of upwind turbines, or even the combined wake from a nearby wind farm, has to be taken into consideration. Wakes that hit downwind rotors can also be a major cause of fatigue loads. A large number of flow models exist to assist in computing the various aspects of wakes and the interaction of wakes with rotors, see Vermeer, Sørensen and Crespo (2003) and Frandsen, Jørgensen, Barthelmie, Rathmann, Badger, Hansen, Ott, Rethore, Larsen and Jensen (2009) for reviews of wake models and experimental data. Their complexity and demand for computer resources range from simple, analytical models that run in virtually no time, over models based on the Reynolds Averaged Navier-Stokes equations (referred to here as RANS or CFD models) that may take several hours to run, to high resolution, time resolved large eddy simulations (LES models), where a computation may take several weeks to complete even on a large cluster. The computational costs of direct numerical simulation (DNS) is even more excessive, currently prohibiting its use in industrial applications, but the other model types could prove useful. Each type of model serves a purpose. Thus a time resolved LES model can be used for detailed studies of the interaction of turbulent flow with a rotor blade or the interactions between wakes. In this way LES calculations could serve as a source of validation or calibration data for simpler models such as RANS models. It is, however, difficult to use LES to compute the flow field in a whole wind farm and impossible to use it for annual energy production (AEP) estimates. In order to estimate the AEP of a large offshore wind farm we need the power production for a range of wind speeds combined with a range of wind directions and possibly even a range of atmospheric stabilities. This easily amounts to several hundreds of flow cases. On top of that we may even want to repeat the whole exercise a large number of times, e.g. in order to optimize the configurations of turbine positions. We need a fast model to do such things.

This report describes a particularly promising approach, linearized CFD models. A linearized CFD model is a 'cheap' version of a CFD model. It mimics the full CFD model's behaviour very well in regions where the perturbations are small, i.e. near the ground and in the far field of wakes. Very close to the rotor the behaviour is not entirely correct because the linearization spoils the momentum budget. It would therefore be natural to expect that the spoiled momentum balance in the near field behind the rotor would spoil the whole wake. However, experience shows that there is a tendency for the linearized wake to repair the damage done to the momentum balance in the near field and return to reasonable momentum deficits in the far field. This very convenient feature seems to make linearized models relatively accurate. At the same time they are also very fast. Depending on the size of the problem a linearized model can be 10^4 or 10^5 times faster than the corresponding CFD model. Another advantage of linearized models is that they can be solved without using a computational grid. This entirely eliminates numerical diffusion, which can otherwise be a problem, especially for large computational domains. A related problem is the generation of spurious mean pressure gradients caused by systematic errors in the momentum balance. This problem is also entirely eliminated in the linearized models. There is a price to pay for these advantages in terms of other types of numerical difficulties, and finding a useful solver for the linearized equations is the main problem. It took many failed attempts before the orthogonal chasing method was discovered. It is a new method and therefore described in some details below.

The linearization technique is completely general, and can be applied to any set of governing equations, but we shall concentrate on only three different closures: the 'simple closure', the mixing length closure and the $E-\varepsilon$ closure (often called $k-\varepsilon$, but we have other uses for the letter k). The closures are defined and shortly discussed in section 3. In section 4 the principles of the derivation of the linearized model equations are demonstrated using the simple closure as example. When the work with linearized CFD was initiated it was not clear

which CFD model was the best and the choice was delayed. Since then more experience has been gained with CFD (and LES) applied to wakes, but without pointing out a specific CFD model as the best one. Instead there has been a growing concern for ability of present day CFD models to cope with wakes. This does not necessarily make linearized CFD a bad idea; but we just may have to wait for the proper CFD model to be invented. The parallel use of three closures reflects this state of affairs. The validation exercise concluding this report gives preference to the simple closure which clearly beats the other two. In the simple closure any influence the wake may have on the eddy viscosity is ignored. The other two closures have such a feed back, but the result turns out to be worse than no feed back at all. This is quite an embarrassment for turbulence theory.

The report contains parts that can be read separately. Section 2 describes the Fuga model. Sections 3–5.6 describe the mathematical details of linearized CFD models and solution methods, and these sections can be skipped or read separately from the rest of the report. It should also be possible to jump directly to the validation in section 6 or to section 7.2 on inter-farm shadow effects. Conclusions are drawn in section 8.

2 Fuga

The methods presented here were developed in the WINDSHADOW and TOPFARM projects and via internal funding. Carbon Trust project sponsored the implementation of the method in a PC based application as well as a series of validation exercises. An important outcome of the project is the PC application which we have called Fuga. Fuga is a tool that can be used to estimate wake effects on the power production in a cluster of wind turbines. It applies to offshore sites or, more generally, to homogeneous terrain. Fuga can be adapted to all the three closures studied here.

In this report we concentrate on validations of model results made by Fuga. Prior to Fuga the model results were produced on a more or less ad hoc basis by adapting various Mathematica notebooks. The risk of making errors was quite large, and many were actually made. The new code, made in Fortran, C++ and Delphi, has been subject to intense debugging and we believe that it produces bug free results. This is more than we will claim for results made with the old notebooks. Therefore we have chosen to validate the three linearized models exclusively with results made with Fuga (version 1.3).

The model has been optimized for fast computations on an ordinary PC. One of the ways to achieve computational speed is to use a system of look-up tables, where some are general and some are turbine specific. These tables are used to construct velocity fields behind a single turbine, and the combined effect of multiple turbines is evaluated as the sum of all velocity perturbations. Wind conditions at turbine sites inside the wind farm will depend on wakes from neighbour turbines. For a given wind direction the turbines sites are therefore first sorted according to their upwind distance, and then the local wind speed and thrust coefficient is evaluated starting with undisturbed upwind turbines sites and progressively evaluating sites in the downwind direction. When the thrust of all turbines is know, we can evaluate the combined wake velocity deficit anywhere. Estimates of annual energy production are calculated as probability-weighted integrals of power output at all wind speeds and directions.

Calculations are done by a suite of programs operating on the file system described in Ott and Nielsen (2010). All programs can be called from a Windows command line, but it is often easier to work with Fuga, which has a graphical user interface. Fuga is responsible for combining wakes from multiple turbines and presenting the results graphically. It also maintains the file structure, see figure 1, and calls the two programs, Preludium and Trafalgar, whenever new lookup tables and single-turbine wake velocity fields are needed. New tables are needed for each turbine type and combinations of boundary-layer height and surface roughness. Wake velocity deficits can, however, be scaled for variable turbine thrust

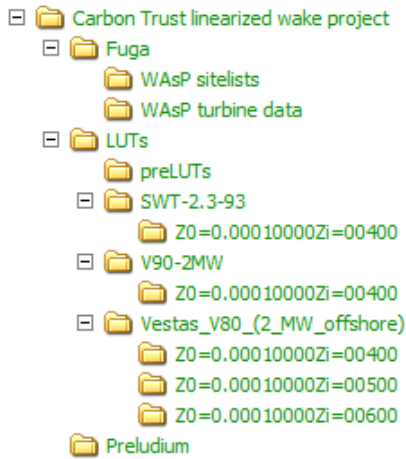


Figure 1. Fuga file structure. Subfolders to turbine type folders contain look-up tables for different atmospheric boundary-layer cases.

and thereby for variable wind speed.

The ambition is to integrate Fuga in WASP as a supplement to the traditional wake model, and the model input and calculations are consequently organized in nearly the same way as in WASP. Here, annual energy production is predicted by a flow model translating observed wind climates at reference sites to wind climates at individual turbine sites. In preparation for Fuga, the user must first set up a WASP project; do a WASP wind-farm calculations; export a so-called windfarm file (*.wwf) containing turbine positions and site-specific wind climates; and finally import this file into Fuga. Turbine data are read from a wind turbine generator file (*.wtg) as in WASP. A sample collection of turbine data is available and new ones can be generated by the WASP Turbine editor.

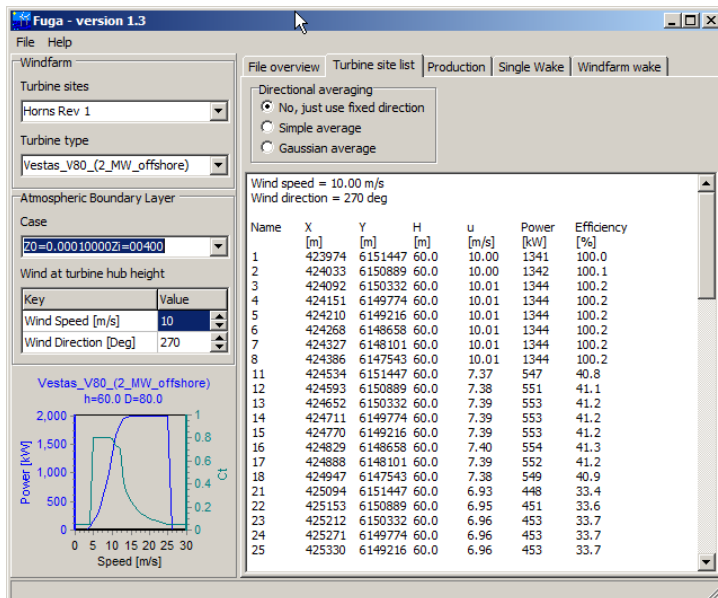


Figure 2. The Fuga graphical interface

Perhaps the best way to get acquainted with Fuga is to run it and use the help facility. Here you will find instructions on how to set up a project and how to generate various kinds of output. Figure 2 shows the Fuga user interface. The top-left frame contains two drop-down lists with available WASP windfarm files and WASP turbine files, which together

with the below boundary-layer case list defines a project. The free-stream wind speed and direction are chosen in the table below the boundary-layer selector. The right-hand side of program shows various pages:

- An overview of look-up tables;
- A list of turbine sites with sheltered wind speeds, power production and efficiency for the current free-stream wind;
- A list of annual energy productions including wake effects for individual turbine sites - either calculated by Fuga or imported from WASP . These results can also be shown for individual wind sectors;
- A display of the single-wake velocity field;
- A display of the combined wind-farm wake velocity field.

Initial comparison indicated narrower model wakes with lower centre-line velocities than could be observed in the field. We believe this to be an effect of variable and non-uniform wind direction causing wake meandering, as will be further discussed in section 6 of this report. The effect is not included in the present version of the model, but what we can do is to average the results for a range of wind speeds. This option is shown above the turbine site list.

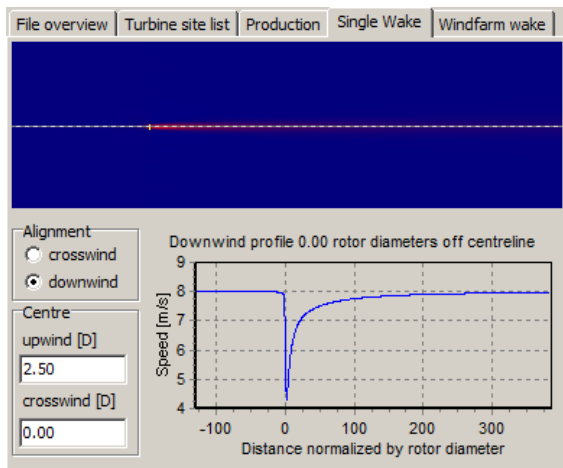


Figure 3. Fuga display of a single wake

Figure 3 shows the single wake velocity field at the selected wind speed. Local wind speeds are shown at the status bar at the bottom of the program window when the mouse cursor is moved over the wake display. Clicking on the wake field will change the position of the below cross profile, which is also indicated by a dotted line in the wake field display. A more precise positioning of the profile is done by the edit boxes left of the profile view.

Figure 4 shows the wind farm wake at the selected wind speed and direction. It is possible to adjust the main plot scales and change the reference turbine or reference position for the below charts. Two chart types are available - a power efficiency plot and a wind profile along a transect line. The first chart type shows power efficiency or local speed reduction as function of wind direction. These values are normalized by the undisturbed wind speed or the production of a turbine without wake effects. The chart can both be shown for a specific turbine or for the entire wind farm. The second chart type shows the wind speed along a transect line with downwind, crosswind or flexible alignment. The centre position is selected by clicking on the wind-farm wake plot.

Fuga has several data export facilities, which are invoked from its main menu. Graphics and data used for charts in the user interface can be exported and, in addition, you can

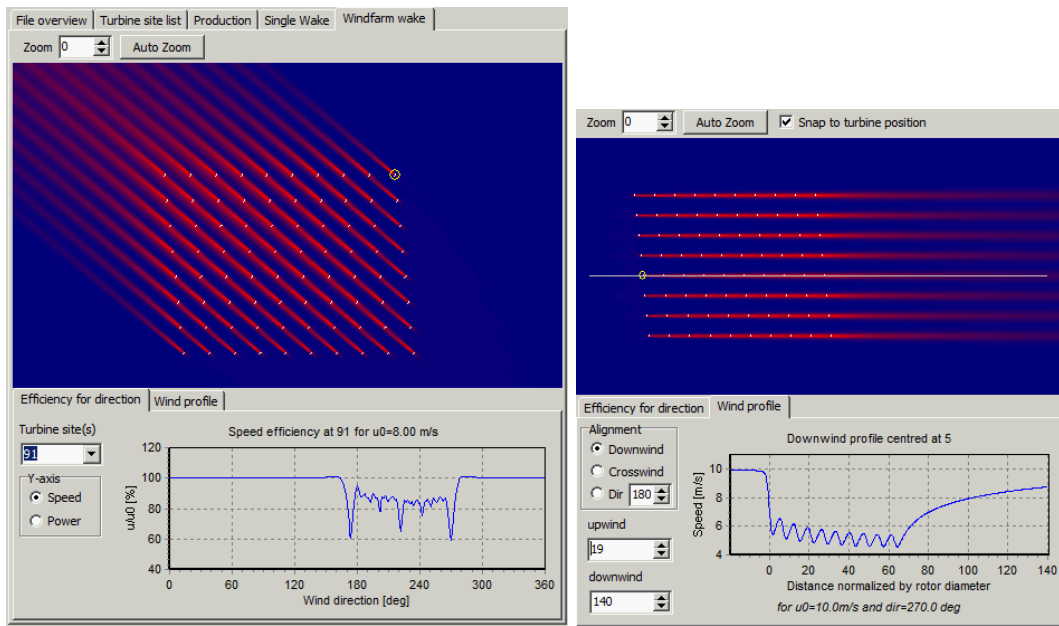


Figure 4. Fuga display of the combined wind-farm wakes: a) efficiency as a function of wind direction and b) wind speed along a transect line.

construct a result table with results from a range of wind speeds and wind directions, either for a single turbine site, for all the sites, or accumulated for the entire wind farm. For some computations, like systematic testing of a range of wind conditions, it might be more practical to call the scriptable FugaBatch program, which has no graphical user interface. A practical working method would be to 1) set up a WASP project with reliable climate statistics and export the windfarm file, 2) load that file and WASP turbine data into the interactive Fuga program, 3) generate look-up tables for appropriate boundary-layer cases, 4) execute FugaBatch calculations from a script and 5) analyse the results in programs like Excel or Mathematica.

A Fuga project is currently limited to wind farms with a single turbine type and uniform hub height, where the same single-turbine wake can be used for all sites and information is needed only at turbine hub height. In the near future Fuga will be able to work with 3D wakes and complex WASP projects including a mixture of turbines in cluster of wind farms, like in section 7.2 of this report. Later on an attempt to model wake meandering will also be made. A Fuga limitation is that surface roughness and wind field have no horizontal variation. It could be argued that wakes should follow the curved flow modified by non-uniform terrain. However, since this is a second order effect, the wakes produced by the linearized flow model in Fuga only follow the undisturbed, horizontally homogeneous, flow field. This is no problem for an offshore site, but we recommend that the present version of the model is not used in complex terrain. On the other hand, the model works with site-specific wind climates calculated by WASP which do depend on the specific terrain, and in this way the model takes the influence of coast lines into account.

3 The governing equations

The starting point is the Reynolds averaged Navier-Stoke's (RANS) equation for a quasi-steady flow. Setting $\partial u/\partial t = 0$ we have¹

$$u_j \frac{\partial u_i}{\partial x_j} = \frac{\partial \tau_{ij}}{\partial x_j} - \frac{\partial p}{\partial x_i} + f_i + \nu \nabla^2 u_i \quad (1)$$

where \mathbf{u} is the mean velocity, $p = P/\rho$ is the pressure scaled with the (uniform) density ρ and $f_i = F_i/\rho$ is the bulk force (i.e. drag force field from turbines) also scaled with ρ . We are neglecting buoyancy and can therefore only model neutral stratification. The Coriolis force has also been neglected. The Reynolds stress tensor τ_{ij} needs to be determined by some kind of closure. The ones we will consider all model τ_{ij} via an eddy viscosity K :

$$\tau_{ij} = K \left(\frac{\partial u_i}{\partial x_j} + \frac{\partial u_j}{\partial x_i} \right) + \frac{1}{3} \delta_{ij} \tau_{kk} \quad (2)$$

Equation (1) is solved together with the continuity equation for incompressible fluid:

$$\frac{\partial u_j}{\partial x_j} = 0 \quad (3)$$

Inserting (2) into (1) leaves a term $\frac{\partial \frac{1}{3} \tau_{kk}}{\partial x_i}$ which is the gradient of a scalar and can be absorbed into the pressure gradient (we will still call it p). $K \gg \nu$ so the real viscous term can be neglected.

3.1 Closures

Next point is to specify K . We consider three possibilities:

Simple closure

$$K = \kappa u_* z \quad (4)$$

This closure is about as simple as it can get. K is just taken as the free stream value without considering any effects from the perturbed flow field in the wake.

Mixing length closure

$$K = l_m^2 \sqrt{2S_{ij}S_{ij}} \quad (5)$$

where

$$l_m = \kappa z \quad (6)$$

is the mixing length and

$$S_{ij} = \frac{1}{2} \left(\frac{\partial u_i}{\partial x_j} + \frac{\partial u_j}{\partial x_i} \right) \quad (7)$$

is the rate-of-strain tensor.

The mixing length closure is based on classical turbulence theory of Prandtl (1925). It is used intensively in atmospheric applications.

¹Here and in the following a summation over repeated subscripts is understood.

$E - \varepsilon$ closure

$$K = C_\mu \frac{E^2}{\varepsilon} \quad (8)$$

Where C_μ is a constant, E is the turbulent kinetic energy (TKE) and ε is the dissipation of TKE². Two additional transport equations govern the two extra variables

$$\frac{\partial}{\partial x_j} v_j E = \frac{\partial}{\partial x_j} \frac{\nu}{\sigma_E} \frac{\partial E}{\partial x_j} + \Pi - \varepsilon \quad (9)$$

$$\frac{\partial}{\partial x_j} v_j \varepsilon = \frac{\partial}{\partial x_j} \frac{\nu}{\sigma_\varepsilon} \frac{\partial \varepsilon}{\partial x_j} + \frac{\varepsilon}{E} (C_{\varepsilon 1} \Pi - C_{\varepsilon 2} \varepsilon) \quad (10)$$

where σ_E , σ_ε , $C_{\varepsilon 1}$ and $C_{\varepsilon 2}$ are model constants and Π is the TKE production given by

$$\Pi = \nu \frac{\partial v_i}{\partial x_j} \left(\frac{\partial v_i}{\partial x_j} + \frac{\partial v_j}{\partial x_i} \right) = \frac{\nu}{2} \left(\frac{\partial v_i}{\partial x_j} + \frac{\partial v_j}{\partial x_i} \right)^2 \quad (11)$$

With a body force (the turbine drag) present we might expect an extra production term in (9) or even an extra term in (10). Such extensions of the $E - \varepsilon$ model have been discussed by Kasmi and Masson (2008) and for canopy drag also by Sanz (2003) and Sogachev and Panferov (2006).

The $E - \varepsilon$ model and similar so called one-and-a-half order closures are very popular for industrial applications, see Wilcox (2002) for details. It should be noted that the model constants are not supposed to be free parameters that can be used to fit specific data. The intension is that the model constants should reflect universal properties of turbulent flow and hence a single set of constants should fit all possible flows. Comparison with data from a variety of experimental flows has resulted in a set of 'standard' constants:

$$C_\mu = 0.09 \quad \sigma_E = 1 \quad \sigma_\varepsilon = 10/9 \quad C_{\varepsilon 1} = 1.44 \quad C_{\varepsilon 2} = 1.92 \quad (12)$$

We are not supposed to deviate from these constants unless we have good arguments. A re-calibration of the constants should involve new as well as old data.

It should be mentioned that Yakhot, Orszag, Thangam, Gatski and Speziale (1992) managed to derive the $E - \varepsilon$ model equations more or less from scratch using renormalization group (RNG) theory, a technique originally developed for quantum field theory. The derivation yields a theoretical estimate of the values of the constants³ which are not far from the standard values. It is worth noting that the RNG derivation involves the assumption that the $E - \varepsilon$ model actually works. If a particular flow is poorly represented by the RNG (or standard) model results, it could therefore be taken as an indication that the $E - \varepsilon$ model just does not work for that flow, so that re-adjustment of model constants would be in vain or even misleading. Unfortunately, this seems to be the case for wakes where the standard model makes a very poor performance. This observation has been made by Kasmi and Masson (2008), Rados, Prospathopoulos, Stefanatos, Politis, Chaviaropoulos and Zervos (2009), Réthoré (2009) and many others. The possible causes for this failure were discussed in Réthoré (2009) and Réthoré, Sørensen and Bechmann (2010) where the usefulness of the eddy viscosity concept is seriously questioned. One of the problems is that a wake in the atmosphere is influenced by turbulence on a very wide range of scales. The small scale turbulence, i.e. eddies with sizes less than the wake width, tend to mix the wake with the surroundings in an essentially diffusive manner which is well described by an eddy viscosity. However, in the atmosphere a large portion of the turbulent kinetic energy resides on scales that are larger than the wake width, and these large eddies tend to move the wake as a whole without causing much mixing. The effect of large eddies is therefore to produce meandering motion, which leads to an uncertainty in the side-to-side wake position, but does not lead

²'Specific dissipation' is more correct - ε is measured in $W/kg = m^2 s^{-3}$

³ $C_{\varepsilon 2}$ is actually given by an expression involving the rate of strain ($\sqrt{2S_{ij}S_j}$) and a constant β which must be determined from experiments

to decay of the wake by mixing. The best we can hope for using eddy viscosity is therefore to model the influence of the small scale turbulence on the mean flow. If we want also to represent the large scale part of the turbulent kinetic energy, we must of course incorporate the mechanisms responsible for it. These are specific, atmospheric processes such as convective rolls, gravity waves, the occasional, spontaneous creation of large descending jets, differential heating by passing clouds and possibly more mechanisms. In order to include these processes we would have to use a time resolved model that includes thermal effects and the Coriolis force. The conventional RANS/CFD framework is inadequate, but it could be done with Large Eddy Simulations that include temperature. However, only at rather extreme computational costs. The sad conclusion is that simple CFD models lack the features necessary to represent meandering.

The logarithmic profile

In flat terrain all these closures yield the usual logarithmic profile

$$u^0(z) = \frac{u_*}{\kappa} \log z/z_0 \quad (13)$$

where u_* is the friction velocity, z_0 is the surface roughness and $\kappa = 0.4$ is the von Karman constant. We will regard κ as fixed which poses the following constraint on the $E-\varepsilon$ model constants

$$C_\mu^{1/4} \sigma_\varepsilon^{1/2} (C_{\varepsilon 2} - C_{\varepsilon 1})^{1/2} = \kappa \quad (14)$$

Since the model does not include the Coriolis force, the surface layer fills the whole boundary layer. The logarithmic wind profile, which is a consequence of surface layer scaling, is therefore valid all the way up to the upper boundary.

Over land the surface roughness is often assumed to be a constant independent of the wind speed. Over water the roughness is created by waves and hence z_0 depends on the wind speed as well as other local factors that determine the local wave characteristics. These other factors include fetch (distance to shore) and the orography of the seabed. The surface roughness increases with the wind speed and is often assumed to follow the Charnock (1955) relation

$$\frac{gz_0}{u_*^2} = A_C \quad (15)$$

where A_C is the Charnock parameter. The relation is limited to 'normal' wind speeds, neither too low or too high. At very low wind speeds z_0 approaches a value appropriate for a smooth boundary, and at very large wind speeds, where water droplets can have a kind of lubricating effect, z_0 even decreases with increasing wind speed, thus contradicting (15). However, turbines usually operate in the 'normal' range of wind speeds where Charnock's relation can be applied. The relation only yields a rough estimate of z_0 , a fact reflected in a wide range of experimental values of $A_C \sim 0.012-0.035$. It should also be noted that swell can cause relatively large waves to inject momentum into the air rather than extracting it. In other words, the waves push the air forward and act as a kind of negative friction. In order to representing this in framework of (13) would require $u_* < 0$ and $z_0 \gtrsim z_h$. This is rather bizarre, so we have to disregard such special situations. Perhaps this could amount to about 1% of the cases, but mainly low wind speeds.

For a fixed wind speed at hub height, $U_h = u^0(z_h)$, we can use (13) and (15) to determine u_* and z_0 . Using the empirical relation $\sigma_u \approx 2.5u_*$ (Panofsky and Dutton 1984) we then have fixed the turbulence intensity $Ti \equiv \sigma_u/U_h$ at hub height, in fact we have

$$Ti = \frac{\sigma_u}{U_h} \approx \frac{2.5\kappa}{\log z_h/z_0} \approx \frac{1.0}{\log z_h/z_0} \quad (16)$$

Real data always show some spread of Ti even for constant U and neutral conditions. We could therefore turn the argumentation around and determine z_0 by means of (16) using U_h and Ti from data. The wide range of experimental values of A_C justifies this procedure.

3.2 Actuator disk model

The actuator disk model is used for the forcing term \mathbf{f} . The drag force is determined by the free wind i.e. the wind speed at hub height determined after removing the turbine. For a given free wind U_{free} along with the x -axis and the hub placed at (x_h, y_h, z_h) the drag force can be written as

$$f_1 = -\frac{1}{2}C_T U_{\text{free}}^2 \delta(x - x_h) \Theta(R^2 - (y - y_h)^2 - (z - z_h)^2) \quad (17)$$

where δ is a Dirac δ -function and Θ is a step function (zero for negative arguments, 1 for positive). In calculations the force is always smeared out a bit for numerical reasons.

3.3 Boundary conditions

The flow will be assumed to be *lid driven* with vanishing mean pressure gradient. At the upper boundary $z = z_i$, the velocity is assumed to be fixed. The lower boundary is imposed at $z = z_0$ where we $\mathbf{u} = 0$. This gives 6 boundary conditions in all:

$$\begin{aligned} u(x, y, z_0) &= 0 \\ v(x, y, z_0) &= 0 \\ w(x, y, z_0) &= 0 \\ u(x, y, z_i) &= u^0(z_i) \\ v(z_i) &= 0 \\ w(z_i) &= 0 \end{aligned} \quad (18)$$

This is sufficient both for the simple closure and for the mixing length closure, but the E - ε model has two more variables and needs two more conditions. These are:

$$\begin{aligned} E'(x, y, z_0) &= 0 \\ \varepsilon(z_0) z_0 &= C_\varepsilon E^{3/2}(z_0) \\ E'(z_i) &= 0 \\ z_i \varepsilon'(z_i) + \varepsilon(z_i) &= 0 \end{aligned} \quad (19)$$

where $E' = \partial E / \partial z$ and $C_\varepsilon = C_\mu^{3/4} / \kappa$.

These boundary conditions describe a lid driven flow where momentum is injected at the top. This can be realized by means of various different upper boundary conditions: constant velocity, constant momentum flux, constant energy flux and combinations of the three, but in practice it makes little difference. A consequence of lid driven flow is that wind farms get more efficient the shallower the boundary layer is. One might expect a blocking effect, which perhaps would be more realistic for a real boundary layer, but such an effect is dominated by the efficiency gain caused by the 'engine' in the lid moving closer to the rotors. It is a small effect, however, with almost no dependence on z_i . The real atmospheric boundary layer is driven by a pressure gradient and the Coriolis force. They cancel each other at the top, so the flow is anything but lid driven. We could of course include the Coriolis force and model the boundary layer in a more realistic manner, but the Coriolis parameter introduces an additional dimension in the look-up tables (see Section 5.3) which makes everything more complicated. An alternative would be to replace the lid driven flow with

one driven by a pressure gradient without Coriolis force but with a given, fixed boundary layer height. However, this possibility has not been pursued.

4 Linearization

In the section we describe how the equations are linearized and set up the problem in a standard form. In the following we use the simple closure as example. The principles are the same for other closures even if the actual equations may differ. Linearization can mean different things. Sometimes it just means 'throwing away terms until the problem becomes linear with an analytical solution'. Belcher, Jarram and Hunt (2003) divided the flow into three regimes (layers) each with its own set of linear equations. These were then solved analytically and pieces together by the asymptotic matching technique. The present model uses a different strategy. We make a formal perturbation expansion and keep all terms, large or small, and numerical rather than analytical solutions are sought. The advantage is that we do not have to worry about asymptotic matching or how to define the regimes, and it becomes less problematic to treat higher orders. Below we describe the perturbation expansion and phrase the problem in a standard form. We use the simple closure as an example.

4.1 The perturbation expansion

With the simplifications described in the previous section, the momentum equation can be written as

$$u_j \frac{\partial u_i}{\partial x_j} = \frac{\partial}{\partial x_j} \kappa u_* z \left\{ \frac{\partial u_i}{\partial x_j} + \frac{\partial u_j}{\partial x_i} \right\} - \frac{\partial p}{\partial x_i} + \xi f_i \quad (20)$$

Note that an extra factor ξ appears on the forcing. The idea is to regard \mathbf{u} and p as functions of the parameter ξ . If we set $\xi = 0$ there is no drag, and the solution is given by (13) and a constant pressure e.g. $p^0 = 0$. For finite ξ a perturbation expansion is made using the external drag force as a 'small' term. Formally, this is done by writing all variables as Taylor series in ξ , vis.

$$\begin{aligned} u_i &= u_i^0 + u_i^1 \xi + u_i^2 \xi^2 + \dots \\ p &= p^0 + u_i^1 \xi + p^2 \xi^2 + \dots \\ E &= E^0 + E^1 \xi + E^2 \xi^2 + \dots \\ \varepsilon &= \varepsilon^0 + \varepsilon^1 \xi + \varepsilon^2 \xi^2 + \dots \\ f_i &= f_i^1 \xi + f_i^2 \xi^2 + \dots \end{aligned} \quad (21)$$

When this is inserted into (20) we get an equation for each power ξ^n . For $n = 0$ we get the zeroth order equation which is just (20) with $f_i = 0$. This is a non-linear equation, but not difficult. For $n = 1$ we get the following first order equations

$$\begin{aligned} u^0 \frac{\partial u^1}{\partial x} + w^1 \frac{\partial u^0}{\partial z} &= \frac{\partial}{\partial x_j} K \left(\frac{\partial u^1}{\partial x_j} + \frac{\partial u_j^1}{\partial x} \right) - \frac{\partial p^1}{\partial x} + f_1^1 \\ u^0 \frac{\partial v^1}{\partial x} &= \frac{\partial}{\partial x_j} K \left(\frac{\partial v^1}{\partial x_j} + \frac{\partial u_j^1}{\partial y} \right) - \frac{\partial p^1}{\partial y} \\ u^0 \frac{\partial w^1}{\partial x} &= \frac{\partial}{\partial x_j} K \left(\frac{\partial w^1}{\partial x_j} + \frac{\partial u_j^1}{\partial z} \right) - \frac{\partial p^1}{\partial z} \\ \frac{\partial u^1}{\partial x} + \frac{\partial v^1}{\partial y} + \frac{\partial w^1}{\partial z} &= 0 \end{aligned} \quad (22)$$

K is given by (4) and the fourth equation comes from the continuity equation. It has been assumed that the forcing is longitudinal, i.e. parallel with the incoming flow so that $f_2 = 0$. This corresponds to an ideal situation with no yaw error. It is possible to take a (known or assumed) yaw error into account by considering transverse forcing, where $f_1^1 = 0$ and $f_2^1 \neq 0$, and obtain the appropriate solution by superposition. This is allowed because the equations are linear in the variables (u^1, v^1, w^1, p^1) . In the following we concentrate on longitudinal forcing since the treatment of transverse forcing is very similar. We also limit the number of turbines to just one because the solution for a cluster of turbines can be obtained by superimposing the wakes (velocity deficits) calculated for each turbine separately. The drag force is proportional to $C_T U_{\text{free}}^2$, and, due to linearity, the first order solution can simply be scaled with this factor. We can therefore set the factor equal to 1, solve the equations, and scale the solution later with the correct factor before the wakes are superimposed. We start with the most upwind turbine which is not in the wake of any of the others. The free stream velocity is therefore equal to the velocity at hub height for the approach flow. Then we proceed downwind to the next turbine, which might be in the wake of the first one. If so we calculate U_{free} (and the corresponding C_T) taking the wake of the first turbine into account, and so forth. In principle the procedure should be iterated on order account for the upstream influence, but in practice convergence is reached after the first iteration.

We will not study higher orders here, but just mention that all the higher order equations are linear in the variables (u^n, v^n, w^n, p^n) and only differ by a source term which is non-linear in the lower order variables. All higher orders can therefore be solved in succession using the same linear solver.

4.2 The mixed-spectral formulation

The governing first order equations (22) are simplified considerably in the mixed-spectral formulation. This is effectuated by Fourier transformations in the two horizontal coordinates x and y . In other words we introduce mixed-spectral variables, e.g.

$$\hat{u}(k_1, k_2, z) = \frac{1}{(2\pi)^2} \int_{-\infty}^{\infty} dx \int_{-\infty}^{\infty} dy u(x, y, z) e^{-i(xk_1 + yk_2)} \quad (23)$$

with the inverse transformation

$$u(y, x, z) = \int_{-\infty}^{\infty} dk_1 \int_{-\infty}^{\infty} dk_2 \hat{u}(k_1, k_2, z) e^{i(xk_1 + yk_2)} \quad (24)$$

The mixed-spectral equations corresponding to (22) read

$$u^0 ik_1 u^1 + w^1 \frac{\partial u^0}{\partial z} = -\mathbf{k}^2 K u^1 + \frac{\partial}{\partial z} K \frac{\partial u^1}{\partial z} + \frac{\partial K}{\partial z} ik_1 w^1 - ik_1 p^1 + f_1^1 \quad (25)$$

$$u^0 ik_1 v^1 = -\mathbf{k}^2 K v^1 + \frac{\partial}{\partial z} K \frac{\partial v^1}{\partial z} + \frac{\partial K}{\partial z} ik_2 w^1 - ik_2 p^1 \quad (26)$$

$$u^0 ik_1 w^1 = -\mathbf{k}^2 K w^1 + \frac{\partial}{\partial z} K \frac{\partial w^1}{\partial z} + \frac{\partial K}{\partial z} \frac{\partial w^1}{\partial z} - \frac{\partial p^1}{\partial z} \quad (27)$$

$$ik_1 u^1 + ik_2 v^1 + \frac{\partial w^1}{\partial z} = 0 \quad (28)$$

Where $\mathbf{k}^2 = k_1^2 + k_2^2$. We have not bothered to put hats on the variables; u^1 really should have been $\hat{u}^1(\mathbf{k}, z)$. Note that most terms can be written as a product of two functions, one that depends on \mathbf{k} and one that depends on z . The only exception is the forcing $f_1^1(\mathbf{k}, z)$, but we can approximate it to any desired accuracy as a sum of such terms: $f_1^1(\mathbf{k}, z) = \sum_n f_{n,\mathbf{k}} \phi_n(z)$. The solution can then be obtained as the sum of the responses to each of the terms $f_{n,\mathbf{k}} \phi_n(z)$, or even better, we can find the response to $\phi_n(z)$ and multiply by $f_{n,\mathbf{k}}$ afterwards. The advantage of this procedure is that $f_{n,\mathbf{k}}$, which contains the information

of turbine geometry and thrust coefficient, does not have to be known when the equations are solved. The functions $\phi_n(z)$ can be chosen in many ways. We choose a set of chapeau functions of the form

$$\Delta_n(z) = \begin{cases} \frac{z-z_{n-1}}{z_n-z_{n-1}} & \text{for } z_{n-1} < z < z_n \\ \frac{z-z_{n+1}}{z_n-z_{n+1}} & \text{for } z_n < z < z_{n+1} \\ 0 & \text{elsewhere} \end{cases} \quad (29)$$

where $\{z_n\}$ is a set of sufficiently closely spaced levels. We set $z_n = z_0 e^{nds}$, where $ds = 0.1$ seems to be a good choice. Note that $\Delta_n(z_m) = 0$ for $n \neq m$ while $\Delta_n(z_n) = 1$. In other words, $\Delta_n(z)$ is a sort of piecewise linear version of a δ function from which we can construct any piecewise linear function with elbows points in $\{z_n\}$.

The big advantage of this formulation is that variables for different wave vectors \mathbf{k} do not mix. We therefore only have to solve four coupled ordinary differential equations, belonging to a given \mathbf{k} , at a time. The mixed-spectral formulation therefore allows calculations to be broken down into relatively simple, independent sub-problems that can be handled by a PC or by a cluster working in parallel. This is in contrast to (22), which involves partial differential equations, and where a representation of the field by values on a grid results in one, very large, set of coupled, algebraic equations.

Some more manipulations are made to (25–28):

1. Use (28) to eliminate $\frac{\partial w^1}{\partial z}$ in (27).
2. Define a new independent variable $s = kz$.
3. Set $k_1 = k \cos \beta$ and $k_2 = k \sin \beta$.
4. Define new dependent variables $\tilde{u} = u^1 u_* k / f_{n,\mathbf{k}}, \tilde{v} = v^1 u_* k / f_{n,\mathbf{k}}, \tilde{w} = w^1 u_* k / f_{n,\mathbf{k}}$ and $\tilde{q} = p^1 k / (f_{n,\mathbf{k}} s)$
5. Isolate $\frac{\partial^2 \tilde{u}}{\partial s^2}$ on the left hand side of (25)
6. Isolate $\frac{\partial^2 \tilde{v}}{\partial s^2}$ on the left hand side of (26)
7. Isolate $\frac{\partial \tilde{p}}{\partial s}$ on the left hand side of (27)
8. Isolate $\frac{\partial \tilde{w}}{\partial s}$ on the left hand side of (28)

This leads to the following equations

$$\begin{aligned} \frac{\partial^2 \tilde{u}}{\partial s^2} &= \left(1 + \frac{i \cos \beta \log \frac{s}{kz_0}}{\kappa^2 s}\right) \tilde{u} - \frac{1}{s} \frac{\partial \tilde{u}}{\partial s} + \left(\frac{1}{(\kappa s)^2} - \frac{i \cos \beta}{s}\right) \tilde{w} \\ &\quad + \frac{i \cos \beta}{\kappa} \tilde{q} - \frac{\Delta_n(s)}{\kappa s} \end{aligned} \quad (30)$$

$$\frac{\partial^2 \tilde{v}}{\partial s^2} = \left(1 + \frac{i \cos \beta \log \frac{s}{kz_0}}{\kappa^2 s}\right) \tilde{v} - \frac{1}{s} \frac{\partial \tilde{v}}{\partial s} - \frac{i \sin \beta}{s} \tilde{w} + \frac{i \sin \beta}{\kappa} \tilde{q} \quad (31)$$

$$\frac{\partial \tilde{w}}{\partial s} = -i \cos \beta \tilde{u} - i \sin \beta \tilde{v} \quad (32)$$

$$\begin{aligned} \frac{\partial \tilde{q}}{\partial s} &= -\frac{2i\kappa}{s} \cos \beta \tilde{u} - i\kappa \cos \beta \frac{\partial \tilde{u}}{\partial s} - \frac{2i\kappa}{s} \sin \beta \tilde{v} - i\kappa \sin \beta \frac{\partial \tilde{v}}{\partial s} \\ &\quad - \left(\kappa + \frac{i \cos \beta \log \frac{s}{kz_0}}{\kappa s}\right) \tilde{w} - \frac{1}{s} \tilde{q} \end{aligned} \quad (33)$$

where $\Delta_n(s)$ is a chapeau function with top point $s_n = k z_n$. These equations are well suited for the upper part where $s > 1$, but for small s they are very unstable. We therefore use an alternative formulation for $s < 1$. It is derived in the same way except that $t = \log \frac{z}{z_0}$ is used as independent variable and $\tilde{p} = p^1 / (k f_{n,\mathbf{k}})$ is used instead of \tilde{q} . The result is

$$\frac{\partial^2 \tilde{u}}{\partial t^2} = \frac{e^{2t} k z_0^2 + i t e^t \cos \beta}{\kappa^2} \tilde{u} + \left(\frac{1}{\kappa^2} - i e^t k z_0 \cos \beta \right) \tilde{w} + \frac{i e^t k z_0 \cos \beta}{\kappa} \tilde{p} - \frac{e^{2t} \Delta_n}{\kappa} \quad (34)$$

$$\frac{\partial^2 \tilde{v}}{\partial t^2} = \frac{e^{2t} k z_0^2 + i t e^t \cos \beta}{\kappa^2} \tilde{v} - i e^t k z_0 \sin \beta \tilde{w} + \frac{i e^t k z_0 \sin \beta}{\kappa} \tilde{p} \quad (35)$$

$$\frac{\partial \tilde{w}}{\partial t} = -i k z_0 e^t \cos \beta \tilde{u} - i k z_0 e^t \sin \beta \tilde{v} \quad (36)$$

$$\begin{aligned} \frac{\partial \tilde{p}}{\partial t} &= -2i e^t k z_0 \kappa \cos \beta \tilde{u} - i e^t k z_0 \kappa \cos \beta \frac{\partial \tilde{u}}{\partial t} - 2i e^t k z_0 \kappa \sin \beta \tilde{v} \\ &\quad - i e^t k z_0 \kappa \sin \beta \frac{\partial \tilde{v}}{\partial t} - \frac{e^{2t} (\kappa k z_0)^2 + i t e^t k z_0 \kappa \cos \beta}{\kappa} \tilde{w} \end{aligned} \quad (37)$$

These equations work much better than (30–33) near the ground, which can be judged from the singular value decomposition. The most extreme singular values are obtained for $k z_0 = 1$, i.e. $s = 1$ or $t = -\log k z_0$, and this point is therefore used to switch between the two formulations.

Note that k and z_0 only appears in the combination $k z_0$. We can therefore solve the equations without knowing k and z_0 separately. Apart from the independent variable (s or t), the solution only depends on four parameters: n , β , $k z_0$ and $k z_i$. In the next section we show that $k z_i$ can be eliminated.

5 Numerical solution method

During his PhD study Corbett (2007) discovered that the linearized equations can be hard to solve. He was solving a linearized model for flow in complex terrain, but linearized wake models present the same difficulties. One of the difficulties is that it is a *two-point problem* with boundary conditions at both ends. *Initial value* problems are usually more benign and can be solved using a standard method such as Runge–Kutta integration. Corbett observed that the problem tends to become numerically ill-posed for small values of $k z_0$ where extremely high working precision had to be used. In some cases, which can be conceived to be encountered in practice, a working precision of as much as 50 decimals is needed, which is more than most conventional programming languages can deal with. Mathematica can, but at a very high cost in terms of computation time. Corbett (2007), see also Corbett, Ott and Landberg (2008), used a shooting technique where solutions obtained by integration from below and from above were matched at a suitably chosen midpoint. Small values of $k z_0$ are relevant for offshore wind farms because wakes are long and the roughness at sea is small, hence there was a need for a more powerful numerical method. All existing methods we have tried fail, including the state-of-the-art algorithms of Mathematica, and it therefore was necessary to invent a new method, which will be described in some detail in this section.

5.1 Standard form

Note that \tilde{u} , $\partial \tilde{u} / \partial s$, \tilde{v} , $\partial \tilde{v} / \partial s$, \tilde{w} and \tilde{q} (or \tilde{p}) appear on the right hand sides of (30–33) or (34–37). The equations are second order in \tilde{u} and \tilde{v} and first order in \tilde{w} and \tilde{q} (or \tilde{p}). First order equations are more practical so we define two new variables \tilde{u}' and \tilde{v}' and two more equations

$$\begin{aligned} \frac{\partial \tilde{u}}{\partial s} &= \tilde{u}' \\ \frac{\partial \tilde{v}}{\partial s} &= \tilde{v}' \end{aligned}$$

Defining $\mathbf{x} = (x_1, x_2, x_3, x_4, x_5, x_6) = (\tilde{u}, \tilde{u}', \tilde{v}, \tilde{v}', \tilde{w}, \tilde{q} \text{ or } \tilde{p})$, the linearized equations (30–33) or (34–37) can then be cast in the general form

$$\frac{dx_i}{ds} = A_{ij} x_j + g_i \quad (38)$$

where both A_{ij} and g_i are functions of s . In addition there are boundary conditions at $s = s_a$ (the ground at $z = z_0$) and $s = s_b$ (the upper boundary at $z = z_i$).

Equation (38) is inhomogeneous, which is impractical, so we use a trick to turn it into a homogeneous problem. First rewrite (38) in the form

$$\frac{dx_i}{ds} = g_i x_0 + A_{ij} x_j \quad (39)$$

which is the same as (38) provided that $x_0 = 1$, which in turn can be expressed by means of the differential equation with the solution $x_0 = 1$:

$$\frac{dx_0}{ds} = 0 \quad (40)$$

with the boundary condition

$$x_0(s_0) = 1 \quad (41)$$

In (38) j runs from 1 to n , say, but we can include x_0 as a variable and write (39) and (40) as

$$\frac{dx_i}{ds} = A_{ij} x_j \quad (42)$$

where we i and j now run from 0 to n . This only requires that we enlarge A_{ij} by defining an extra (upper) row and an extra (left) column

$$\begin{aligned} A_{0j} &= 0 & j &= 0 \dots n \\ A_{i0} &= g_i & i &= 1 \dots n \end{aligned} \quad (43)$$

Using shorthand vector/matrix notation we can write (42) as

$$\frac{d\mathbf{x}}{ds} = \mathbf{A}\mathbf{x} \quad (44)$$

The vector valued function $\mathbf{x}(s) = (x_0(s), \dots, x_n(s))$ can be thought of as a map from the interval $[s_a, s_b]$ into the complex linear space \mathbb{C}^{n+1} . Here we define the usual inner product

$$\langle \mathbf{x} | \mathbf{y} \rangle \equiv \mathbf{x}^\dagger \mathbf{y} = x_i^* y_i \quad (45)$$

where the dagger (\dagger) denotes the conjugate transpose and the asterisk denotes complex conjugation. A boundary conditions at $s = s_a$, say, can then be expressed as

$$\langle \mathbf{b} | \mathbf{x}(s_a) \rangle = c \quad (46)$$

where $c = 0$ for all the original boundary conditions while $c = 1$ for the 'extra' boundary condition $x_0(s_a) = 1$.

5.2 Linear chasing

Consider now the *dual* problem⁴

$$\frac{d\mathbf{y}}{ds} = -\mathbf{A}^\dagger \mathbf{y} \quad (47)$$

where \mathbf{A}^\dagger is the Hermitian adjoint of \mathbf{A} , i.e. $A_{ij}^\dagger = A_{ji}^*$. The dual problem is interesting because solutions to it can be used to move boundary conditions. Suppose that \mathbf{y} is a solution to (47) with the $n + 1$ boundary conditions $y(s_a) = c$ and \mathbf{x} is a solution to (44) with (46) as one of its boundary conditions. Then we have

$$\frac{d\langle \mathbf{y} | \mathbf{x} \rangle}{ds} = \langle -\mathbf{A}^\dagger \mathbf{y} | \mathbf{x} \rangle + \langle \mathbf{y} | \mathbf{A} \mathbf{x} \rangle = \langle \mathbf{y} | -\mathbf{A} \mathbf{x} \rangle + \langle \mathbf{y} | \mathbf{A} \mathbf{x} \rangle = 0 \quad (48)$$

⁴The term *auxiliary* problem is often used, but we prefer *dual*.

and it follows that

$$\langle \mathbf{y}(s) | \mathbf{x}(s) \rangle = c \quad (49)$$

holds for all value of s . Setting $s = s_b$ we therefore get a boundary condition on $\mathbf{x}(s_b)$ equivalent to the original boundary condition (46) at s_a . Note that solving (47) is relatively easy because it is an initial value problem (i.e. all boundary conditions are at the same point). Moving all boundary conditions to s_b we end up with an *initial value* problem for \mathbf{x} starting from s_b . This is the linear chasing method, which is the default method for solving linear two-point problems with NDSolve in Mathematica. A non-linear method similar to a method proposed by Gel'fand and Lokutsiyevskii in an unpublished paper is also offered. Unfortunately the documentation of the method found in the Mathematics help system does not allow us to figure out exactly what NDSolve does when this method is enforced.

Linear chasing works well in many cases, but not always. After moving all boundary conditions to s_b we need to solve a set of linear equations in order to determine the initial value $\mathbf{x}(s_b)$, and that may turn out to be numerically impossible. This can happen if two or more boundary conditions at s_a effectively translate into the same boundary condition at s_b and extraordinarily high working precision is required to distinguish the small differences. Even if an initial value $\mathbf{x}(s_b)$ can be determined the numerical solution may end up violating the boundary conditions at s_a after integrating down from s_b . This is due to the accumulation of numerical inaccuracies which tends to wipe out the 'memory' of the lower boundary conditions. Solutions to (44) may increase or decrease fast for $s \rightarrow \infty$ and we are generally interested solutions that decrease when approaching a boundary. However, when the equations are integrated upwards from s_a small numerical errors tend to excite the increasing the solutions which soon begin to dominate. We can therefore end in a situation where different boundary conditions effectively translate into only one condition because we do not have enough working precision to distinguish them. Integrating from above will excite the decreasing solutions, which is more healthy, at least for as long as s is large. But near the lower boundary the solutions once again tend to explode, and it becomes difficult to get the lower boundary conditions right. The effect of the upper boundary conditions just drown in numerical noise, and the solution seriously violate the original lower boundary conditions.

5.3 Orthogonal chasing

In section 5.2 we saw how a dual equation can be used move boundary conditions from one boundary to another. We can also use them to move boundary conditions to positions in between. If all boundary conditions are moved to the same point s we have enough conditions to determine $\mathbf{x}(s)$. So the idea is to determine $\mathbf{x}(s)$ from the conditions imposed by the dual equations. This is better than solving the original equation, as in the linear chasing methods, because the boundary conditions are enforced directly and not via 'memory' kept through long integrations.

It is most practical to work with inhomogeneous equations, hence we drop the trick with the extra variable $x_0(s)$ and go back to (38)

$$\frac{dx_i}{ds} = A_{ij} x_j + g_i \quad (50)$$

where $\mathbf{x} = (x_1, x_2, \dots, x_n)$.

We define dual variables $\mathbf{y}^p(s) = (y_1^p(s), y_2^p(s), \dots, y_n^p(s))$ where $p = 1, 2, \dots, n$ and impose the following equation on them:

$$\frac{d\mathbf{y}^p}{ds} = -\mathbf{A}^\dagger \mathbf{y}^p \quad (51)$$

Defining the square matrix

$$Y_{ij} \equiv y_i^j \quad (52)$$

we may also write (51) as

$$\frac{d}{ds} \mathbf{Y} = -\mathbf{A}^\dagger \mathbf{Y} \quad (53)$$

For each p , $\mathbf{y}^p(s)$ is used to specify a (boundary) condition on \mathbf{x} :

$$\langle \mathbf{y}^p(s) | \mathbf{x}(s) \rangle = c_p(s) \quad (54)$$

At the lower boundary $s = s_a$ the first m conditions (for $p \leq m$) should coincide with the lower boundary conditions. Thus the boundary condition $u(z_0) = 0$ can be written as $x_1(s_a) = 0$ corresponding to $\mathbf{y}(s_a) = (1, 0, 0, 0, 0, 0)$ and $c(s_a) = 0$. Without loss of generality we can assume orthogonality:

$$\langle \mathbf{y}^p(s_a) | \mathbf{y}^q(s_a) \rangle = \delta_{pq} \quad (55)$$

For $m < p \leq n$ it would seem natural to choose initial values at s_b so that $\mathbf{y}^p(s_b)$ is given by the upper boundary conditions, and integrate down from s_b to s_a . This would ensure n conditions at every s from which $\mathbf{x}(s)$ could be determined. However, in practice the n conditions tend to degenerate and sometimes a numerical solution cannot be obtained. Instead we choose some lower boundary conditions with $c_p(s_a) = 0$ for $p > m$ so that the orthogonality condition (55) extends to the whole set of \mathbf{y} s. In other words, $Y_{ij}(s_a)$ is a unitary matrix. With these initial conditions we can integrate (53) upwards and determine $\mathbf{Y}(s)$ up to a value of s which is larger than any s_b we can think of. Note that we do not have to know s_b or the form of the upper boundary conditions or the functional form of the forcing \mathbf{f} (which determines \mathbf{g}) to obtain \mathbf{Y} . This makes $\mathbf{Y}(s)$ very versatile because it only depends only on the two parameters $s_a = kz_0$ and β while it is independent of s_b and the wind turbine type which dictates \mathbf{f} . More calculations need to be done before we can determine a specific \mathbf{x} , but these calculation are relatively fast compared to calculating \mathbf{Y} , and therefore it is advantageous to store \mathbf{Y} as a look-up-table (LUT). Actually $\mathbf{x}(s)$ is used to construct the wake of a solitary turbine which is also used as a look-up-table. The tables containing \mathbf{Y} are therefore very general look-up tables from which more specific look-up-tables can be constructed. We will refer to the \mathbf{Y} tables as preLUTs - preliminary look-up tables. The preLUTs are so general that they can be made once and for all at installation.

Once $\mathbf{Y}(s)$ is known we find $\mathbf{x}(s)$ by first finding \mathbf{c} and then solving (54), which can also be written as

$$\mathbf{Y}^\dagger(s)\mathbf{x}(s) = \mathbf{c}(s) \quad (56)$$

The equation for \mathbf{c} is simply

$$\frac{dc_p}{ds} = \langle \mathbf{y}^p | \mathbf{g} \rangle \quad (57)$$

For a given turbine type the right hand side is known and the integration is fast and easy. We need an initial value which we only have for $p \leq m$ where $c_p(s_a)$ is dictated by the lower boundary conditions. We therefore integrate these equations from s_a to s_b to get $\mathbf{y}^p(s)$ for $p \leq m$. When we arrive at s_b we have m conditions in addition to the $n - m$ upper boundary conditions, which is enough to determine $\mathbf{x}(s_b)$ and subsequently calculate $\mathbf{c}(s_b) = \mathbf{Y}^\dagger(s_b)\mathbf{x}(s_b)$. Knowing $c_p(s_b)$ we can then integrate the remaining equations for $p > m$ down from s_b to s_a . This yields $\mathbf{c}(s)$ and we finally solve (56) to get $\mathbf{x}(s)$.

The algorithm outlined above illustrates the main principles, most notably the use of preLUTs which only depend on kz_0 and β , but some additional tricks are necessary to eliminate the problem with rapidly growing modes so that the matrix \mathbf{Y} becomes (almost) singular. To avoid this we use the set $\{s_j\}$ as 'stations' to divide the interval of integration $[s_a, s_b]$ into sub-intervals $[s_j, s_{j+1}]$. The same set of points was used to define chapeau functions for the forcing term. The idea is to avoid that \mathbf{y} s grow too much from one station to the next. At each station we then make a Gram-Schmidt orthonormalization and restart the integration with \mathbf{y} s that can be clearly distinguished numerically. Formally this is achieved by a so called QR decomposition

$$\mathbf{Y} = \hat{\mathbf{Y}} \mathbf{T}^\dagger \quad (58)$$

where $\hat{\mathbf{Y}}$ is a unitary matrix and \mathbf{T}^\dagger is an upper triangular matrix. The integration is restarted with the value $\mathbf{Y} = \hat{\mathbf{Y}}$ at each station. The advantage of changing to new \mathbf{y} s every

now and then is that we avoid that the \mathbf{y} s all take off in the direction of the fastest growing mode. Because \mathbf{T}^\dagger is upper triangular, the first j th column of \mathbf{Y} span the same subspace as the first j columns of $\hat{\mathbf{Y}}$. Thus \mathbf{y}^1 is just normalized at each station and will tend to grow in the direction of the fastest growing mode. When the rest of the \mathbf{y} s are forced to be perpendicular to \mathbf{y}^1 this tendency is reduced for them. Note also that we can still solve \mathbf{y}^p for $p = 1, \dots, m$ separately because they never mix with the remaining \mathbf{y}^p with $p > m$.

The condition $\mathbf{Y}^\dagger \mathbf{x} = \mathbf{c}$ translates into the condition

$$\hat{\mathbf{Y}}^\dagger \mathbf{x} = \hat{\mathbf{c}} \quad (59)$$

where

$$\hat{\mathbf{c}} = \mathbf{T}^{-1} \mathbf{c} \quad (60)$$

Note that because $\hat{\mathbf{Y}}^\dagger$ is unitary the solution to (59) is straight forward

$$\mathbf{x} = \hat{\mathbf{Y}} \hat{\mathbf{c}} \quad (61)$$

The preLUTs contain $\hat{\mathbf{Y}}(s_j)$, $\mathbf{T}^{-1}(s_j)$ and $\mathbf{T}(s_j)$ for every station s_j . In addition there are results from the integration of (57) with four different forcings: either constant or proportional to s and either longitudinal or transversal. This allows us to model any forcing which is a chapeau function with elbow points at three consecutive stations. Furthermore, in our case the boundary conditions are homogeneous in the sense that $\mathbf{c}(s_a) = 0$ and $\mathbf{c}(s_b) = 0$. If s_j is the 'central station' (i.e. $f(s_j) \neq 0$) we have $c^p(s) = 0$ for $s < s_{j-1}$ allowing us to start the integration at s_{j-1} . Integrating up to $s = s_j$ gives the response to half as chapeau function. The second half is obtained from the integrations on $[s_j, s_{j+1}]$. No more integration is needed because $c^p(s)$ remains constant for $s > s_{j+1}$. It is therefore sufficient to find the results of the integrations just from one station to the next, and store them in the preLUTs. The preLUTs therefore contain three matrices and four vectors for each station and further are indexed by the two parameters β and kz_0 .

We mentioned that it is advantageous to use a logarithmic coordinate for $s < 1$. The procedure is therefore slightly modified and some care should be taken when crossing $s = 1$. This is straight forward and we will spare the reader from further details.

5.4 Numerical integration scheme

Explicit Runge–Kutta methods with built in step size control were used for the numerical integration of (53) and (56). At first the fifth–order Runge–Kutta–Fehlberg (Cash and Karp 1990) used by Corbett et al. (2008) was tried, but found to be rather slow. A simpler third–order method described in Press, Teukolsky, Vetterling and Flannery (1992) turned out to be much faster for the same accuracy. It therefore seems as if slow convergence of the Taylor series prevents us from taking advantage of high order methods. This suggests that the Burlirsh–Stoer method (Press et al. 1992), which is based on a clever extrapolation of results from a low order scheme, could be efficient for this problem, but it was not tried since the third order scheme already worked satisfactory.

5.5 FFIT

A conventional Fast Fourier Transform (FFT) can be used to construct the wind and pressure fields from its Fourier components. FFT is a discrete transform resulting in periodic fields. The calculated wake is therefore the response to an infinite, periodic array of turbines. We want the response from a single, solitary turbine which can be approximated if we make the periodic domain large enough. In practice this means extremely large because the drag from the turbine should be negligible compared to the friction of the surface of the domain, and water is very smooth. It would be better to use a Fourier Integral Transforms, which can be regarded as the limit as the domain size goes to infinity. The problem is that we need to do a numerical Fourier integral for each point where we want output and that takes very

long time. Fortunately there is a technique where all the numerical Fourier integrals can be made in one batch which makes use of the FFT. The result is the fast Fourier integral transform (FFIT) which we now describe in more detail. For simplicity we will restrict the explanations to the 1D case which can easily be generalized to the 2D case we are interested in here. Thus the problem is to find

$$f(x) = \int_{-\infty}^{\infty} \hat{f}(k) e^{ikx} dx \quad (62)$$

for a representative set of x -values. Numerical Recipes (Press et al. 1992) offers a method which is intended for cases where \hat{f} is rather smooth and has compact support (so that the integration goes over a finite interval). We can get compact support if we restrict the calculation to the set of points $x_j = x_0 + a j$, where $j = 0, 1, \dots, n-1$ and x_0 is an offset. Then we can rewrite (62) as

$$f(x_j) = \int_0^{2\pi/a} \hat{F}(k) e^{ikx_j} dk \quad (63)$$

where

$$\hat{F}(k) = \sum_{p=-\infty}^{\infty} \hat{f}(k + 2p\pi/a) \quad (64)$$

where it in practice is sufficient to sum a finite number of terms.

We evaluate the integral as a sum using the rectangular rule. Thus we choose n equally spaced points on the k -axis k_0, k_1, \dots, k_{n-1} with $k_q = k_0 + b q$ and evaluate $f(x)$ as

$$f(x) \approx b \sum_{q=0}^{n-1} \hat{F}(k_q) e^{ik_q x} \quad (65)$$

For $x_j = x_0 + a j$ we can write (65) as

$$f(x_j) \approx b e^{ik_0 a j} \sum_{q=0}^{n-1} \left\{ \hat{F}(k_q) e^{ik_q x_0} \right\} e^{iabqj} \quad (66)$$

Taking a look at the sum we note it is of the form

$$\sum_{q=0}^{n-1} g_q e^{iabqj} \quad (67)$$

This in fact is a discrete Fourier transform for certain choices of a , b and n , namely those where

$$ab = 2\pi/n \quad (68)$$

Assuming this restriction holds we can use FFT to evaluate *all* the integrals in one go and it appears that we have a fast method. We should of course make sure that we cover a decent range of k -values and the spacing b should also be small enough to ensure an accurate evaluation of the integral. Because of (68) the only way to get b small enough is to make na large and that is the main problem with the method. Experience shows that increasing n for fixed a has little effect, hence a good resolution on the k -axis is obtained at the expense of a poor resolution on the x -axis and *visa versa*.

According to Numerical Recipes (65) is a really lousy approximation when na is not large enough. A better approximation can be made if it can be assumed that \hat{F} is slowly varying so that it can be approximated by a piecewise linear function (or more generally a higher order spline). In that case we can write \hat{F} as

$$\hat{F}(k) \approx \sum_q \hat{F}(k_q) \phi(k - k_q) \quad (69)$$

where ϕ is a triangular *chapeau* functions: $\phi(k) = 1 - |k/b|$ for $|k| < b$ and zero for $|k| > b$. The point is that with this approximation we can do (63) analytically:

$$f(x_j) \approx \sum_{q=0}^n \hat{F}(k_q) \int_0^{2\pi/a} \phi(k - k_q) e^{ikx_j} dk = bW(bx_j) \sum_{q=0}^{n-1} \hat{F}(k_q) e^{ikx_0} e^{i2\pi qj/n} \quad (70)$$

Here we notice that the sum is a Fourier sum that can be done with FFT. The so called attenuation factor W is given by

$$W(s) = \frac{2(1 - \cos s)}{s^2} \quad (71)$$

Our experience with attenuation factors is that they do not cure the main problem, which arises from the reciprocal relation (68) between a and b . Fortunately, there exists a method that eliminates this restriction. It is based on a trick due to Bailey and Swarztrauber (1991), see also Bailey and Swarztrauber (1994) and Inverarity (2002). First note that qj can be written as

$$qj = \frac{1}{2}(q^2 + j^2 - (q - j)^2) \quad (72)$$

so that (66) can be written as

$$f(x_j) \approx b e^{ik_0 a j + \frac{1}{2} i a b j^2} \sum_{q=0}^{m-1} \left\{ \hat{f}(k_q) e^{ik_q x_0 + \frac{1}{2} i a b q^2} \right\} e^{-\frac{1}{2} i a b (j-q)^2} \quad (73)$$

The sum looks like a circular convolution of two vectors of length $2n$.

$$\sum_{q=0}^{2n-1} g_q h_{j-q} \quad (74)$$

It *is* in fact a convolution if we define

$$g_q = \begin{cases} \hat{f}(k_q) e^{ik_q x_0 + \frac{1}{2} i a b q^2} & \text{for } 0 \leq q < n \\ 0 & \text{for } n \leq q < 2n \end{cases} \quad (75)$$

and

$$h_j = \begin{cases} e^{-\frac{1}{2} i a b j^2} & \text{for } 0 \leq j < n \\ e^{-\frac{1}{2} i a b (2n-j)^2} & \text{for } n \leq j < 2n \end{cases} \quad (76)$$

With the sum written in this form we can make use of FFT to do the convolution all in one go. Simply apply FFT to g and h separately, multiply and take the inverse transform. We need $2n$ points instead of n , but that's a reasonably small price to pay for the freedom to choose a and b independently.

It should be emphasized that FFIT is an approximation and that there are a number of choices to make. Approximating \hat{F} with piecewise cubic functions (instead of piecewise linear) leads to a different attenuation function. More fancy integration schemes have also been suggested, e.g. Simpson's rule (Simonen and Olkkonen 1985). FFIT can of course be used for the inverse transformation but unlike FFT we do not return to where we started when we transform back and forth. Worst of all is the lack of error estimates which means that we have little guidance in choosing a , b and n . Firmer FFIT theory is badly needed.

5.6 Code verification and accuracy issues

The numerical solver was implemented in two different programs, Preludium and Trafalgar, and a graphical user interface called Fuga was also made. Fuga takes input from the user and from WASP files containing wind turbine data and wind farm layouts and controls the execution of Preludium and Trafalgar. Fuga also calculates the wake from a whole wind farm on the basis of a solitary turbine wake. The solitary wake is made by the C program Trafalgar, which performs a FFIT on LUT data. The LUTs, containing $\mathbf{x}(z_j)$ for a range of wave vectors \mathbf{k} are made by the Fortran program Preludium which can also make preLUTs.

The complexity of the calculations and the fact that intermediate results can only be checked at a late stage in a long series of manipulations makes debugging very hard. The situation changed when an analytical solution was found for a special case. It is for the LUT with $\beta = \pi/2$. It represents the response to a vertically chapeau shaped and horizontally harmonic forcing and the analytical solutions is for the $u_1(s_c)$ where s_c is the level where the chapeau function has its maximum. For $\beta = \pi/2$ the problem reduces to a solvable Sturm–Liouville problem. When the forcing is a chapeau function with elbows at s_{c-1} , s_c and s_{c+1} we find

$$\begin{aligned}
u(s_c) &= \frac{K_0(s_c)I_0(s_b) - I_0(s_c)K_0(s_b)}{2(s_{c-1} - s_c)(K_0(s_a)I_0(s_b) - I_0(s_a)K_0(s_b))} \\
&\times (I_0(s_a) (-\pi s_{c-1}^2 L_{-1}(s_{c-1})K_0(s_{c-1}) + \pi s_{c-1} s_c L_{-1}(s_c)K_0(s_c) + s_c K_1(s_c)(\pi s_{c-1} L_0(s_c) + 2) \\
&\quad - s_{c-1}(\pi s_{c-1} L_0(s_{c-1}) + 2)K_1(s_{c-1})) \\
&\quad + K_0(s_a) (s_{c-1}^2 (\pi L_1(s_{c-1}) + 2)I_0(s_{c-1}) - s_{c-1} s_c (\pi L_1(s_c) + 2)I_0(s_c) + s_c I_1(s_c)(\pi s_{c-1} L_0(s_c) + 2)) \\
&\quad - s_{c-1} K_0(s_a)(\pi s_{c-1} L_0(s_{c-1}) + 2)I_1(s_{c-1})) \\
&+ \frac{K_0(s_a)I_0(s_c) - I_0(s_a)K_0(s_c)}{2(s_{c+1} - s_c)(K_0(s_a)I_0(s_b) - I_0(s_a)K_0(s_b))} \\
&\times (I_0(s_b) (-\pi s_{c+1}^2 L_{-1}(s_{c+1})K_0(s_{c+1}) + \pi s_{c+1} s_c L_{-1}(s_c)K_0(s_c) + s_c K_1(s_c)(\pi s_{c+1} L_0(s_c) + 2) \\
&\quad - s_{c+1}(\pi s_{c+1} L_0(s_{c+1}) + 2)K_1(s_{c+1})) \\
&\quad + K_0(s_b) (s_{c+1}^2 (\pi L_1(s_{c+1}) + 2)I_0(s_{c+1}) - s_{c+1} s_c (\pi L_1(s_c) + 2)I_0(s_c) + s_c I_1(s_c)(\pi s_{c+1} L_0(s_c) + 2)) \\
&\quad - s_{c+1}(\pi s_{c+1} L_0(s_{c+1}) + 2)I_1(s_{c+1})K_0(s_b))
\end{aligned} \tag{77}$$

where I_n and K_n are modified Bessel functions of the first and second kind, respectively and L_n is a modified Struve function. An analytical expression for $u(s)$ with $c \neq s_c$ exists, but it is too complicated to write down here. The solution was found with the aid of Mathematica, and Mathematica can also be used to evaluate the expression. This is a bit tricky because some of the terms can get very large while almost cancel each other. Mathematica therefore sometimes give up due to lack of precision, but it was possible to get representative values to compare with numerical values generated from preLUTs. The comparison of numerical and analytical results is very satisfactory indeed, not worse than a relative accuracy of 10^{-6} , i.e. 6 significant digits. This is much better than expected from the conservative error estimates used for error control. The agreement is so substantial that it must be safe to declare major parts of the code bug free. We note that a similar analytical solution can be found for the mixing length closure and a similar good accuracy of the numerical solution is found. We did not manage to find analytical solutions for the $E - \varepsilon$ closure.

Figure 5 shows a 3D 'blanket plot' of $\text{Re } u^1(s_a)$. The analytical solution is the intersection between the blanket and the right, vertical face. The curve on the left, vertical face was obtained from a (very long) analytical expression representing the limit $kz \rightarrow 0$. The fact that the numerical solution connects smoothly to this theoretical limit is a further check of the correctness of the numerical solution.

Although there are strong indications that the look-up tables are accurate, the accuracy of the final result also depends other factors as well. Inaccuracies sneak in when we make interpolations in the tables and when the FFIT is applied. The interpolation errors are probably most severe. This could be the cause of the tiny, but spurious, oscillations seen in the calculated velocity profiles. Perhaps the simple bi-linear interpolation scheme used by the Trafalgar module in Fuga should be replaced with something better.

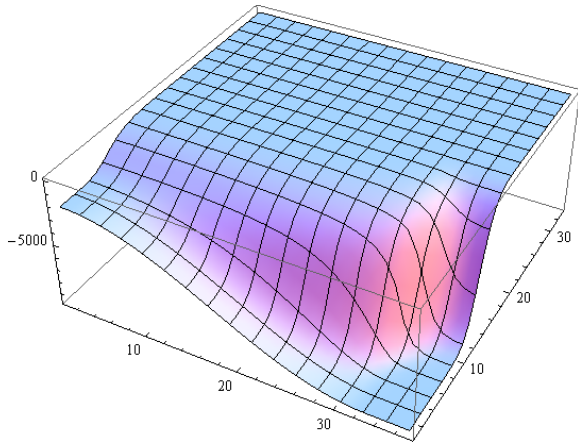


Figure 5. Numerical results for $\text{Re } u^1(s_c)$. The text explains further.

6 Validation against data

In this section we present validations of the model (Fuga version 1.3) against data using three different datasets. Two of the sets are production data from the offshore wind farms Horns Rev I and Nysted and a third contains velocity measurements in the wake of an onshore turbine placed in homogeneous terrain.

The offshore data were extracted from the database generated within the UpWind project (Hansen, Barthelmie, Cabezon and Politis 2008, Barthelmie, Frandsen, Rathmann, Hansen, Politis, Prospathopoulos, Schepers, Rados, Cabezn, Schlez, Neubert and Heath 2011). They have also been used within the TOPFARM project (Hansen 2009). The data consist of production data for all turbines in the park averaged over a 1m/s wide free wind speed interval in five degree wind direction bins. The wind direction bins were centered around a 'critical' direction, where the wind is parallel with the rows. This happens for direction 278° at Nysted and 270° at Horns Rev I. The extracted data set is based on raw data measured up to November 2009, thus including more raw data than e.g. Barthelmie, Rathmann, Frandsen, Hansen, Politis, Prospathopoulos, Rados, Cabezon, Schlez, Phillips, Neubert, Schepers and van der Pijl (2007). For each turbine care has been taken only to select periods where all relevant upwind turbines are producing. Extra selection criteria were imposed requiring the preceding 10 minute period to fall within the same wind speed and wind direction bins (Hansen 2009). This was done in order to filter out data for situations where the wind was changing too much in time or space.

We need the surface roughness z_0 and the inversion (lid) height z_i as input to the model. For the offshore cases $z_0 = 0.1\text{mm}$ was used. The value is based on (15) using $A_{\text{Ch}} = 0.012$ as determined by Peña and Gryning (2008) for Horns Rev 1 met mast data. Via (16) this corresponds to $\text{Ti}=7.4\%$. The same value was used for Nysted, but $z_0 = 0.2\text{mm}$ could also be justified. In all cases the inversion height was set to $z_i = 400\text{m}$. This is an average offshore value, but choosing $z_i = 1000\text{m}$ does not change the results very much and would not lead to any changes of conclusions.

Very narrow wind directions bins, only two degrees wide, have been used for production data, e.g. Barthelmie et al. (2007) and Frandsen et al. (2009). The intension has been to use the multiple wake situation as a model test case. There are several problems with this. Firstly, the experimental data series is not stationary, hence it could be relevant to represent a ten minutes series as a mixture of realizations with different mean values. If so the only way to compare a model with data is to make several runs for a range of mean directions and make an appropriate, weighed average of the results. A theory that could tell us how to make such an average is unfortunately lacking. Secondly, we feed the models with a horizontally

homogeneous free wind, but in reality conditions are not strictly homogeneous over a 5–6 km wide wind park. The stationarity selection criterion is an attempt to compensate for this. We don't know how successful this compensation is, but it seems unlikely that it can guarantee uniformity to within two degrees. Finally, for Horns Rev the wind direction was taken from the yaw angle of one of the western turbines. This was done because the wind vane at met mast M2 was not working while the vanes on M6 and M7 were disqualified because they were located in the wake. It is therefore possible that narrow wind direction bins correspond to fairly wide model input bins, and that the experimental data contain very few multiple wake situations. Due to these uncertainties we will only use wide bins covering 15, 25 and 35 degrees. This should make a more fair comparison because relatively fewer wind directions are 'misplaced' in the wide bins. The averages were taken from model results with wind directions in one degree steps, which is close enough to represent a continuum.

Inhomogeneity seems to be a worse problem for Nysted than for Horns Rev. Nysted is located about 5 km to the South of Lolland and with more islands further to the East. In westerly winds it is characteristic that the turbines generally produce less energy the nearer they are to the coast. The wind speed bins were selected according to the production of one of the turbine in the front row. This turbine therefore served as anemometer. It might have been better to estimate free stream velocities in a way that takes spatial variations across the farm into account, but that is easy to say in hindsight. Horns Rev I is located about 12km to the West of Jutland and with the whole North Sea acting as fetch for westerly winds. This should result in more homogeneous flow field and a much better agreement between productions from turbines in the first, undisturbed row is in fact seen. This might explain a somewhat better model performance for Horns Rev I than for Nysted.

Three linearized models were tested. They are based on 1) the simple closure, 2) the mixing length closure and 3) the $E-\varepsilon$ closure. The following set of model constants for the $E-\varepsilon$ model were suggested by Gribben (2010)

$$C_\mu = 0.0293 \quad \sigma_E = 1 \quad \sigma_\varepsilon = 0.8 \quad C_{\varepsilon 1} = 1.44 \quad C_{\varepsilon 2} = 2.67 \quad (78)$$

Figure 6a–c shows that the three closures give quite different results. The results for the simple closure are very close to the measured productions for the two widest bins, while they fall below the measurements for the 15 degree bin. It could be a bin size effect, but it could also be a genuine flaw of the model. The mixing length closure is less successful, consistently over-predicting the production. The $E-\varepsilon$ closure consistently under-predicts the production. The same trends can be seen in the comparisons with data from the Nysted wind farm in figure 7. The simple closure again performs best, and this time the results for the 15 degree bin look better. The mixing length closure again consistently over-predicts the production. The $E-\varepsilon$ closure reproduces the measured energy production in the second row almost exactly, but it vastly under-predicts the energy production in the downwind parts of the farm.

A comparison was also made with wake data for the Nibe B turbine published by Taylor (1990). The turbine is placed onshore 1km to the East of a coast line extending N–S. Data were taken for southerly winds where the upwind fetch is flat, rural terrain. The case is interesting because of the larger roughness. According to the data report it is as large as 10cm, while Hassan, Taylor and Garrad (1988) has $z_0=4$ cm. Both estimates appear to be based on fits to velocity profile data. The reported turbulence intensity around 10–15% would suggest a lower value around $z_0=1$ cm. For wake calculations it is more important to reproduce the correct turbulence level than the correct velocity profile, because the decay of the wake is governed by turbulent mixing. We have therefore chosen $z_0=1$ cm.

Figure 8a–c shows the comparison. It appears that none of the closures capture the near wake at $x = 2.5D$. We cannot expect linearized models to do that. However, at the two longer distances $x = 4D$ and $x = 7.5D$ the results tend to be more reasonable. All the models under-predict the deficit, but the simple model makes the best performance, both with respect to the width and the depth of the wake. The mixing length closure predicts practically the same (slightly too narrow) width as the simple model, but the wake is more

shallow than the data. Finally the $E-\varepsilon$ closure over-predicts the width and under-predicts the depth. For higher values of z_0 all the closures would yield even more shallow velocity deficits and all would make poorer performances, but the simple closure would still be best.

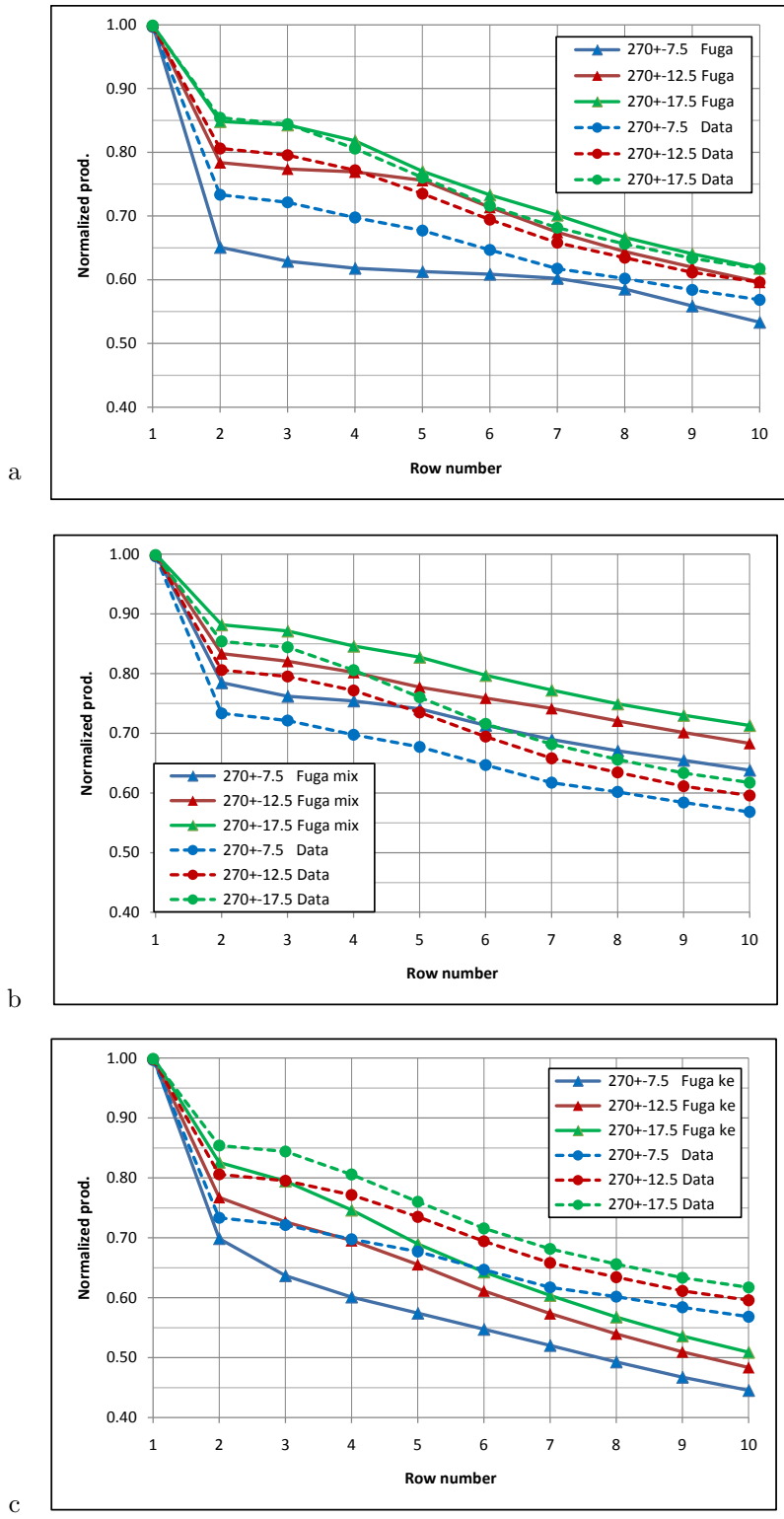


Figure 6. Comparison of Fuga results with data from the Horns Rev I wind farm. $U=10\text{m/s}$, $z_0=0.1\text{mm}$, a: simple closure. b: mixing length closure. c: $E-\varepsilon$ closure.

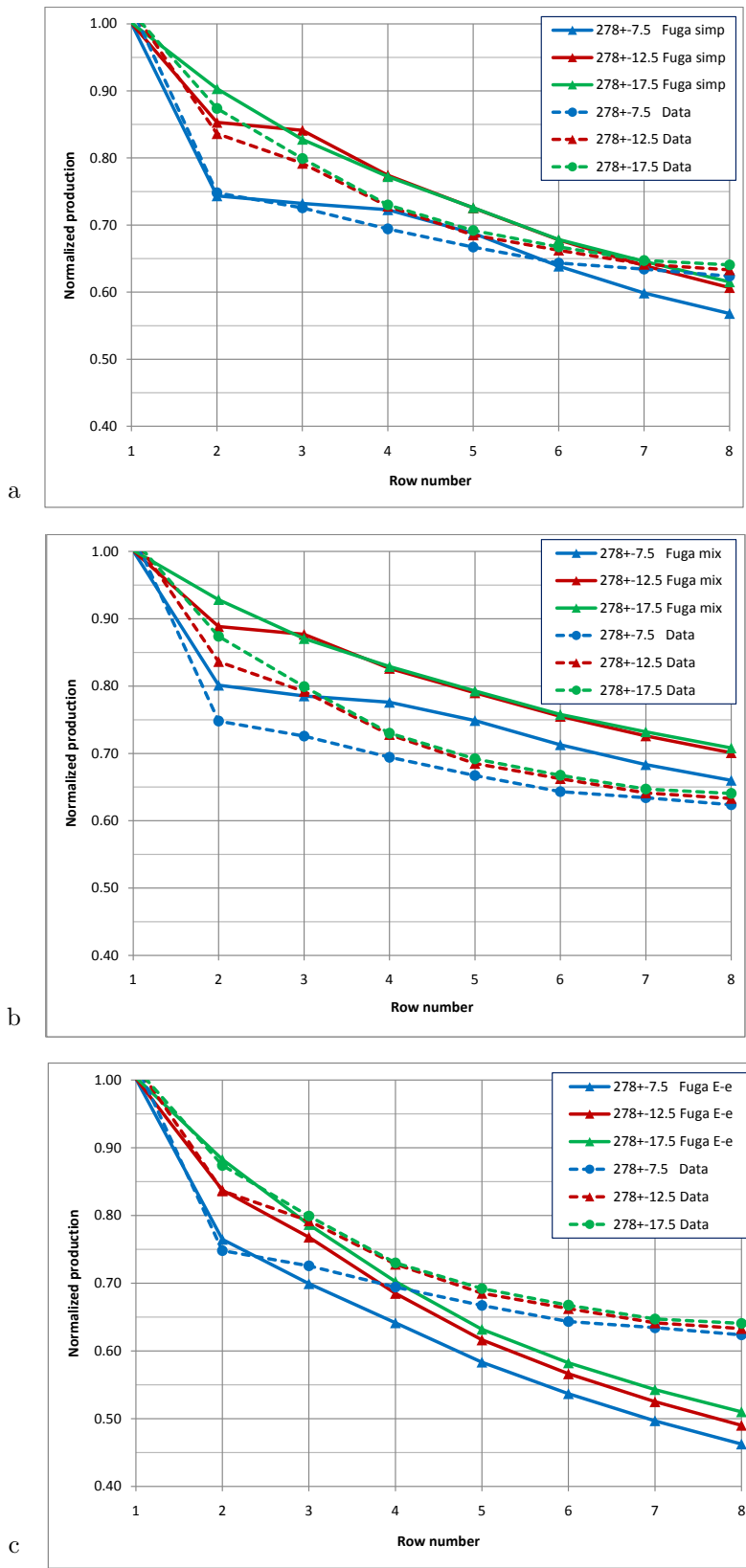


Figure 7. Comparison of Fuga results with data from the Nysted wind farm. $U = 8\text{m/s}$, $z_0=0.1\text{mm}$, a: simple closure. b: mixing length closure. c: $E-\epsilon$ closure.

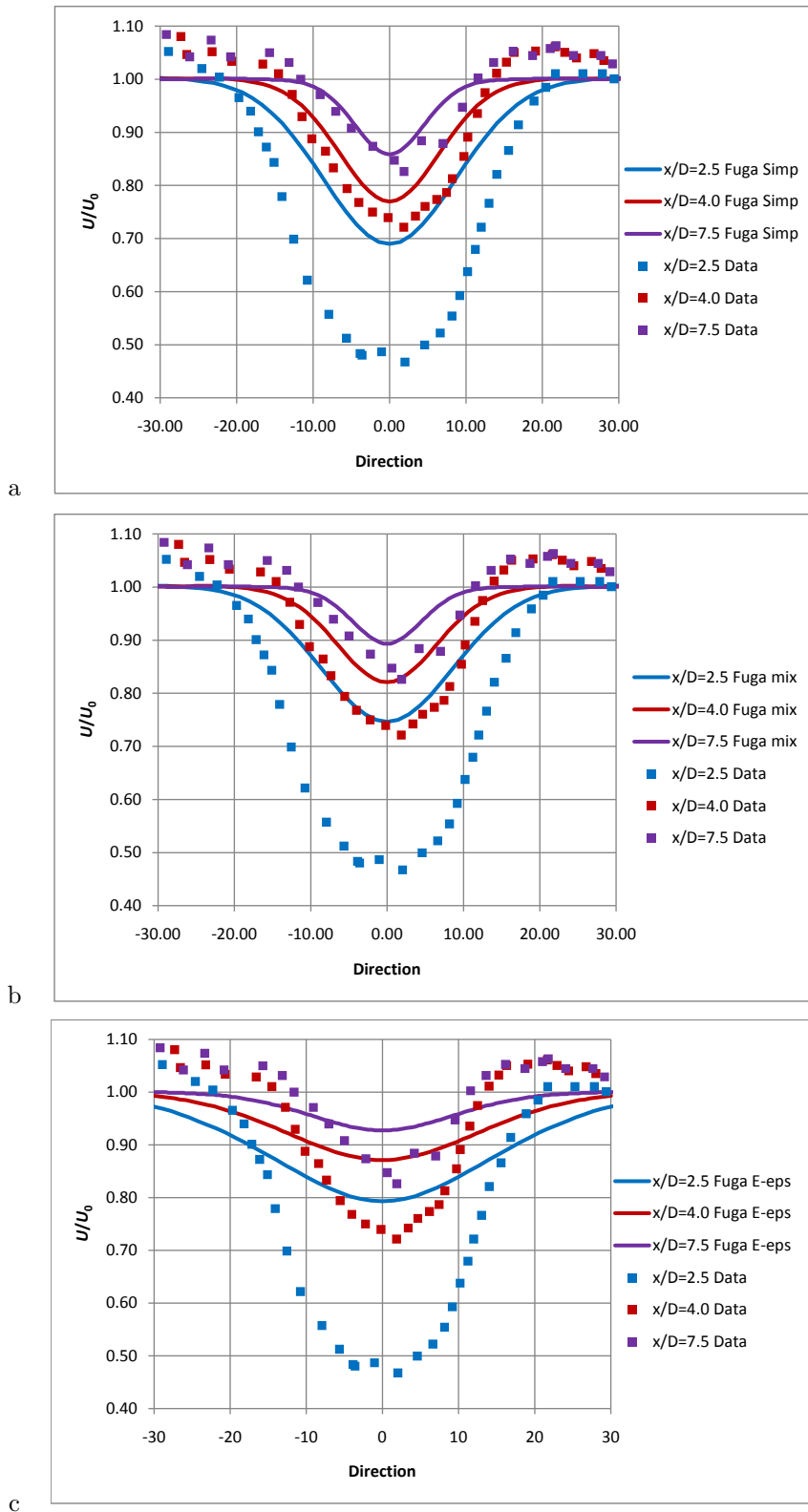


Figure 8. Comparison of Fuga results with data for a solitary Nibe B turbine. $U = 8.55$ m/s, $z_0 = 1$ cm, $C_T = 0.82$, a: simple closure, b: mixing length closure, c: $E-\epsilon$ closure.

7 Inter farm shadow effects

7.1 Farm wake validation

The long-range behaviour of the model is obviously important if the model is to be used to estimate shadow effects between wind farms. Not much data has been available for validations, but the met mast data from Horns Rev 1 can be used. For westerly winds met masts M6 and M7 are in lee of the farm and the reduction of wind speed has been measured, see figure 9. Data were selected from the same periods as in the validation of production predictions in Section 6. Thus wind direction data were inferred from the yaw angle of turbine 07 (green dot in figure 9). The yaw angle is related to the wind direction through the action of the control system in a complicated way, so the method adds an unknown amount of uncertainty to the wind direction data. The bin size of five degree is therefore probably too small so that many measurements may have ended up in the 'wrong' bin.

Data for free wind speeds of 8 m/s and 10m/s are shown in figure 10. M6 is located 2 km behind the last row in the farm. For M7 the distance is 6 km. At M6 the model yields a pronounced peak around 270 degree which is hard to see in the data. This is probably due to the uncertainty in the binning of the data. The reason why the peak is positive is that the met masts are not located exactly behind an West-East row of turbines, but between two rows. The wakes from the two turbine rows therefore tend to miss M6 when the wind direction is exactly 270. The model therefore predicts more shadow effect for the two neighbouring bins at 265 and 275 where the mast is hit more directly by individual wakes. It is likely that the model exaggerates the peak because in reality meandering will blur the picture. At M7 the peak has disappeared leaving an almost perfect agreement between model and measurements. This demonstrated the model's ability to predict wind farm wakes, at least out to distances out to about 6 km.

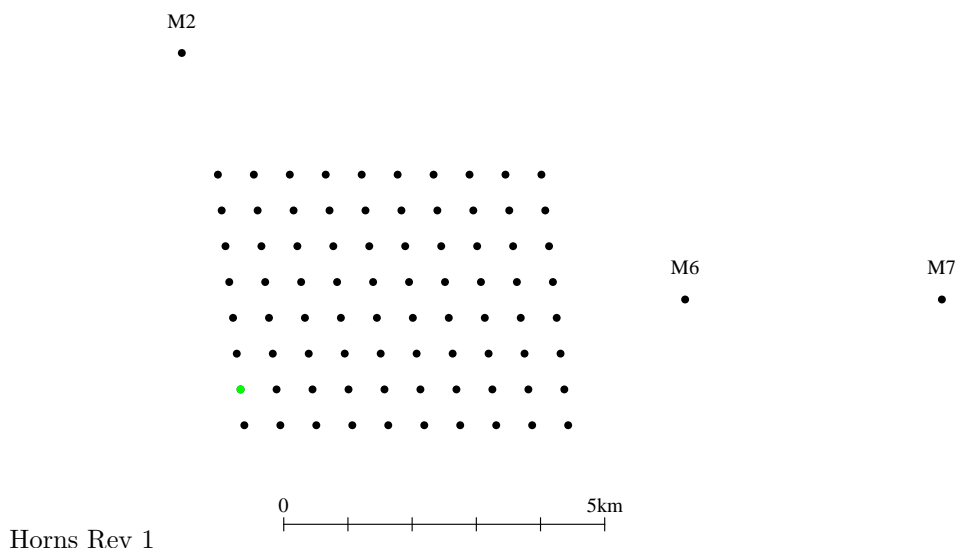
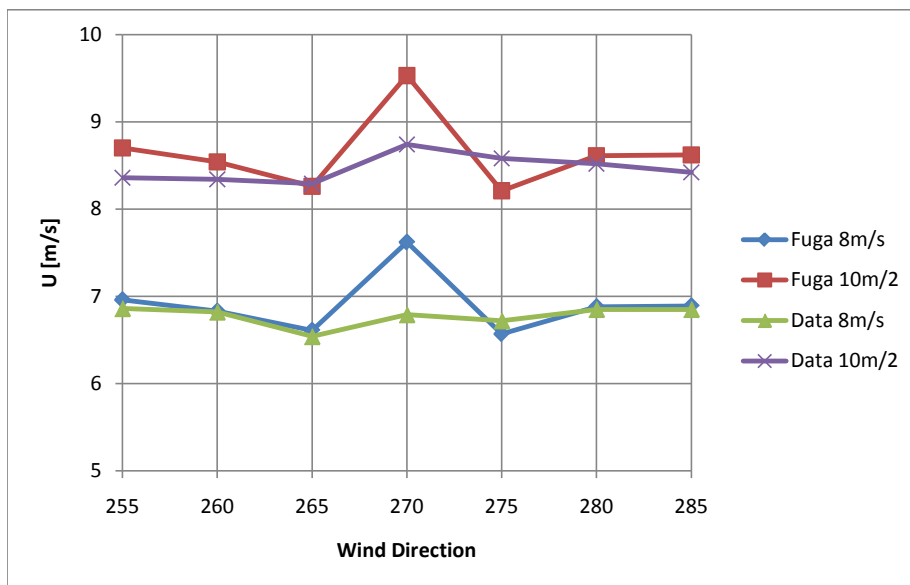


Figure 9. Layout of Horns Rev 1 showing wind turbines and met masts. Production and yaw angle from turbine 07 (green dot) was used to estimate wind speed and wind direction.

M6



M7

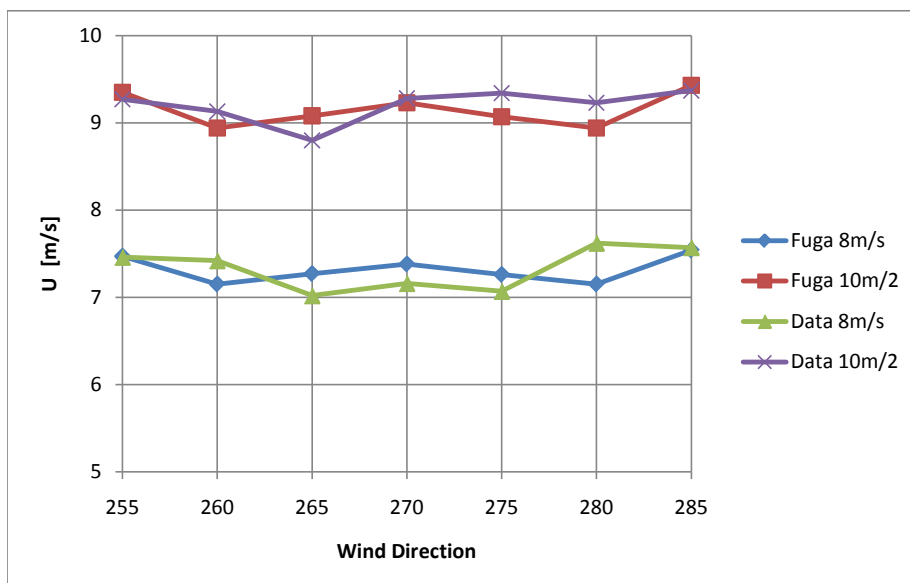


Figure 10. Measured and predicted wind speeds at the two met masts in the lee of Horns Rev 1 for westerly winds. Data and predictions were collected in 5 degree bins.

7.2 A case study: Rødsand 1 and 2

The ability of the model to predict farm-to-farm shadow effects is illustrated below by way of an example. We have chosen the Nysted and Rødsand 2 wind farms, which are two offshore farms located relatively close to each other, see figure 11. Nysted wind farm was finished in December 2003 and consists of 72 Bonus 2.3 MW turbines with 80 m rotor diameter and 69 m hub height. It is placed in an area called Rødsand (with red sand) and has therefore sometimes been referred to as Rødsand 1. Rødsand 2 consists of 90 Siemens 2.3 MW turbines with 93 m rotor diameter and 68.5 m hub height. It started operating in August 2010.

Production data for the period where both farms have been operating are, unfortunately, not yet available. Therefore we cannot make a validation exercise at this point, but must suffice with certain predictions.

The present (June 2011) version of the Fuga program does not allow for different turbine types. Predictions of shadow effects between the two farms can therefore only be made if the same turbine type is assumed for both farms. However, an implementation in the form of a Mathematica notebook exists which can cope with different turbine types, and it is this version that has been used to produce the results that follow.

The distance between the two wind farms is only 3 km, and judging from the wind rose (figure 12), Rødsand 1 should often be in the wake of Rødsand 2. The shadow effect of Rødsand 2 is illustrated in figure 13 which shows the net energy production of Rødsand 1 with and without Rødsand 2 as a function of wind speed. The model was run for 360 directions and results were subsequently collected in 5 degree bins. In the calculations the free windspeed at hub height is fixed at 10 m/s and the roughness is set to 0.1 mm. There is not much shadow effect except for westerly winds. Here the net power reduction amounts to as much as 30% of the free stream value. Figure 14 shows similar graphs for an WestEast line of turbines in Rødsand 1. The line is shown with red dots in figure 11. The most severe power reduction is found for a5 located closest to Rødsand 2. The worst case for a5 is a normalized loss of 60%. The production of a5 averaged over the sector $270^\circ \pm 15^\circ$ is reduced by 42%. For the same sector h5, the most easterly turbine in the line, suffers a reduction of only 14%, much less than the 38% at h5 caused by the other Rødsand 1 turbines, but still not negligible. In all other 30 degree sectors the production losses are rather small and the total loss of annual power production from Rødsand 1 is less than 5%.

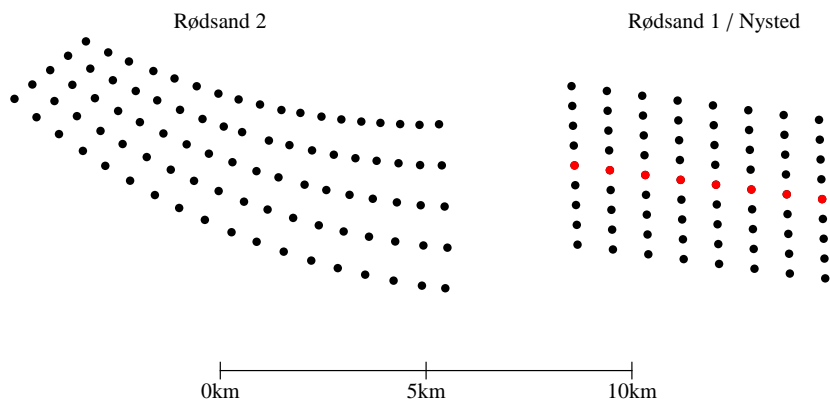


Figure 11. Layout and positioning of Nysted/Rødsand 1 and Rødsand 2 wind farms. The red dots are the turbines used for figure 14

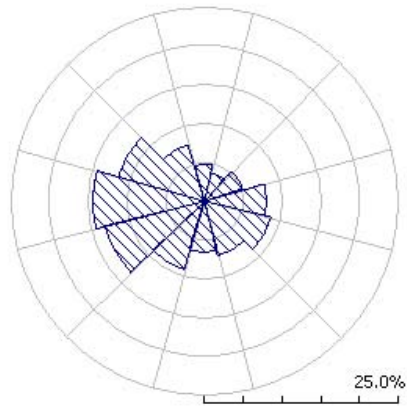


Figure 12. Wind rose for Rødsand.

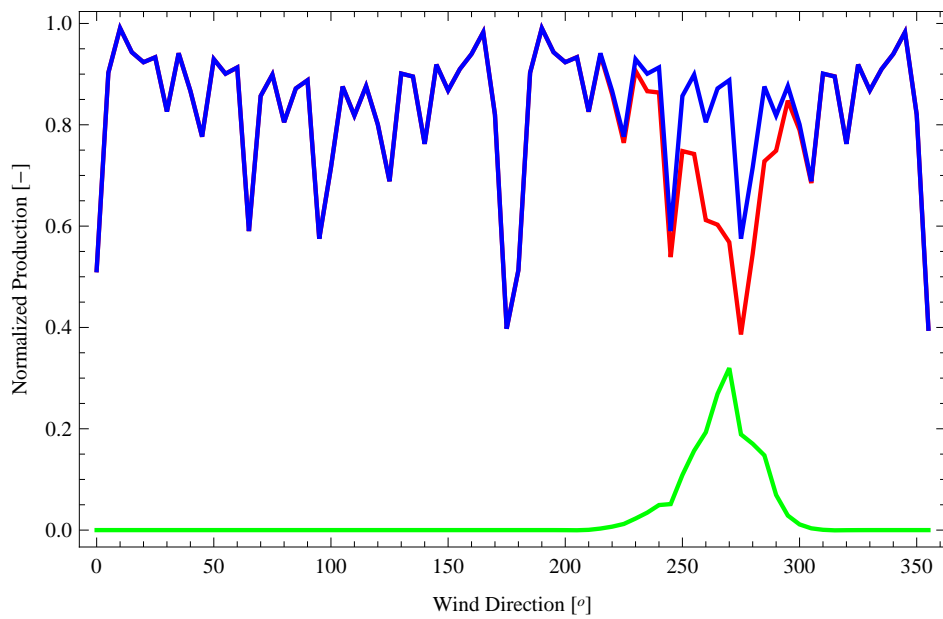


Figure 13. Net production of Rødsand 1 at 10 m/s normalized with free stream value as a function of wind direction. Blue line: without Rødsand 2. Red line: with Rødsand 2). Green line: Normalized power reduction.

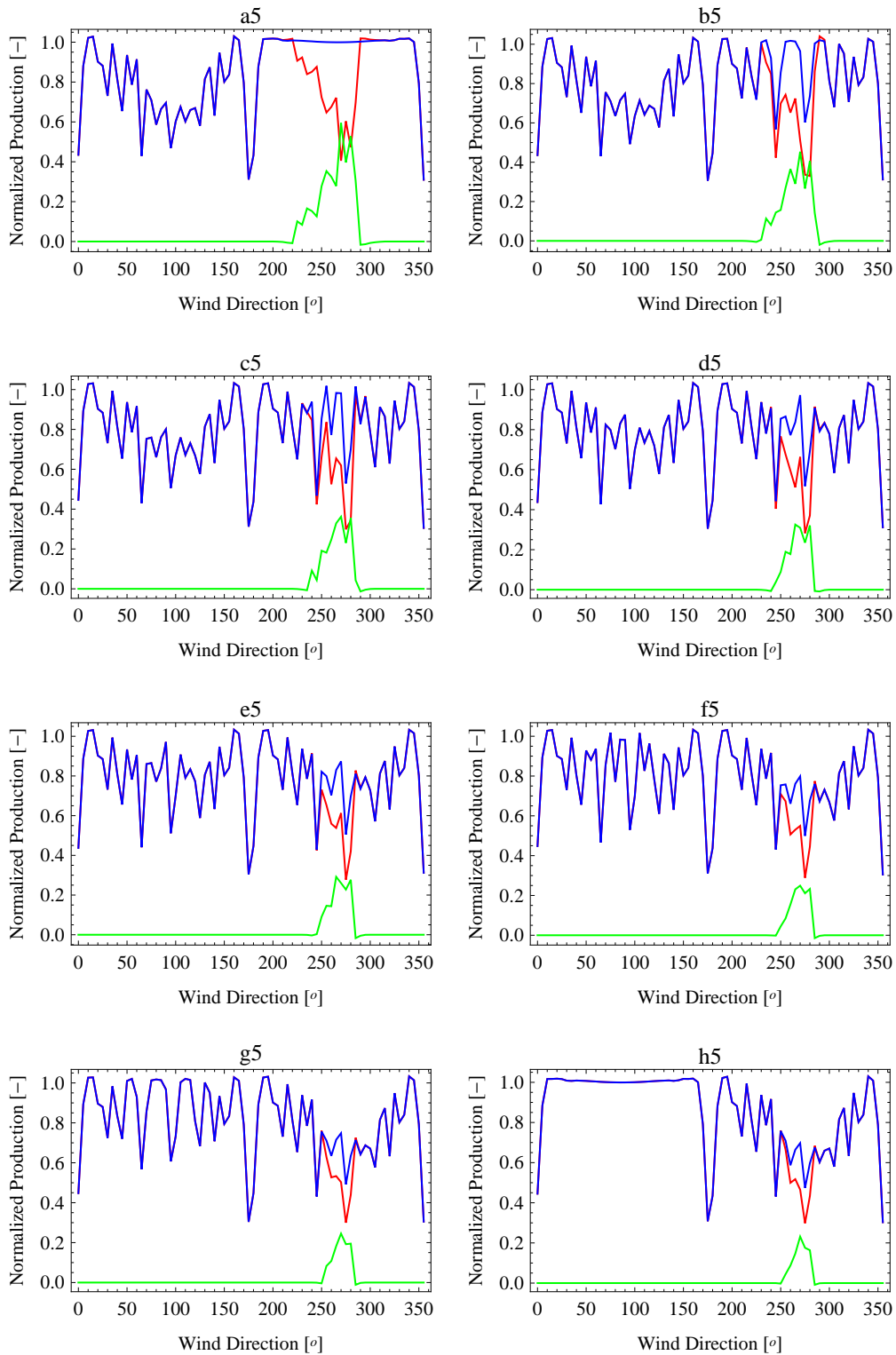


Figure 14. As in fig. 13 except for the line of individual turbines marked with red dots in fig. 11. Turbine identifiers listed from West to East are: a5, b5, c5, d5, e5, f5, g5 and h5.

8 Conclusions

A general linearization procedure has been suggested that applies to any set of CFD equations. The resulting linear equations are further simplified by using a mixed-spectral formulation. This breaks the problem up into independent sets of coupled, ordinary differential equations for which a new solution technique is suggested. The method involves the use of pre-calculated look-up tables which considerably speeds up the solution. The linearized model is typically about 10^6 times faster than the CFD model which it was constructed from.

Three different closures have been tried: the 'simple', the mixing length and $E - \varepsilon$. A validation exercise with production data from the Horns Rev 1 and Nysted wind farms and wake measurements from the Nibe turbines shows that the simple closure is clearly superior to the two other closures. This closure is therefore suggested for future, commercial versions of Fuga. The simple closure further validated against direct measurements in the wake of Horns Rev 1 taken with met masts M6 and M7 in the lee of the farm. The predictions are in almost perfect agreement with the measurements.

The agreement with data collected in narrow wind direction bins is, however, not very good. The problem arises when the wind comes straight down turbine rows. In such situations the model tends to exaggerate the wake losses caused by multiple wakes that accumulate momentum deficit from several turbines. At the same time the data are probably not binned very accurately because the wind direction is inferred from the yaw angle of one of the turbines (wind vane data were not reliable). This leads to less pronounced variations with the (ten minutes average) wind direction in the production data than in the model results. Imperfect data is part of the problem, but it is not the whole explanation. It is most likely that meandering should be allowed to smear out the model results. The wakes produced by the model are very straight in contrast to real wakes. The wakes made in LES simulations by Calaf, Meneveau and Meyers (2010), which are adjusted to offshore roughness, show considerable meandering, and it appears to be very unlikely to have more than double wakes. In other words, the wake from a turbine from time to time hits the next downwind turbine to form a double wake, but the double wake only very seldom hits the next turbine to form a triple wake, even if the mean wind points in that direction. This behaviour is caused by large scale eddies, larger than the wake cross section, that twist and turn the wake centreline. The RANS models we have linearized, on the other hand, only have one length scale and therefore cannot distinguish between large scale eddies that produce meandering, and small scale eddies that produce mixing. In the 'simple' closure the eddy viscosity is set equal to the unperturbed value in a statistically homogeneous and stationary background flow field. The eddy viscosity is therefore essentially determined by the mean vertical momentum flux, which is not very much influenced by meandering, since meandering is dominated by side-to-side motion. Large scale eddies that cause meandering are therefore not present in the model universe and meandering effects will have to be added in order to interpret model results in a real world context. We should allow for some random variations added to the straight centrelines of the calculated wakes.

Fuga is useful for the prediction of power production. The model's neglect of meandering makes predictions more sensitive to the wind direction than data can account for. However, the annual production is not so much affected by this. Multiple wake situations are, after all, not very common, and although the model probably predicts too much penalty in multiple wake situations, it also predicts too little penalty in situations where the wakes are not predicted to hit downwind rotors, but meandering in reality sometimes makes it happen from time to time.

The inclusion of meandering effects will be the next step in the development of Fuga. The influence of atmospheric stability and non-uniform terrain are other aspects that will be subject to future work.

9 Acknowledgements

This work was funded by

- Danish Public Service Obligation (PSO) as part of the WindShadow project (Energinet.dk 10086)
- The European Commission in the framework of the Non Nuclear Energy Programme Sixth Framework, Contract REN07/FP6EN/S07.73680/038641 (TOPFARM - Next Generation Design Tool for Optimization of Wind Farm Topology and Operation)
- Carbon Trust as part of the *Offshore Wind Accelerator* project

Notation

Variable	Explanation
A_{Ch}	Charnock constant
A_{ij}	Matrix in the standard form the linearized equations
C_T	Thrust coefficient
$C_{\varepsilon 1}$	E - ε model constant
$C_{\varepsilon 2}$	E - ε model constant
C_μ	E - ε model constant
C_ε	E - ε model constant = $\sqrt{\frac{C_\mu}{\sigma_\varepsilon(C_{\varepsilon 2} - C_{\varepsilon 1})}}$
D	Rotor diameter
F	Drag force = $-T$
f	= F/ρ
K	Eddy viscosity
k	Horizontal wave number = $ \mathbf{k} $
\mathbf{k}	Wave number vector = $(k_1, k_2, 0) = k(\cos \beta, \sin \beta, 0)$
l_m	Mixing length
P	Pressure
p	= $P/\rho - \frac{1}{3}\tau_{jj}$
Q^*	The complex conjugate of the quantity Q
Q^\dagger	Complex conjugate transpose of the matrix Q . $(Q^\dagger)_{ij} = Q_{ji}^*$.
R	Rotor radius
s	kz
S_{ij}	Rate of strain tensor, cfr. (7)
t	$\log \frac{z}{z_0}$
T	Thrust
Ti	Turbulence intensity = $\frac{\sigma_u}{U}$
U_{free}	Free stream velocity at hub height
u_*	Friction velocity
\mathbf{u}	Mean velocity field = $(u, v, w) = (u_1, u_2, u_3)$
\mathbf{u}^0	Unperturbed velocity = $(u^0(z), 0, 0)$
\mathbf{u}^1	First order perturbed velocity = $(u^1, v^1, w^1) = (u_1^1, u_2^1, u_3^1)$
(x, y, z)	Coordinates: x -axis downwind, z -axis upwards
\mathbf{x}	Linear variables = e.g. (u, u', v, v', w, p)
\mathbf{y}^q	Dependent variable in the dual equation for the q th boundary condition
\mathbf{Y}	$Y_{ij} = y_i^j$
z_h	Hub height
z_0	Surface Roughness
β	Angle from \mathbf{u}^0 to \mathbf{k}
κ	von Karman constant = 0.4
ν	Molecular viscosity
ρ	Air density
σ_E	E - ε model constant
σ_ε	E - ε model constant
τ_{ij}	Reynolds stress tensor = $-\langle u'_i u'_j \rangle$
ξ	Expansion parameter for perturbation series

References

- Bailey, D. H. and Swarztrauber, P. N.: 1991, The fractional fourier transform and applications, *SIAM Review* **33**, 389–404.
- Bailey, D. H. and Swarztrauber, P. N.: 1994, A fast method for the numerical evaluation of continuous fourier and laplace transforms, *SIAM J. Sci. Comput.* **15**, 1105–1110.
- Barthelmie, R., Frandsen, S. T., Rathmann, O., Hansen, K. S., Politis, E. S., Prospathopoulos, J., Schepers, J. G., Rados, K., Cabezn, D., Schlez, W., Neubert, A. and Heath, M.: 2011, Flow and wakes in large wind farms:final report for upwind wp8, *Technical Report Risø-R-1765(EN)*, Risø-DTU.
- Barthelmie, R. J., Rathmann, O., Frandsen, S. T., Hansen, K. S., Politis, E., Prospathopoulos, J., Rados, K., Cabezon, D., Schlez, W., Phillips, J., Neubert, A., Schepers, J. G. and van der Piljl, S.: 2007, Modelling and measurements of wakes in large offshore wind farms, *Conference on the science of making torque from wind*, Journal of Physics Conference Series, Vol. 75, 012049., Danish Technical University, p. 8 p.
- Belcher, S. E., Jarram, N. and Hunt, J. C. R.: 2003, Adjustment of a turbulent boundary layer to a canopy of roughness elements, *J. Fluid Mech.* **488**, 369–398.
- Calaf, M., Meneveau, C. and Meyers, J.: 2010, Large eddy simulations study of fully developed wind-turbine array boundary layers., *Physics of Fluids* **22**, 015110.
- Cash, J. R. and Karp, A. H.: 1990, A variable order runge-kutta method for initial value problems with rapidly varying right-hand sides, *Transactions of Mathematical Software* **16**, 201–222.
- Charnock, H.: 1955, Wind stress on a water surface, *QJRMS* **81**, 639–640.
- Corbett, J.-F.: 2007, Ramsim: A fast computer model for mean wind flow over hills., *Technical Report Risø-PhD-17*, Ph. D. thesis from Copenhagen University, Denmark. Available from Risø National Laboratory.
- Corbett, J.-F., Ott, S. and Landberg, L.: 2008, A mixed spectral–integration model for neutral mean flow over hills, *Boundary-Layer Meteorol.* **128**, 229–254.
- Frandsen, S. T., Jørgensen, H. E., Barthelmie, R. J., Rathmann, O., Badger, J., Hansen, K., Ott, S., Rethore, P.-E., Larsen, S. E. and Jensen, L.: 2009, The making of a second-generation wind farm efficiency model-complex, *Wind Energy* **12**, 445–458.
- Gribben, B.: 2010. Private communication. The constants were suggested by Carbon Trust in connection with the Offshore Wind Accelerator project.
- Hansen, K. S.: 2009, Analysed data for the topfarm project. Private communication.
- Hansen, K. S., Barthelmie, R. J., Cabezon, D. and Politis, E.: 2008, Wake measurements used in the model evaluation. Deliverable D8.1 of the UpWind project.
URL: <http://www.upwind.eu/Shared%20Documents/WP8%20-%20Flow/D8.1%20-%20Wake%20measurements%20used%20in%20the%20model%20evaluation.pdf>
- Hassan, U., Taylor, G. J. and Garrad, A. D.: 1988, The dynamic response of wind turbines operating in a wake flow, *Journal of Wind Engineering and Industrial Aerodynamics* **27**, 113–126.
- Inverarity, G. W.: 2002, Fast computation of multidimensional fourier integrals., *SIAM J. SCI. COMPUT.* **24**, 645–651.
- Kasmi, A. E. and Masson, C.: 2008, An extended k - ε model for turbulent flow through horizontal-axis wind turbines, *J. of Wind Eng. and Ind. Aerodyn.* **96**, 103–122.

- Ott, S. and Nielsen, M.: 2010, Fuga files and scripts. Note on Fuga input and output files and how to run batch mode. Fuga documentation file FilesAndScripts.pdf.
- Panofsky, H. A. and Dutton, J. A.: 1984, *Atmospheric Turbulence*, John Wiley & Sons, New York.
- Peña, A. and Gryning, S.-E.: 2008, Charnock's roughness length model and non-dimensional wind profiles over the sea, *Boundary-Layer Meteorology* **128**, 191–203.
- Prandtl, L.: 1925, Über die ausgebildete Turbulenz, *Zeitschrift für Angewandte Mathematik und Mechanik* **5**, 136–139.
- Press, W. H., Teukolsky, S. A., Vetterling, W. T. and Flannery, B. P.: 1992, *Numerical Recipes*, 2nd edn, Cambridge University Press.
- Rados, K., Prospathopoulos, J., Stefanatos, N., Politis, E., Chaviaropoulos, P. and Zervos, A.: 2009, CFD modeling issues of wind turbine wakes under stable atmospheric conditions, *EWECC 2009*.
- Réthoré, P.-E.: 2009, Wind turbine wake in atmospheric turbulence., *Technical Report AAU-DCE Thesis No. 22*, Ph. D. thesis from Aalborg University & Risø-DTU, Denmark. Available from Risø National Laboratory: RIS-PhD-53(EN).
URL: <http://windenergyresearch.org/?p=115H>
- Réthoré, P.-E., Sørensen, N. and Bechmann, A.: 2010, Modelling issues with wind turbine wake and atmospheric turbulence., *TORQUE Conference proceedings*.
URL: <http://windenergyresearch.org/?p=76H>
- Sanz, C.: 2003, A note on $k - \epsilon$ modelling of vegetation canopy air-flows, *Boundary-Layer Meteorology* **108**, 191–197.
- Simonen, P. and Olkkonen, H.: 1985, Fast method for computing the fourier integral transform via simpsons numerical integration, *J. Biomed. Eng.* **7**, 337–340.
- Sogachev, A. and Panferov, O.: 2006, Modification of two-equation models to account for plant drag, *Boundary-Layer Meteorology* **121**, 229–266.
- Taylor, G. J.: 1990, Wake measurements on the nibe wind turbines in denmark, *Technical Report ETSU WN 5020*, Department of Energy, National Power.
- Vermeer, L. J., Sørensen, N. J. and Crespo, A.: 2003, Wind turbine wake aerodynamics, *Progress in Aerospace Sciences* **39**, 467–510.
- Wilcox, D. C.: 2002, *Turbulence Modeling for CFD*, 2nd edn, DCW Industries.
- Yakhot, V., Orszag, S. A., Thangam, S., Gatski, T. B. and Speziale, C. G.: 1992, Development of turbulence models for shear flows by a double expansion technique, *Physics of Fluids A* **7**, 1510–1520.

 Title and author(s)

Linearised CFD Models for Wakes

Søren Ott, Jacob Berg and Morten Nielsen

 ISBN

978-87-550-3892-9

ISSN

 Dept. or group

Wind Energy Department

Date

September 23, 2011

 Groups own reg. number(s)

Project/contract No.

1120183-01

 Pages

39

Tables

Illustrations

References

 Abstract (Max. 2000 char.)

This report describes the development of a fast and reasonably accurate model for the prediction of energy production in offshore wind farms taking wake effects into account. The model has been implemented as a windows application called Fuga which can run in batch mode or as a graphical user interface. Fuga is briefly described. The model is based on a linearization technique which is described in some detail, and linearized, governing equations are derived and written in a standard form based on a mixed-spectral formulation. A new solution method is used to solve the equations which involves intensive use of look-up tables for storage of intermediate results. Due to the linearity of the model, multiple wakes from many turbines can be constructed from the wake of a single, solitary turbine. These are in turn constructed from Fourier components by a fast Fourier integral transform of results derived from generic look-up tables. Three different models, based on three different closures, are examined:

- the 'simple closure' using an unperturbed eddy viscosity $\kappa u_* z$
- the mixing length closure
- the $E-\varepsilon$ closure

Model results are evaluated against offshore wind farm production data from Horns Rev I and the Nysted wind farm, and a comparison with direct wake measurements in an onshore turbine (Nibe B) is also made. A very satisfactory agreement with data is found for the simple closure. The exception is the near wake, just behind the rotor, where all three linearized models fail. The mixing length closure underestimates wake effects in all cases. The $E-\varepsilon$ closure overestimates wake losses in the offshore farms while it predicts a too shallow and too wide the wake in the onshore case. The simple closure performs distinctly better than the other two. Wind speed data from the the Horns rev met masts are used to further validate Fuga results with the 'simple' closure.

Finally, Rødsand 1 and 2 are used as an example to illustrate the interaction between wind farms.

 Descriptors

 Available on request from:

 Information Service Department, Risø National Laboratory
 (Afdelingen for Informationservice, Forskningscenter Risø)

Risø DTU is the National Laboratory for Sustainable Energy. Our research focuses on development of energy technologies and systems with minimal effect on climate, and contributes to innovation, education and policy. Risø has large experimental facilities and interdisciplinary research environments, and includes the national centre for nuclear technologies.

Risø DTU
National Laboratory for Sustainable Energy
Technical University of Denmark

Frederiksborgvej 399
PO Box 49
DK-4000 Roskilde
Denmark
Phone +45 4677 4677
Fax +45 4677 5688

www.risoe.dtu.dk